Università di Bologna

Dipartimento di Scienze della Terra e Geologico-Ambientali

DOTTORATO DI RICERCA IN SCIENZE DELLA TERRA
XXIV CICLO
Coordinatore: Prof. Roberto Barbieri

Tesi di Dottorato

INDOOR AND OUTDOOR NATURAL RADIOACTIVITY IN THE VULSINI VOLCANIC DISTRICT (CENTRAL ITALY): ESTIMATION OF DOSES AND RADIOLOGICAL RISKS

Settore concorsuale:

04/A1 – GEOCHIMICA, MINERALOGIA, PETROLOGIA, VULCANOLOGIA, GEORISORSE ED APPLICAZIONI

Presentata da:

Giorgia Cinelli

Relatore

Prof. Bruno Capaccioni

Co-relatori

Prof.ssa Laura Tositti

Prof. Domiziano Mostacci

Ciclo di studi 2009-2011

Abstract

Terrestrial radioactivity for most individual is the major contributor to the total dose and is mostly provided by ^{238}U, ^{232}Th and ^{40}K radionuclides. In particular indoor radioactivity is principally due to ^{222}Rn, a radioactive noble gas descendent of ^{238}U, second cause of lung cancer after cigarettes smoking.

Vulsini Volcanic District is a well known quaternary volcanic area located between the northern Latium and southern Tuscany (Central Italy). It is characterized by an high natural radiation background resulting from the high concentrations of ^{238}U, ^{232}Th and ^{40}K in the volcanic products. In this context, subduction-related metasomatic enrichment of incompatible elements in the mantle source coupled with magma differentiation within the upper crust has given rise to U, Th and K enriched melts. Almost every ancient village and town located in this part of Italy has been built with volcanic rocks (particularly tuffs, due to their mechanical properties) pertaining to the Vulsini Volcanic District. The radiological risk of living in this area has been estimated considering separately:

a. the risk associated with buildings made of volcanic products and built on volcanic rock substrates
b. the risk associated to soil characteristics (permeability, soil radon concentration).

The former has been evaluated both using direct ^{222}Rn indoor measurements and simulations. Direct ^{222}Rn indoor measurements, carried out in the Bolsena village, have revealed extremely high values in the old centre due to the combined effect of building materials, volcanic basement and low air exchange rates. Simulations of "standard rooms" built with the tuffs and lavas from the Vulsini Volcanic District investigated in this work, have provided estimations of the effective doses and lifetime risk for radiogenic cancer.

The latter has been carried out by using *in situ* measurements of ^{222}Rn activity in the soil gases. A radon risk map for the Bolsena village has been developed using soil radon measurements integrating geological information. According to this, this area can be defined with no doubts a radon-prone area.

Available epidemiological data have not been fully utilizable to research an eventual increase of cancer in this area, but useful for some remarks.

Data of airborne radioactivity in ambient aerosol at two elevated stations in Emilia Romagna (North Italy) under the influence of Fukushima plume have been collected, effective doses have been calculated and an extensive comparison between doses associated with artificial and natural sources in different area have been described and discussed.

Riassunto

Per la maggior parte della popolazione il contributo predominante all'esposizione annuale alle radiazioni ionizzanti è rappresentato dalla radioattività naturale dovuta in maggior parte ai radionuclidi ^{238}U e ^{232}Th, alle loro catene di decadimento e al ^{40}K. In ambienti chiusi la radioattivà è principalmente dovuta al ^{222}Rn, gas nobile radioattivo presente nella catena di decadimento dell'^{238}U, che è stato riconosciuto essere la seconda causa di tumore al polmone dopo il fumo di sigaretta.

Il Distretto Vulcanico Vulsino, area vulcanica localizzata tra il nord del Lazio e il sud della Toscana (Italia centrale), è caratterizzato da un alto fondo di radioattività naturale derivante dalle alte concentrazioni di ^{238}U, ^{232}Th e ^{40}K presenti nei prodotti vulcanici. In questo contesto le sorgenti mantelliche metasomatizzate arricchite di elementi incompatibili, insieme alla differenziazione magmatica all'interno della crosta superiore, ha dato origine a fusi ricchi di U, Th e K.

La maggior parte delle città storiche localizzate in questa area dell'Italia sono state edificate utilizzando roccia vulcanica estratta nel Distretto Vulcanico Vulsino, in particolare il tufo grazie alle sue buone proprietà meccaniche. E' stato perciò stimato il rischio radiologico per i residenti in quest'area e sono stati considerati separatamente:

a. il rischio associato all'utilizzo di prodotti vulcanici come materiali da costruzione per edifici costruiti su un substrato di roccia vulcanica,

b. il rischio legato alle caratteristiche del suolo (concentrazione di radon nel suolo, permeabilità).

Il primo è stato valutato mediante misure di concentrazione di ^{222}Rn in ambienti chiusi e attraverso simulazioni di una stanza tipo. Le misure dirette di ^{222}Rn in ambienti chiusi sono state effettuate nella città di Bolsena e hanno rilevato valori estremamente alti soprattutto nel centro storico, dovuti all'effetto combinato di: materiali da costruzione, basamento vulcanico e bassi ricambi d'aria.

Le simulazioni della stanza tipo, costruita con tufi e lave del Distretto Vulcanico Vulsino studiate in questo lavoro, hanno fornito una stima della dose efficace e del rischio di sviluppare un tumore radiogenico nel tempo vita.

Il secondo è stato valutato utilizzando misure di concentrazione di ^{222}Rn nei gas del suolo con cui è stata sviluppata una mappa di rischio per la città di Bolsena in cui vengono prese in

considerazione anche le informazioni geologiche. Dalla mappatura appare senza alcun dubbio che questa è un'area ad elevata probabilità di alte concentrazioni di radon (radon prone area).

I dati epidemiologici disponibili ad oggi non sono pienamente utilizzabili per studiare un eventuale aumento di tumori nella popolazione di quest'area, ma utili per fare osservazioni e considerazioni più generali.

A seguito dell'incidente nella centrale nucleare di Fukushima sono stati raccolti dati di radioattività nell'aerosol ambientale in due stazioni dell'Emilia Romagna (Nord Italia) e sono state ricavate le dosi efficaci ricevute dalla popolazione. Inoltre dosi associate a sorgenti naturali ed artificiali in diverse aree sono state confrontate e discusse.

Contents

Chapter 1 - Introduction

The human population is continuously exposed to ionizing radiation from several natural sources, this exposure is a continuing and inescapable feature of life on Earth. Natural sources can be classified in two broad categories: high-energy cosmic rays incident on the Earth's atmosphere and releasing secondary radiation (cosmic contribution); radioactive nuclides generated during the formation of the Earth and still present in the Earth's crust (terrestrial contribution). Among the natural radionuclides (the so-called primordial radionuclides), only those having half-lives comparable to the age of the Earth, together with their decay products, exist in significant quantities on the planetary scale. Terrestrial radioactivity is mostly provided by ^{238}U, ^{235}U, ^{232}Th radioactive families together with ^{40}K, which is a long lived radioactive isotope of the elemental potassium.
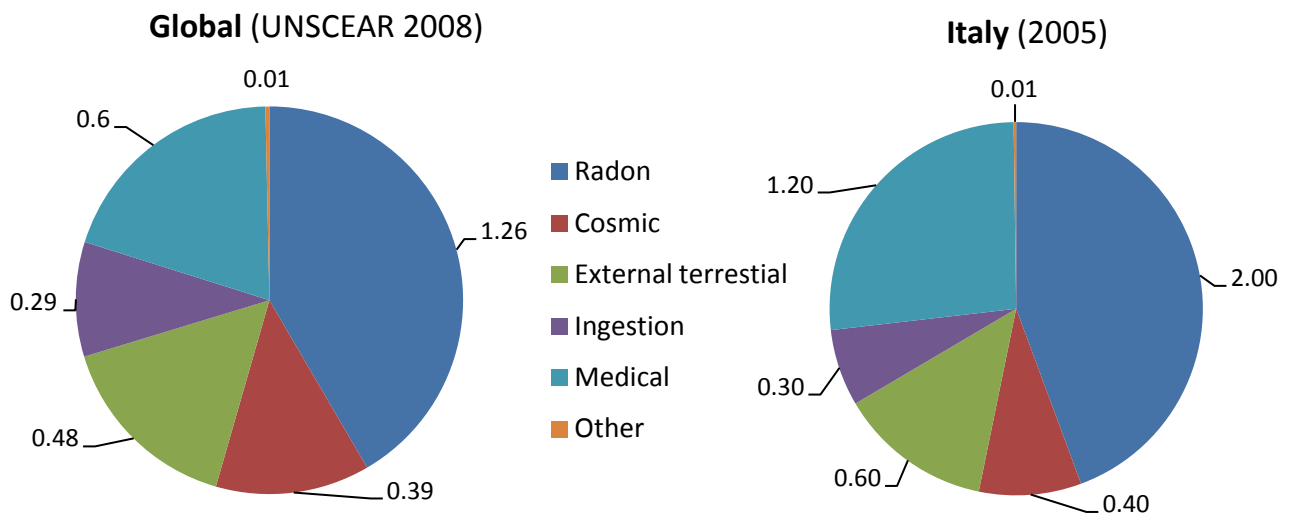
Fig. 1.1 Estimated contributions to public exposure (mSv/y) from different sources for Italy (Dionisi, 2005) and UNSCEAR estimates of worldwide average exposure.

For most individuals, exposure to ionizing radiation from natural sources exceeds that from all man-made sources combined (Fig.1.1), in most circumstances ^{222}Rn (Radon), produced in the radioactive decay of the ^{238}U progeny, is the major contributor to the total dose. Radon is a

radioactive noble gas, exhaled form the earth's surface or from other materials into the atmosphere is rapidly dispersed while in confined air spaces such as houses and underground mines the radon concentration increases with decreasing ventilation rate. Recent studies on indoor radon and lung cancer in Europe, North America and Asia provide strong evidence that radon causes a substantial number of lung cancers in the general population, therefore representing the second cause of lung cancer after smoking. The proportion of lung cancers attributable to radon range from 3 to 14%, depending on the average radon concentration in the country concerned and the calculation methods (Zeeb and Shannoun, 2009).

Throughout the world there are small areas of markedly high absorbed dose rates in air that are associated with thorium-bearing and uranium-bearing minerals in the rock-soil. In those areas, absorbed dose rates in air of several hundred nanograys per hour are not uncommon.
In Italy the contributions to public population due to natural sources appear higher than those considering the worldwide average (Fig.1.1) in particular for radon 2 mSv/y versus 1.26 mSv/y, for external terrestrial 0.6 mSv/y versus 0.48 mSv/y.
In the UNSCEAR report (2000) areas of high natural background are listed, and between these some Italian volcanic areas are named (Lazio, Campania, Orvieto town, South Toscana).

In the present work the attention has been focused on the Vulsini Volcanic District, a large volcanic area located between northern Latium and southern Tuscany (Central Italy) active during the period 590 – 127 ka (Gillot et al., 1991, Nappi et al.,1995). On the basis of temporal and spatial distribution of the eruptive activity, it has been subdivided into four volcanic complexes: Paleobolsena, Bolsena, Latera and Montefiascone (Nappi et al., 1991). The volcanic complexes display similar eruptive styles, characterized by ignimbrite-forming events preceded and followed by effusive and strombolian activities, usually taking place along peripheral circum-calderic fault systems. These volcanic products contain high concentrations of ^{238}U, ^{232}Th and ^{40}K due to subduction-related metasomatic enrichment of incompatible elements in the mantle source coupled with magma differentiation within the upper crust.
Almost every ancient village and town located in the northern part of Latium (Bolsena, Montefiascone, Gradoli, Pitigliano, Sovana etc.) has been built with volcanic rocks pertaining to the Vulsini Volcanic District. Among them, Bolsena is one of the most important, located on the shore of the homonymous lake, along the ancient "Francigena" road (historically connecting the northern Europe with the city of Rome) and with remarkable architectural and archeological features. In this area volcanic stones have been widely used to build walls and graves during the Etruscan period,

amphitheater and walls during Roman dominion and private and public buildings through Middle Age and Renaissance. Nowadays, concrete and bricks have largely replaced natural materials.

There is no specific values of doses or of activity concentrations in the environmental that defines what constitutes an "enhanced natural radiation area" (UNSCEAR, 2008). Some references cite criteria on the dose rate, indoor and soil radon concentrations, contents of radionuclides in building materials that can be used for this purpose.

The first step of the present work was to analyze different environmental matrices (i.e., rock, soil, air, etc.) to estimate quantitatively natural radioisotopes. Rock and soil samples were collected at different sites between Latera and Bolsena volcanic complexes and analyzed by γ-spectrometry and X-ray fluorescence in laboratory. *In situ* γ-spectrometry have been performed directly in the ground and in indoor building materials. Soil gas radon measurements have been carried out and soil permeability has been estimated in an area around Bolsena village, where also indoor radon measurements have been made.

So all these different data of radioactivity have been collected with the aim to confirm the fact that this area is an "enhanced natural radiation area" and quantify the exposure in term of doses and the radiological risk for inhabitants of this volcanic area.

In this area population is currently exposed to high chronic levels of radiation and it is interesting consider the relevance of such exposure to epidemiological studies on the effect of low-dose and low-dose-rate exposures. For this reasons the available epidemiological data from the Italian Network of Cancer Registries (AIRTUM) have been analyzed. The scope was to find if there is a correlation between epidemiological data and radiological risk estimated for people living in the Vulsini Volcanic District.

During the thesis period a relevant event happened: the accident in the Fukushima Dai-ichi nuclear power plant after the devastating tsunami in Japan on the March 11th 2011. These event has been an occasion to compare doses due to natural sources and due to the artificial radionuclides released in air during the nuclear accident. Radioactivity data in air samples have been collected by our research group at Monte Cimone and Montecuccolino stations. Effective doses to the population of Bologna (Italy) due to inhalation of the radionuclides detected from Fukushima plume have been estimated. Moreover some measures of radioactivity have been carried out in the area around Chernobyl reactor, where on 26 April 1986 a nuclear disaster happened. All these data have provided the possibility to made a comparison between doses due to the presence of artificial radioactivity and to high level of natural radioactivity that can be found in the Vulsini Volcanic District.

References

Gillot, P.Y., Nappi, G., Santi, P. and Renzulli, A., 1991. *Space-time evolution of the Vulsini Volcanic Complexes, central Italy*. EUG VI, Strasburg, 24-28 March 1991. Terra Abstract, 3-1, 446.

Nappi, G., Renzulli, A. and Santi, P., 1991. Evidence of incremental growth in the vulsinian calderas (Central Italy). *J. Volcanol. Geotherm. Res*. 47, 13–31.

Nappi, G., Renzulli A., Santi, P. and Gillot, Y.P. 1995. Geological evolution and geochronology of the Vulsini volcanic district (central Italy): Bollettino della Società Geologica Italiana, v.114, 599-613.

United Nations Scientific Committee on the effects of Atomic Radiation (UNSCEAR), 2000. Sources and Effects of Ionizing Radiation. Report to General Assembly, Annex B, United Nations, New York, NY. 156 pp.

United Nations Scientific Committee on the effects of Atomic Radiation (UNSCEAR), 2008. Sources and Effects of Ionizing Radiation. Report to General Assembly, Annex B, United Nations, New York, NY.245 pp.

Zeeb H, Shannoun F, eds. WHO Handbook on Indoor Radon: A Public Health perspective. Geneva, Switzerland: World Health Organization; 2009.

Chapter 2 - Natural Radioactivity

2.1 Introduction

Natural radionuclides can be classified in three major categories:

i.   cosmic radionuclides continuously produced by bombardment of stable nuclides by cosmic rays, primarily in the atmosphere;

ii.   primordial radionuclides having half-lives sufficiently long that they have survived since their creation;

iii. secondary radionuclides derived from radioactive decay of the primordials.

2.2 Cosmic radiation

The primary radiations that originates in outer space and impinge isotropically on the top of the earth's atmosphere, consist of 87% protons, 11% α particles, about 1% nuclei of atomic number Z between 4 and 26, and about 1% electrons of very high energy. These radiations originate outside the solar system and only a small fraction is normally of solar origin, however the solar component becomes significant during solar flares, which follows an 11-year cycle.

Primary cosmic rays predominate above 25 km of altitude. The specific character of primary cosmic rays is their high energy (with a mean energy of about 10^{10} and maximum energies of as much as 10^{20} eV) which implies a low stopping power and higher penetration capability than is usual for heavy particles. The interactions of the primary particles with atmospheric nuclei produce electrons, γ rays, neutrons, and mesons. At sea level the dominant component of the cosmic-ray field is muons with energy mostly between 1 and 20 GeV, only the 0.05% of primary protons penetrate at sea level (UNSCEAR, 2008; Eisenbud, 1997).

2.3 Cosmogenic radionuclides

Cosmic irradiation of the atmosphere produces neutrons and protons which react with N_2, O_2, Ar resulting in the production of radioactive nuclides, listed in table 1. These nuclides are produced at constant rates and brought to the earth surface by rain water. Equilibrium is assumed to be established between the production rate and the mean residence time of these radionuclides in terrestrial reservoirs (atmosphere, sea, lakes, soil, plants, etc) leading to constant specific radioactivities of the elements in each reservoir. If a reservoir is closed from the environment, its specific radioactivity decreases and this can be used to date marine sediments (using ^{10}Be, ^{26}Al), groundwater(^{36}Cl), glacial ice (^{10}Be), dead biological materials (14C) etc. The shorter-lived cosmogenic radionuclides have been used as natural tracers for atmospheric mixing and precipitation processes (e.g.^{39}Cl or ^{38}Sr)(Choppin, 2002). Of the 22 identified cosmogenic nuclides (Table 2.1), only four, ^{14}C, ^{3}H, ^{22}Na, and ^{7}Be, are of any consequences whatsoever from the perspective of dose to humans.

Radionuclide	Half-life	Major Radiations	Target nuclides	Typical concentrations (Bq/ kg)		
				Air (troposphere)	Rainwater	Ocean water
^{10}Be	$1.6*10^6$ y	β	N,O			$2*10^{-8}$
^{26}Al	$7.2*10^{-5}$ y	β+	Ar			$2*10^{-10}$
^{36}Cl	$3*10^{-5}$ y	β	Ar			$1*10^{-5}$
^{8}0Kr	$2.3*10^{-5}$ y	K X ray	Kr			
^{14}C	5730 y	β	N,O			$5*10^{-3}$
^{32}Si	~650 y	β	Ar			$4*10^{-7}$
^{39}Ar	269 y	β	Ar			$6*10^{-8}$
^{3}H	12.33 y	β	N,O	$1.2*10^{-3}$		$7*10^{-4}$
^{22}Na	2.6 y	β+	Ar	$1*10^{-6}$	$2.8*10^{-4}$	
^{35}S	87.4 d	β	Ar	$1.3*10^{-4}$	$7.7-107*10^{-3}$	
^{7}Be	53.3 d	γ	N,O	0.01	0.66	
^{37}Ar	35.0 d	K X ray	Ar	$3.5*10^{-5}$		
^{33}P	25.3 d	β	Ar	$1.3*10^{-3}$		
^{32}P	14.28 d	β	Ar	$2.3*10^{-4}$		
^{38}Mg	21.0 h	β	Ar			
^{24}Na	15.0 h	β	Ar		$3.0-5.9*10^{-3}$	
^{38}S	2.83 h	β	Ar		$6.6-21.8*10^{-2}$	
^{31}Si	2.62 h	β	Ar			
^{18}F	109.8 m	β+	Ar			
^{39}Cl	56.2 m	β	Ar		$1.7-8.3*10^{-1}$	
^{38}Cl	37.29 m	β	Ar		$1.5-25*10^{-1}$	
^{34m}Cl	31.99 m	β+	Ar			

Table 2.1 Radionuclides Induced in the Earth's Atmosphere by Cosmic Rays (Eisenbud, 1997).

2.4 Primordial radionuclides

2.4.1 Non series primordial radionuclides

Primordial radionuclides, not belonging to the natural radioactive decay series of uranium and thorium and ligher than lead (Z<82) are listed in table 2. Only 2 of the 17 nonseries, primordial nuclides, ^{40}K and ^{87}Rb, are of most interest.

Because of the long half-lives of these nuclides they must have been formed at the time of (or possibly even before) the formation of the solar system and of the earth. When the earth's crust solidified, these radionuclides became trapped in rocks. As they decayed, decay products accumulated in the closed rock environment. By measuring the amount of parent and daughter nuclides, it is possible with the half-life to calculate how long this environment (e.g. a rock formation) has existed. This is the bases for *nuclear dating* (also called "radioactive clocks'), and almost all of the nuclides in Table 2.2 can be used for this purpose, e.i. dating methods for the K-Ar and Rb-Sr systems. The potassium isotope ^{40}K has an abundance of about 0.012% of natural potassium, and decays to ^{40}Ca emitting beta radiation (89%). The 11% of the decay of ^{40}K involve in electron capture and ^{40}Ar is the product. This ^{40}Ar is in an non stable excited state; upon returning to its ground-state, it emits the gamma radiation at 1.46 MeV.

The heavy element series beginning with U and Th isotopes are therefore referred to as *long* decay series.

Radionuclide	Half-life (y)	Major Radiations	Typical crustal concentration (Bq kg^{-1})
^{40}K	$1.26*10^9$	β, γ	630
^{50}V	$6*10^{15}$	γ	$2*10^{-5}$
^{87}Rb	$4.8*10^{10}$	β	70
^{113}Cd	$>1.3*10^{15}$	Not reported	$<2*10^{-6}$
^{115}In	$6*10^{14}$	β	$2*10^{-5}$
^{123}Te	$1.2*10^{13}$	X rays	$2*10^{-7}$
^{138}La	$1.12*10^{11}$	β, γ	$2*10^{-2}$
^{142}Ce	$>5*10^{16}$	Not reported	$<1*10^{-5}$
^{144}Nd	$2.4*10^{15}$	α	$3*10^{-4}$
^{147}Sm	$1.05*10^{11}$	α	0.7
^{152}Gd	$1.1*10^{14}$	α	$7*10^{-6}$
^{174}Hf	$2.0*10^{15}$	α	$2*10^{-7}$
^{176}Lu	$2.2*10^{10}$	e-, γ	0.04
^{187}Re	$4.3*10^{10}$	β	$1*10^{-3}$
^{190}Pt	$6.9*10^{11}$	α	$7*10^{-8}$
^{192}Pt	$1*10^{15}$	α	$3*10^{-6}$
^{209}Bi	$>2*10^{18}$	α	$<4*10^{-9}$

Table 2.2 Non series Primordial Radionuclides ligher than Lead (Eisenbud, 1997).

2.4.2 Elements in the natural radioactive decay series

For heavy nuclei it often occurs that the daughter nuclei, which have been formed by radioactive decay, decay again to form new daughter nuclei and so on, until finally, after many decay processes, a stable nucleus is left. In this case, the term *decay series* or *decay chain* is used. In nature four long series of genetically related radionuclides beginning with Th, U or Np and ending with Pb and Bi exist.

The first series in Table 2.3 is known as the *thorium decay series,* and consists of a group of radionuclides related through decay in which all the mass numbers are evenly divisible by four (the *4n* series). It has its natural origin in ^{232}Th which occurs with 100% isotopic abundance. Natural thorium has a specific activity of 4.06 kBq/g, as its half life through α-decay is $1.41*10^{10}$ y. The terminal radionuclide in this decay series is the stable species ^{208}Pb. The longest-lived intermediate is ^{228}Ra (5.76 y).

Radionuclide	Half-life	Major Radiations
^{232}Th	$1.4*10^{10}$ y	α, <1% γ
^{228}Ra	5.75 y	β ,<1% γ
^{228}Ac	6.13 h	β, γ
^{228}Th	1.91 h	α, γ
^{224}Ra	3.66 d	α, γ
^{220}Rn	55.6 s	α, <1% γ
^{216}Po	0.15 s	α, <1% γ
^{212}Pb	10.64 h	β, γ
^{212}Bi	60.55 m	α, γ
^{212}Po(64%)	0.305 μs	α
^{208}Tl(36%)	3.07 m	β, γ
^{208}Pb	Stable	None

Table 2.3. Thorium Series (Eisenbud, 1997)

The uranium decay series, reported in table 2.4, consist of a group of nuclides that, when their mass number is divided by 4, have a remainder of 2 (the 4n + 2 series). The parent of this series is ^{238}U with a natural abundance of 99.3 %; it undergoes a decay with a half-life of $4.46 \cdot 10^9$ y. The stable end product of the uranium series is ^{206}Pb. The specific activity of ^{238}U is 12.44 MBq/kg ^{238}U.

Radionuclide	Half-life	Major Radiations
^{238}U	$4.47*10^9$ y	α, <1% γ
^{234}Th	24.1 d	β, γ
^{234m}Pa	1.17 m	α, <1% γ
^{234}Pa	21.8 y	β, γ
^{234}U	$2.44*10^5$ y	α, <1% γ
^{230}Th	$7.7*10^4$ y	α, <1% γ
^{226}Ra	1600 y	α, γ
^{222}Rn	3.8 d	α, <1% γ
^{218}Po	3.05 m	α, <1% γ
^{214}Pb(99.98%)	26.8 m	β, γ
^{218}At(0.02%)	2 s	α, γ
^{214}Bi	19.9m	β, γ
^{214}Po(99.98%)	164 μs	α, <1% γ
^{210}Tl(0.02%)	1.3 m	β, γ
^{210}Pb	22.3 y	β, γ
^{210}Po(~100%)	138.4 d	α, <1% γ
^{206}Tl(0.00013%)	4.20 m	β, <1% γ
^{206}Pb	Stable	None

Table 2.4 Uranium Series (Eisenbud, 1997)

Radionuclide	Half-life	Major Radiations
^{235}U	$7.038*10^8$ y	α, γ
^{231}Th	25.5 h	β, γ
^{231}Pa	$2.276*10^4$ y	α, γ
^{227}Ac	21.77 y	β, <1% γ
^{227}Th(98.62%)	18.72 y	α, γ
^{223}Fr(1.38%)	21.8 m	β, γ
^{223}Ra	11.43d	α, γ
^{219}Rn	3.96 s	α, γ
^{215}Po	1.78 ms	α, <1% γ
^{211}Po(~100%)	36.1 m	β, γ
^{215}Ac(0.00023%)	~0.1 ms	α, <1% γ
^{211}Pb	2.14 m	α, γ
^{211}Pb(0.273%)	0.516 s	α, γ
^{207}Tl(99.73%)	4.77 m	β, <1% γ
^{207}Pb	Stable	None

Table 2.5 Actinium Series (Eisenbud, 1997)

The *actinium decay series* (Table 2.5) consists of a group of nuclides whose mass number divided by 4 leaves a remainder of 3 (the 4n + 3 series). This series begins with the uranium isotope ^{235}U, which has a half-life of 7.04 • 10^8 y and a specific activity of 80 MBq/kg. The stable end product of the series is ^{207}Pb.

	^{234}U	^{235}U	^{238}U	Total
Specific Activity	231.3*10^3 MBq/kg	80 MBq/kg	12.44 MBq/kg	
Atom %	0.0054%	0.72%	99.275%	
Weight %	0.0053%	0.711%	99.284%	
Activity %	48.9%	2.2%	48.9%	
Activity in 1 g of U$_{nat}$	12356 Bq	568 Bq	12356 Bq	25280 Bq

Table 2.6. Properties of Natural Uranium Isotopes.

The uranium normally found in nature consists of three isotopes having mass numbers 234, 235, and 238. In the earth's crust, ^{238}U is present in the amount of 99.28% and is usually in radioactive equilibrium with ^{234}U, which is present in the amount of 0.0054%, ^{235}U is present in the amount of 0.71%. The specific activity of natural uranium is 25.3 MBq/kg considering the natural abundance of the three radionuclides. Some characteristics of natural uranium are summed in table 2.6.

The quantities of the three radionuclides, uranium, thorium and potassium can be expressed in two different and equivalent ways, using:

a. the specific activity in Bq/kg
b. the weight fraction in ppm or %.

The contents are given generally in ppm for uranium and thorium (1 ppm = 10^{-6} kg U and Th for 1 kg rock mass) and in percent (%) for potassium (1%= 10^{-2} kg K for 1 kg rock mass).

Conversion from specific activity (Bq/kg) to bulk elemental weight fraction was obtained with the following conversion factors (Stromswold,1995):

1% K= 309.7 Bq/kg
1 ppm U= 12.35 Bq/kg (^{238}U or ^{226}Ra, both assumed in equilibrium)
1 ppm Th = 4.072 Bq/kg.

2.5 Abundance of uranium, thorium, and potassium in minerals and rocks

Potassium is a constituent of a number of typical and abundant minerals. It is generally chemically combined:

- in clay minerals where it occurs in the clay mineral structures,
- in evaporites where it occurs chemically as salts, such as sylvite, carnallite,
- in rock forming minerals (for example feldspars: orthoclase, microcline and micas: biotite, muscovite) where it is chemically combined into the silicate structure.

The most abundant rock forming minerals contain only small quantities of thorium and uranium. Higher concentrations of U occur in uranium minerals (for example, autunite, bequerelite, carnotite, pechblende, uraninite, tyuyamunite with contents up to 76% U) and uranium-bearing minierals (such as: betafite, chalcolite, fergusonite, pyrochlore, uranotile with contents up to 56% U). Larger quantities of Th are concentrated in some accessory minerals which also contain large quantities of U. However the main portion of Uranium is finely dispersed as submicroscopic, ill defined microinclusions, loosely bound on grain boundaries, fractures and internal surfaces; it can easily be leached by weak acids (Shon, 1998). This cause the high mobility of uranium under geological processes.

Original uranium is generally associated with acid igneous rocks (the average is about 4.65 ppm). It forms soluble salts, especially the uranyl ion (UO_2^{2+}) and it is present in this form in rivers and sea water. The salts are instable and pass easily out of the solution. From the water, uranium can be fixed and pass into sediments in three ways:

- chemical precipitation in acid (pH 2.5..4) ore reducing (pH 0…0.4) environmental,
- adsorption by organic matter,
- adsorption by phosphates.

For the most part, uranium has a very heterogeneous sedimentary distribution, is movable, and can be used as an environmental indicator. Thorium has its main origin in acid and intermediate rocks, but compared with uranium, it is very stable, and will not generally pass into solution.

The natural radioactivity of rocks is due to the contribution of the radiation components U, Th and K. Concentration of the three radionuclides vary widely in crustal rocks as the results of the mineral composition of the rock type and the rock genesis and environment. Mean value for the crust are reported in table 2.7.

	Uranium (ppm)	Thorium (ppm)	Potassium (%)
Earth's crust	2.1	7.8	2.1
Oceanic crust	0.64	2.8	0.87
Continental crust	2.8	10	2.6

Table 2.7 Mean values of the uranium, thorium, and potassium content for the earth' crust after Heier and Rogers, 1963 (Shon, 1998).

2.5.1 Igneous rocks

Generally the concentrations of all three elements in common igneous rocks are distinctly higher (about 10 times) in acidic than in ultrabasic rocks and follow a trend of the SiO_2 content. Higher radioactivity of magmatic rocks is mainly related to the presence of accessory uranium and thorium-bearing minerals. Values and ranges in different igneous rocks are presented in table 2.8.

	U (ppm)	Th(ppm)	K(%)
Acid			
Intrusive			
Granite	4-7	15-40	3.4-4
Extrusive			
Rhyolite	2.5-5	6-15	2-4
Trachyte	2-7	9-25	5.7
Basic			
Intrusive			
Gabbro	0.84-0.9	2.7-3.85	0.46-0.58
Diorite	2.0	8.5	1.1
Granodiorite	2.6	9.3-11	2-2.5
Extrusive			
Alcali basalt	0.99	4.6	0.61
Alcali olivine	1.4	3.9	1.4
basalt	1.2-2.2	5.5-15	1.4-3.23

Table 2.8 U, Th, and K content of some igneous rocks (Shon, 1998)

2.5.2 Metamorphic rocks

The uranium, thorium, and potassium content of metamorphic rocks is a result of the original contents of the educt material (igneous or sedimentary) and may have been changed by metamorphic processes. The content is adsorbed and redistributed according to the degree of metamorphic transformation. Generally radioactive elements are decreased with increasing metamorphism.

2.5.2 Sedimentary rocks

In sedimentary rocks the relative mean abundances are less predictable that in igneous rocks. Carbonates are the lowest in natural radioactivity of the sedimentary rocks and generally shales have an higher level of natural radioactivity than others sediments; consequently the gamma-ray sonde is used to distinguish between shales and other sediments. The correlation between clay content (respectively shaliness) and radiation of sedimentary rocks is important for the reservoir characterization with respect to:

- the distinction between clay and sand layers,
- the determination of the clay content and
- the characterization of "clay types".

2.6 Radon

Radon is a noble gas, colorless, odorless, and radioactive, in nature it presents three isotopes: ^{222}Rn, ^{220}Rn and ^{219}Rn. When ^{226}Ra, descendent of ^{238}U chain, decays by α emission, it transmutes to its decay product ^{222}Rn, called **radon,** with a half-life of 3.8 days. Similarly, ^{224}Ra, which is a descendant of the ^{232}Th chain, decays by α emission to ^{220}Rn historically known as **thoron** having a half-life of about 55.6 seconds. ^{219}Rn, historically called **actinon**, is a member of the ^{235}U chain and decays most rapidly, having a half-life of about 3.92 seconds.

The radon decay products are radioactive isotopes of polonium, bismuth, lead and thallium (see tables 2.3, 2.4 and 2.5), which are produced by decay of the radon isotopes. These daughters of the radioactive gases are isotopes of heavy metals and are easily fixed to existing aerosol particles in the atmosphere. They decay by particle and β/γ emission.

^{222}Rn exhibits the longest radiological half-life (3.82 days) of the radon isotopes and it has a greater opportunity than the shorter-lived radon isotopes to escape to the atmosphere. In the present work the attention has been focused only in the ^{222}Rn, called hereafter just radon.

2.6.1 Emanation and transport in materials

Radon enters the atmosphere mainly by crossing the soil-air or building material-air interface. Because soil and also most earth-building materials have 10^3-10^4 times higher gas concentrations that the atmosphere, there is a great radon concentration gradient between such materials and open

air. This gradient is permanently maintained by the generation of the ^{238}U and ^{232}Th series from long-lived mother nuclides and is responsible for a continuous flux of the radon isotopes into the atmosphere. The amount of activity released per surface and time unit is called the ***exhalation rate*** (Porstendörfer, 1994).

In general two steps determine the radon flux from materials:

a. release from the solid mineral grains to the filled pores, called "emanation",
b. subsequent transport through the pores of the material into the atmosphere.

In open atmosphere, it is rapidly diluted in a large volume of air and its concentration rarely becomes a problem. But if radon enters a building, the volume of air available for dilution may be much smaller and high concentrations become possible.

In many case the soil and the bedrock beneath house are the main source but are known cases of high contents of ^{226}Ra in the building material. In general building materials of natural origin reflect the geological conditions at the site of production, and there are large regional differences even within the same country, as the case described in the present work (Nazaroff and Nero, 1988).

Emanation Power

When radium decay in soil grains, the resulting atoms of radon isotopes must first escape from the mineral grains to air-filled pores. The fraction of radon formed in the soil grains that escape into pores is known as the emanation coefficient, or fraction or power. The emanation fraction is considered to have two components: recoil and diffusion, but the former is the most important. The influence of temperature is small while several studies have demonstrated that moisture have a large impact on the emanation coefficient.

Radon Transport in Material

In order to enter the atmosphere Radon must be transported through the pores of the material by two basic mechanisms: molecular diffusion, and advection (i.e. accompanying a movement of air in the pores). Diffusion is always present, but is normally not a very efficient migration mechanism. Diffusion is a migration from high concentration pores towards low-concentration pores, governed by Fick's law, expressed as:

$$J = -D_e * \nabla C \qquad (1)$$

where J is the radon flux (Bq/m^2/s) across the section of the pores, D_e the effective diffusion coefficient, and C the radon concentration in the pores (Bq/m^3). If diffusion is the only migration mechanism, it is possible to calculate the average migration distance (diffusion length)

$$L = \sqrt{D_e / \lambda_{Rn}} \qquad (2)$$

which is found to be approximately 2.5 m in free (still) air, and 1 m in soil, 0.5 m in building materials.

Advection may be much more efficient, but only in high-permeability materials, i.e., usually coarse-grained materials. Note that high-permeability pathways may exist in low-permeability materials, in case of fractures (macroscopic or microscopic).

Efficient transport is only possible with advection, which is governed by Darcy's law giving the velocity of air in pores

$$v = -k * \nabla P / (\mu \varepsilon) \qquad (3)$$

where the velocity is proportional to the pressure gradient; μ is the viscosity of air and k the permeability.

The pressure gradient is most often created by the house itself, either through the stack effect (warmer air inside the house goes up creating depressurisation in the lowest part of the building) or as an obstacle to the wind (higher pressure on the side where the wind comes, lower pressure on the other side).

The advection current needs some entry path to bring radon into the house. This may be offered by cracks, hollow walls, or bad filling of any hole that makes the subsoil communicate with the house (around water pipes, …).

2.7 Exposure to natural sources

In the previous chapter it has been shown that for most individuals, exposure to ionizing radiation from natural sources exceeds that from all man-made sources combined (Fig.1.1). In the following chapter the different types of exposure are taken into account and described.

Glossary

Absorbed dose (D): the energy absorbed per unit mass $D = \frac{d\varepsilon}{dm}$ where dε is the mean energy imparted by ionizing radiation to the matter in a volume element and dm is the mass of the matter in this volume element. It is expressed in Gray (Gy=J/kg).

Equivalent dose (H_T): the absorbed dose, in tissue or organ T weighted for the type and quality of radiation R. It is given by: $H_T = w_R D_{T,R}$ where $D_{T,R}$ is the absorbed dose averaged over tissue or organ T, due to radiation R and w_R is the radiation weighting factor. The unit for equivalent dose is the sievert (Sv).

Effective dose (E): the sum of the weighted equivalent doses in all the tissues and organs of the body from internal and external irradiation. It is given by: $E = \sum_T w_T H_T = \sum_T w_T \sum_R w_R D_{T,R}$ where w_T is the tissue weighting factor for tissue or organ T. The unit for effective dose is the sievert.

2.7.1 Exposure to cosmic radiations

As said before at the ground level the dominant component of the cosmic-ray field is mouns with energies mostly between 1- 10 GeV. These contributes about 80% of the absorbed dose rate in free air from the directly ionizing radiation; the remainder comes from electrons produced by muons or presents in the electromagnetic cascade (UNSCEAR, 2000; UNSCEAR, 2008).
The dose rate due to cosmic rays in open air on the earth surface depends on altitude and latitude. Data of cosmic radiation from some countries are reported in table 2.9.

The variation with latitude of the dose rate from *the photon and ionizing component* is small. The dose rate is about 10% lower at the geomagnetic equator than at high latitudes. Considering the population distribution with latitude, an average dose rate in free air at sea level of 31 nGy/h has been estimated (0.27 mSv/y). Instead the ionizing component vary strongly with altitude. Cosmic dose rates at elevation above the sea level can be estimated using the following formula (UNSCEAR 2008):

$$\dot{E}_I(z) = \dot{E}_I(0)[0.21e^{-1.649z} + 0.79e^{-0.4528z}] \quad (1)$$

where $\dot{E}_I(0)$ is the dose rate at the sea level and z is the altitude in kilometres.

For the *neutron* both the latitude and altitude strongly affect exposure rates. Researchers suggested that the equatorial neutron fluence rate at sea level is 20% of the polar fluence rate and that the fluence rate at 50° latitude is 80% of the polar fluence rate. For latitude 50° N the effective dose rate for neutron has been derived: 0.08 mSv/y. The world population-weighted average effective dose rate at sea level due cosmic ray neutron thus determined is 0.048 mSv/y. For the neutron component of cosmic rays there is also a substantial altitude effect. The formula allows to calculate the neutron dose rates taking in account the altitude dependence at habitable elevations around the world (UNSCEAR, 2008):

$$\dot{E}_N(z) = \dot{E}_N(0)b_N e^{az}$$

where $\dot{E}_N(0)$ is the effective dose rate at the sea level due to neutron:

$b_N = 1$ and $a = 1$ km^{-1} for $z < 2$ km

$b_N = 2$ and $a = 0.7$ km^{-1} for $z > 2$ km

Exposure at aircraft altitudes

Since the exposure to cosmic radiation increases rapidly with altitude persons who fly frequently are exposed to elevated levels of cosmic radiation of galactic and solar origin and to secondary radiation produced in the atmosphere, aircraft structure, etc. The cosmic particle flux depends on solar activity and solar eruptions. For altitudes of 9-12 km at temperate latitudes, the effective dose rates are in the range 5-8 µSv/h, such that for a transatlantic flight from Europe to North America, the route dose would be 30-45 µSv/h. At equatorial latitudes, the dose rates are lower and in the range of 2-4 µSv/h.

The European directive 96/29/Euratom, which is based on 1990 recommendations of ICRP, has established a specific regime for workers exposed to enhanced levels of natural radiation (EC, 1996). For workers receiving more than 1 mSv/y, the directive foresees the following constraints :

    a) the exposition of the workers must be evaluated

    b) the work programme should reduce the highest exposures

    c) the workers must be informed of the risks

during pregnancy, the dose should not exceed 1 mSv.

Region/country	Outdoors						Indoors					
	Cosmic		Terrestial		Total		Cosmic		Terrestial		Total	
	Mean	Range	Mean	Range	Mean	Range	Mean	Range	Mean	Range	Mean	Range
Cuba Central America	34	32-67	24	4-162	55	38-196	27	26-54	30	10-76	44	37-103
Belgium West Europe	33	32-36	43	13-80	76	45-120	26	20-36	60	32-180	86	55-200
Italy West Europe	38	32-54	74	11-209	112	57-243	31	26-43	105	0-690	136	29-717
Czech Republic East Europe	34	32-62	66	6-245	100	40-285	34		85	42-2000	119	74-2000
Finland North Europe	32		71	45-139	103	77-171	32		73	24-181	105	56-213
Azebaijan East Asia	37	30-45	102	45-160	140	75-205	21	16-26	123	87-160	144	103-186
China-Taiwan East Asia	27	25.7-58	52	24-68	79		24	23-52	101	66-189	125	
Islamic Republic of Iran West Asia	40.5	33.0-57.6	71	36-130	111.5	69-187.6	16.8	13.2-31.3	115	70-165	131.8	83.2-196.3
Median*					57	18-93					75	20-200
Population-weighted Value*					59						84	

Table 2.9 Absorbed dose rates in air (nGy/h) from UNSCEAR(UNSCEAR,2008). *(UNSCEAR,2000).

2.7.2 Exposure to terrestrial radiation

External Exposures

Irradiation of the external human body from external sources is mainly by gamma radiation from radionuclides in the ^{238}U and ^{232}Th series and from ^{40}K. Some other terrestrial radionuclides, including those of the ^{235}U series, ^{87}Ru, ^{138}La, ^{147}Sm, and ^{176}Lu, exist in nature but such low levels that their contribution to the dose in humans are small.

External exposure *outdoors* arise from terrestrial radionuclides present at trace levels in all soils, some value are reported in table 10. The specific levels are related to the types of rock from which the soils originate. There have been many surveys to determine the background levels of radionuclides in soils, which can in turn be related to the absorbed dose rates in air. The latter can easily be measured directly, and provide an evaluation of the background exposure levels in different countries (Tab. 2.9). The absorbed dose rates can be derived from activity concentration in soil using specific coefficient (table 2.11). In the UNSCEAR (UNSCEAR, 2000) between the areas of high natural background listed there is the Orvieto town located in the Vulsini Volcanic District. For this area it is indicated a value of absorbed dose in air (cosmic + terrestrial) of 560 nGy/h, value high in comparison to the world median of 84 nGy/h.

Indoor exposures depend on radionuclide concentrations in outdoor soil and in building material. Information on distribution of indoor exposures derived from direct measurements is not extensive, but these can be assessed in the basis of information on soil, shielding and building material, and then linked with the number of people exposed in order to estimate population exposure (Tab. 9). The indoor exposures are in general 40% greater than outdoor exposures.

To estimate annual effective doses, a value of 0.7 Sv/Gy can be assumed as conversion coefficient from absorbed dose to air to effective dose received by adults and 0.8 for the occupancy factor. The resulting worldwide average of the annual effective dose is 0.48 mSv, with the results for individual countries being generally within the 0.3-0.6 mSv range (UNSCEAR, 2000).

Region/country	Concentration in soil (Bq/kg)							
	^{40}K		^{238}U		^{226}Ra		^{232}Th	
	Mean	Range	Mean	Range	Mean	Range	Mean	Range
Egypt Africa	320	29-650	37	6-120	17	5-64	18	2-96
United States North America	370	100-700	35	4-140	40	8-160	35	4-130
Iran West Asia	640	250-980			28	5-55	22	5-42
Belgium West Europe	380	70-900			26	5-50	27	5-50
Bulgaria East Europe	400	40-80	40	8-190	45	12-210	30	7-160
Portugal South Europe	840	220-1230	49	26-82	44	8-65	51	22-100
Median	400	140-850	35	16-110	35	17-60	30	11-64
Population-weighted value	420		33		32		45	

Table 2.10 Natural radionuclide content in soil (UNSCEAR, 2000).

Radionuclide	Concentration in soil (Bq/kg)		Dose Coefficient (nGy/h per Bq/kg)	Absorbed dose rate in air (nGy/h)	
	Median value	Population-weighted value		Median value	Population-weighted value
^{40}K	400	420	0.0417	17	18
^{238}U series	35	33	0.462	16	15
^{232}Th series	30	45	0.604	18	27
Total				51	60

Table 2.11 External exposure rates calculated from various concentrations of terrestrial radionuclides in soil (UNSCEAR, 2000).

Internal exposures other than radon

Internal exposure arise from the intake of terrestrial radionuclides by inhalation and ingestion.

Doses by *inhalation* result from the presence in air of dust particles containing radionuclides of the ^{238}U and ^{232}Th decay chains. The dominant component of exposure due to inhalation are the

short-lived decay products of radon, while inhalation intake of natural radionuclides other than radon and its decay products makes only a minor contribution to internal exposure.

Ingestion intake of natural radionuclides, mainly ^{40}K and ^{238}U and ^{232}Th, depends on the consumption rates of food and water and on the radionuclide concentration. Concentrations vary widely because of the different background levels, climate, and agricultural conditions that prevail.

The total annual effective dose from inhalation and ingestion of terrestrial is 310 µSv, of which 170 µSv is from 40K and 140 µSv is from the long-lived radionuclides in the uranium and thorium series.

Radon

As underlined in the previous chapter radon and its short-lived decay products in the atmosphere are the most important contributors to human exposure from natural sources. ^{222}Rn gas undergoes radioactive decay, a large percentage of the decay products, which are solid, attach to ambient aerosols. Although some of the decay products remain unattached, others increase their size through various physical and chemical processes. The attachment rate depends on numerous factors such as the size and concentration of ambient particles. Deposition of radon decay products in the lung also depends on numerous factors, including the particle size, breathing frequency, tidal volume, and lung volume. Once inhaled and deposited, alpha particles released during the decay of ^{218}Po and ^{214}Po deliver the majority of radiation dose to the sensitive lung epithelium.

Irradiated cells may undergo DNA breaks, accurate repair, inaccurate repair, gene mutations, apoptosis, chromosomal change, and genetic instability. Alpha particles are unique among environmental carcinogens in their ability to produce double-strand DNA breaks. The resulting DNA breakage and rejoining may produce various outcomes, including the insertion, deletion, or rearrangement of genetic material. The cells that have sustained genetic damage, and do not die, may become cancerous. In fact, cancer is thought to be monoclonal in nature (i.e., cancer can originate from a single cell that has completed the process of malignant transformation). Because even a single alpha particle can cause significant genetic damage to the cell, it is unlikely that there is a threshold for radon-induced lung cancer (Field, 2011).

In developing the risk estimates for residential radon exposures (i.e., extrapolation or interpolation of the miner-based data to the residential setting), the BEIR VI committee assumed that the risk of developing radon induced lung cancer increases linearly as the exposure increases and that even very low exposures carry some risk (e.g., no threshold for risk).

The potential alpha energy concentration PAEC is the total energy of all alpha particles that will be emitted by the short-lived radon progeny present in 1 m^3 of air.

$$PAEC(MeV/m^3) = 13120C(^{214}Bi) + 17830C(^{214}Pb) + 3690C(^{218}Po)$$

The equivalent dose rate to lung is roughly proportional to PAEC. However, the free fraction is more harmful. It is mostly constituted of ^{218}Po, which is nearly in equilibrium with radon (only ~10% is deposited). Hence, the radon concentration may also be a good indicator of the risk.

The range of dose conversion factors for radon, derived from epidemiological studies and physical dosimetry varies from 6 to 15 nSv(Bq*h*m^{-3})$^{-1}$. In the Italian law (Legislative Decree 230/1995, implementing the Council Directive 96/29/EURATOM, based on the recommendations of the ICRP60) for workers a value of 9 nSv(Bq*h*m^{-3})$^{-1}$ is suggested.

References

Choppin, G.R., Liljenzin, J.O, Rydberg, J. *Chapter 5: Radionuclides in Nature.* Radiochemistry and Nuclear Chemistry, Butterworth-Heinemann, 2002, pp. 94 -121.

Eisenbud, M., Gesell, T., 1997. *Chapter 6: Natural radioactivity*. In: Eisenbud, M., Gesell, T. (Eds.), Environmental Radioactivity. Academic Press, London, pp. 134-200.

European Community (1996) Council Directive 96/29/Euratom of 13 May 1996 laying down basic safety standards for the protection of the health of workers and the general public against the danger arising from ionising radiation. Official journal No. L 159, 29 June 1996, 1-114.

Field, R.W. ,2011. *Radon: An Overview of Health Effects*. In: Nriagu JO (ed.) Encyclopedia of Environmental Health, volume 4, Burlington-Elsevier, pp.745-753.

Legislative Decree 230/1995. "Attuazione delle direttive 89/618/Euratom, 90/641/Euratom, 92/3/Euratom e 96/29/Euratom in materia di radiazioni ionizzanti."available at http://www.aimn.it/lex/DLgs_230_modificato.pdf

Nazaroff, W.W., and Nero, A.V., Jr., Eds., 1988, *Radon and its decay products in indoor air.* New York, John Wiley and Sons, Inc., 518 p.

Porstendörfer, J., 1994. *Properties and Behavior of Radon and Thoron and their decay products in the air.* J.Aerosol Sci, Vol. 25, No.2, pp 219-263.

Schon, J.H., 1998. *Physical proprieties of rocks*. Pergamon, pp 583.

United Nations Scientific Committee on the effects of Atomic Radiation (UNSCEAR), 2000. Sources and Effects of Ionizing Radiation. Report to General Assembly, Annex B, United Nations, New York, NY. 156 pp.

United Nations Scientific Committee on the effects of Atomic Radiation (UNSCEAR), 2008. Sources and Effects of Ionizing Radiation. Report to General Assembly, Annex B, United Nations, New York, NY.245 pp.

http://www.wise-uranium.org/rup.html

Chapter 3 - Detection and Measurement of Natural Radioactivity. Calibration procedure of NaI detector for *in situ* γ-spectrometry[1]

3.1 Introduction

The detection and measurement of natural radioactivity represents a fundamental aspect in our work. Because of the need to provide a qualitative and quantitative analysis of natural radioisotopes in different environmental matrices (i.e. rock, soil, air, etc) a large numbers of different detectors has been used and are described in this chapter.

Ionizing radiation is rarely detected directly, detectors usually measure the secondary products arising from the interactions of the radiation with the detector material. For example, as an alpha or beta particle traverses a detector's sensitive volume, electron-ion pairs or electron-hole pairs are created and the subsequent movement and collection of charges gives rise to an electrical pulse or current. Indirectly ionizing radiation such as gamma photons and neutrons must first undergo interactions in the detector material that produce secondary charged particles, recoil atoms or electrons that, in turn, produce charge pairs as they slow down.

The collection of the ionization created by radiation in a detector volume can be used simply to detect the passage of a radiation particle. The rate of generation of radiation-induced pulses can then be used to measure the rate at which radiation particles traverse the detector. Such detectors are termed *radiation counters*. In some detectors, the magnitude of the radiation induced pulse is related to the type of radiation particle and its energy. By measuring both the number of pulses and the distribution of pulse sizes produced by a given type of radiation, both the number and energy distribution of the incident radiation can be determined. These detectors can then be used as *energy spectrometers*. In some detectors the average current can be used as a measure of the amount of ionization or energy deposition, per unit mass of detector material, caused by incident radiation. These detectors can then be calibrated to measure radiation absorbed doses and are thus called *dosimeters* (McGregor, 2007; Knoll, 2000).

---

[1] This study is in collaboration with Jonathan Baré (ISIB, Haute Ecole P.-H.Spaak, Brussels, Belgium) and with Roberto Braga (Dip. di Scienze della Terra e Geologico-Ambientali, Università di Bologna, Italy)

The measurement systems used in the present work can be divided in three main groups according to their use to:

- measure dose exposure rate;
- measure radon concentrations in:
  - indoor air
  - soil gas;
- perform gamma spectrometry analyses:
  - in laboratory (HpGe)
  - *in situ* (NaI).

3.2 Dose Exposure Rate Monitor

Geiger-Müller (GM) tubes are gas-filled radiation detectors that are useful, cheap and robust. A GM tube basically detects the presence and intensity of radiation (particle frequency, rather than energy) but cannot determine the type, energy, or vectors of the detected radiation. It has high sensitivity, versatility with various types of radiation, wide variety of shapes and windows, large output signal and reasonable cost.

The basic design consists of a metal tube, often with a mylar or mica window at one end. At the center of the tube runs a wire with a strong positive charge. The tube is sealed and filled at low pressure with an inert gas such as argon, helium or neon with some gases added. In the absence of radiation, the detector does not conduct charge, whenever ionizing radiation passes through, however, an electric signal is generated because the metal casing of the Geiger-Muller tube acts as a cathode, and the central wire is the anode. The anode transfers the pulses of current through a resistor, where they are converted to pulses of voltage. The voltage pulses are then recorded by a counting device. Finally, an oscilloscope, LED screen, or other display conveys the particle count to the user. In a GM counter, the avalanche produced near the anode wire spreads along its entire length, that is why the output signal is independent of the magnitude of the triggering event.

The direct reading from a Geiger counter provides the count of particles detected, or counts per minute (cpm) but it can offer several standard units of measurement, with the understanding that the readings apply only to the types of radiation that particular model is able to accurately detect. The Sievert for equivalent dose is the most common measures of radiation dosage.

Two Geiger Muller tubes designed by two different companies have been used in the present work: Gamma-Scout® Geiger and RKSB-104 (Belvar).

Fig.3.1 Photograph of Gamma-Scout Geiger counter.   *Fig.3.2 Photograph of РКСБ·104 Geiger counter.*

3.3. Radon Instruments

Many techniques, in various type of detectors, have been established for measuring radon concentration and its decay products in indoor air or in soil gases.

There are 3 classes of measurement techniques that are used:

i.   Grab sampling provides instantaneous measures of radon or radon progeny in air.
The entire measurement is completed within a few tens of minutes, therefore only giving the concentration at a specific time. Considering the potential variability of concentration with time, this does not give a direct measure of the average exposure rate in a home.

ii.   Continuous active sampling, for radon decay products is based on the grab-sample methods, with modifications to permit automatic sampling, counting, and, in some case, analysis. It involves multiple measurements at closely spaced time intervals (from several minutes to an hour) over a long period. These are more costly than integrative devices and only recommended when other measures indicate a problem and the source of radon entry needs to be pinpointed precisely.

iii. Integrative sampling devices are passive, and collect data on radon levels over a fixed period of time. Typical integrative devices are charcoal canisters, alpha track film dosimeters and Electret Ion Chambers, all simple to use.

All the techniques for measuring radon and its decay products are based on the detection of emissions from radioactive decay (Field et al, 2011). The instruments used in the present work to measure radon concentration are presented.

3.3.1. Electret Ion chamber

The *Electret Ion chambers* (EIC) provide a true integrated measurement of the average radon gas concentration during the exposure period. A positively charged electret is used in conjunction with an ionization chamber made of an electrically conductive plastic. All types of these devices have a filter in the opening of the chamber to preclude the passage of particulate radioactive materials, such as radon decay products, into the chamber. The electret, which is an electrically charged plastic disk, functions both as the source of an electric field and as a sensor in the device. As radon and its decay products undergo radioactive decay within the chamber, the emitted radiation ionizes the air (Field et al, 2011).
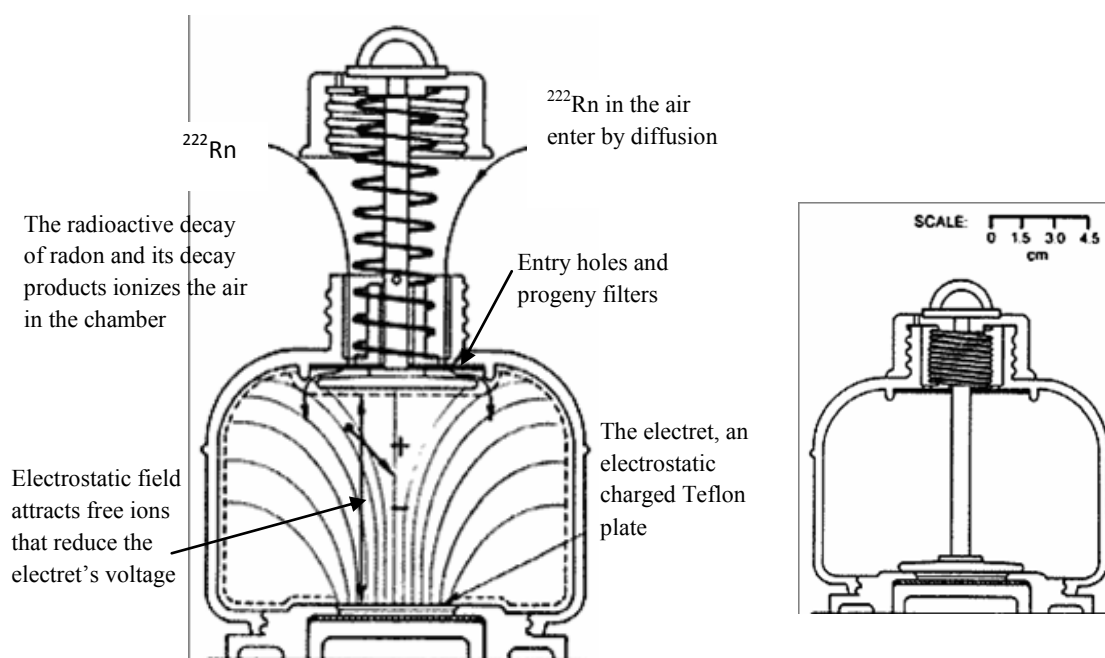

Fig. 3.3 Diagram displaying the functioning of an electret ion chamber (EIC) open (b) and close (b).

The positively charged electret collects negative ions that have been produced in the chamber air, resulting in a discharge of the electret that is related to the integrated ionization during the

measurement period (Fig. 3.3a). At the end of the exposure period, this mechanism is closed such that the electret is exposed to a tiny volume of air, thus effectively 'turning off' the device (Fig. 3.3b).

The electrical potential on the electret is measured before and after the exposure using an electret reader (an electrostatic voltmeter).

In our work for indoor radon measurements we used the E-PERM® (Fig.4) system, that utilizes the Electret Ion Chamber (EIC) technology (RadElec E-Perm, 2008).

An electret is paired with a precision, volumetric E-PERM ion chamber to comprise a working E-PERM Radon Monitor. E-PERM ion chambers are manufactured from electrically conductive polypropylene. Inlets are filtered to allow only radon by passive diffusion. E-PERM radon monitors are also designed to have an insignificant response to thoron. The S (standard) chamber is the most popular because of these special features:

- Spring-loaded cap for turning the device on or off
- Hole through the open stem to allow a 1/8 inch lock tie security seal
- Hanging ring on the cap to suspend the device.

Short-term electrets with the S chamber will measure radon at a level of 200 Bq/m^3 in approximately 48 hours. A 4 to 7-day test is ideal.

Long-term electrets with the S chamber will measure radon at a level of 200 Bq/m^3 in approximately 28 days. A 90-day test is ideal. Appropriate chamber and electret combinations are recommended for high concentration measurements.

To perform short term measurements of indoor radon concentration, in our cases between 2-5 days, the system has been used with the configuration S chamber and short term electrets.

Fig.3.4 Photograph of E-Perm electret ion chambers opened and closed (on the right) and the electret reader (on the left).

3.3.2. Continuous Radon Monitor (CRM)

Continuous radon monitors (CRMs) are electronic instruments that make continuous measurements of radon concentration at least hourly. CRMs are considered to be 'active' devices regardless of whether a pump is used or whether radon enters the detector by passive diffusion.

CRMs are typically used for measurements from 2 to 8 days in duration. The hourly measurements and the average over the measurement period are typically stored for printing or transfer to a computer; however, some CRMs provide measurements in real time.

We have used two types of CRMs that differ depending on the type of detector that is used: the Femto-TECH that uses a pulse-ion chamber as detector and RAD7 based on a solid-state detector (both for continuous monitoring of radon end thoron in soil gas or indoor environments).

Femto-TECH

The *femto*-TECH CRM-510 (Fig. 3.5) is a precision airborne alpha radiation detection and is suited for a wide range of radon measurements. It is truly a portable self-contained continuous radon monitor (CRM) employing passive diffusion sampling in the ambient air environment in which it is situated. Radon decay products are removed and prevented from entering the internal pulse ion sensing volume. As radon atom decays within the sensing volume of the chamber, a burst of ions is produced and is converted to electrical pulses in an electrometer (Detector: Air Ionization Probe).

It can read and store data for four days of stand-alone operation. In addition to the measurement and storage of radon data it provides the measurement and storage of temperature, barometric pressure, and relative humidity. In the Test Report hourly data are given for radon concentration and environmental parameters. In addition the report indicates if the instrument during acquisition was moved or disturbed (tilt). Its working range for radon concentration is between 18 to 74000 Bq/m^3. This instrument has been used to perform radon indoor short term measurements, at least 24 hours long.
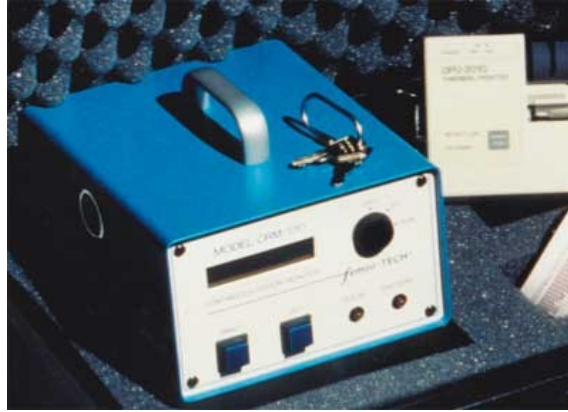
Fig. 3.5 Photograph of a continuous radon monitor (CRM), Femto-TECH.

RAD 7

The Durrige RAD7 is a very highly versatile instrument that can be used in many different modes for different purposes. We mostly used the instrument in 3 different ways:

a) continuous monitoring of radon in air,

b) sniffing for radon and/or thoron,

c) testing soil gas-radon and thoron.

The first two categories have been used to perform measurements of radon concentrations in indoor environments.

The RAD7 uses a solid state alpha detector, that is a semiconductor material (silicon) that converts alpha radiation directly to an electrical signal. It can electronically determine the energy of each alpha particle, technique known as alpha spectrometry.

The RAD7's internal sample cell is a 0.7 liter hemisphere, coated on the inside with an electrical conductor. A solid state Silicon alpha detector is at the center of the hemisphere. The high voltage power circuit charges the inside conductor to a potential of 2000 to 2500 volts, relative to the detector, creating an electric field throughout the volume of the cell. The electric field propels positively charged particles onto the detector.

The RAD7 pulls samples of air through a fine inlet filter, which excludes the progeny, into a chamber for analysis. A ^{220}Rn or ^{222}Rn nucleus that decays within the cell leaves its transformed nucleus, ^{218}Po or ^{216}Po respectively, as a positively charged ion. The electric field within the cell drives this positively charged ion to the detector, to which it sticks. When the short-lived ^{218}Po or ^{216}Po nucleus decays upon the detector's active surface, its alpha particle has a 50% probability of entering the detector and producing an electrical signal proportional in strength to the energy of the alpha particle. Subsequent decays of the same nucleus produce beta particles, which are not

detected, or alpha particles of different energy. Different isotopes have different alpha energies, and produce different strength signals in the detector. The RAD7 amplifies, filters, and sorts the signals according to their strength.

The RAD7 spectrum is a scale of alpha energies from 0 to 10 MeV. Of particular interest are the radon and thoron daughters that produce alpha particles in the range of 6 to 9 MeV (Fig. 3.6).

^{222}Rn (3.82 days)

α (5.49 MeV)

^{214}Po (164 μsecs)

^{218}Po (3.05 min)

β

α (7.69 MeV)

α (6.00 MeV)

^{214}Bi (19.9 min)

^{214}Pb (26.8 min)

β

^{210}Pb (22.3 yr)
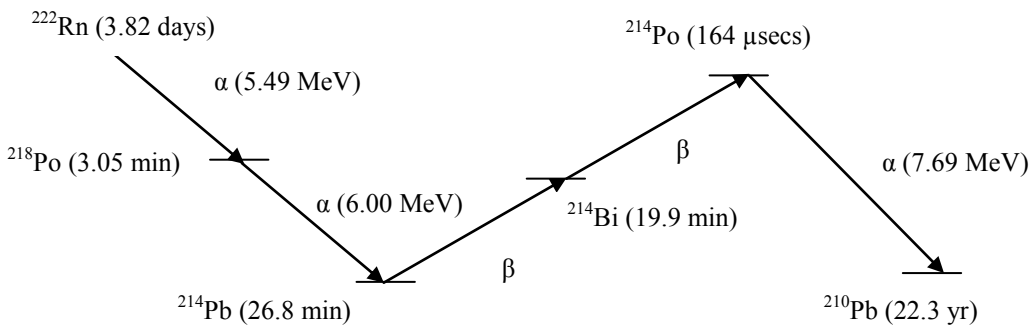
Fig. 3.6a Radon Decay Chain

^{220}Rn (55.6 sec)

α (5.29 MeV)

^{212}Po (0.3 μsec)

^{212}Bi (50.6 min)

^{216}Po (0.15 sec)

β

α (8.78 MeV)

α (6.79 MeV)

α (6.05 MeV)

^{212}Pb (10.6 hrs)

β

^{208}Tl (3 min)

β

^{208}Pb
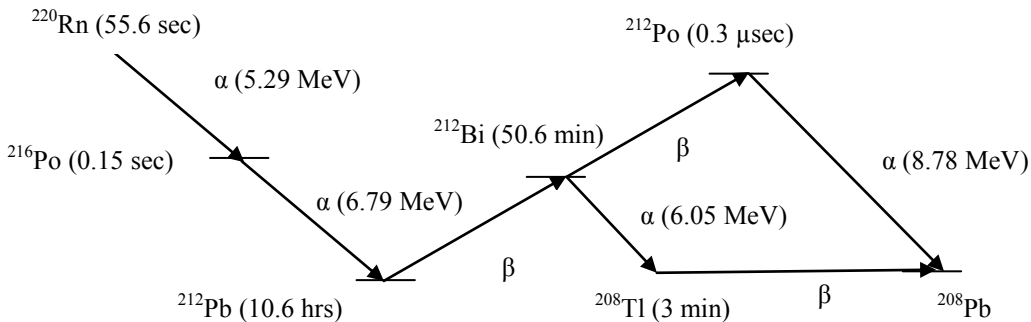
Fig. 3.6b Thoron Decay Chain

When the radon and thoron daughters, deposited on the surface of the detector, decay, they emit alpha particles of characteristic energy directly into the solid state detector. The detector produces an electrical signal. Electronic circuits amplify and condition the signal, then convert it to digital form. The RAD7 's microprocessor picks up the signal and stores it in a special place in its memory according to the energy of the particle. The accumulations of many signals results in a spectrum. The RAD7 divides the spectrum's 0 to 10 MeV energy scale into a series of 200 individual counters, each representing a 0.05 MeV channel.

In Sniff mode, the RAD7 uses only the ^{218}Po signal to determine radon concentration, and the ^{216}Po (thoron mode) to determine thoron concentration, ignoring the subsequent and longer-lived radon

daughters. In this way, the RAD7 achieves fast response to changes in radon concentration, and fast recovery from high concentration, the instrument responds to changes almost instantaneously.

Normal mode is required for continuous monitoring in one location over many hours, the RAD7 uses both radon peaks, ^{218}Po and ^{214}Po to calculate concentration, with double the count rate you increase precision of the measurement.

Soil Gas Sampling and Measurement

To determine the radon concentration in soil gas at a specified depth within the soil the gas must be removed from the soil and delivered to a RAD7 without dilution by outside air. A probe, with a hollow tube and sampling holes near the tip may be inserted into the soil, and gas drawn up the tube, and into the RAD7.

Fig.3.7 Photograph taken during a soil gas measurement.

There are three modes of measurement: one is by grab sample, another by continuous monitoring in standard protocol and the third in THORON mode, with the pump running continuously. In our measurements we used THORON MODE. Thoron protocol uses 5-minute cycles and prints out both the radon and thoron concentrations at the end of every cycle. However, thoron has a short half-life (one minute) so that the pump has to run continuously. The first two cycles should be ignored, while the radon reading equilibrates. Thereafter, there will be a reading every five minutes. Because of the short thoron half life, some estimate of sample acquisition time is needed if the thoron readings are to be properly interpreted. During acquisition, a flow meter may be connected

to the RAD7 outlet. This will show how fast the air is flowing from the sampling point. An estimate of the sample acquisition volume will then allow a calculation of the time delay between sampling and measuring.

Instruments for Radon and Thoron measurements			
Detector Type	**Principle of Operation**	**Measurement Modes**	**Sampling Mode**
E-Perm	Electret Ion Chamber	Radon in air	Passive Air Diffusion
Femto-Tech	Air Ionization Probe	Radon in air	Passive Air Diffusion
RAD7	Electrostatic collection of alpha-emitters with spectral analysis	Radon and thoron in air and soil	Monitor/Sniffer

Table 3.1 Summary of the instruments used in Radon and Thoron measures including some technical specifications.

3.4. Gamma Spectrometry

Gamma and X-ray transfer energy that is stored in their electromagnetic field and the individual wave packets of this radiation are called photons. Apart from the energy carried by gamma and X-ray photons, the main difference between gamma rays and X-ray is their origin, while X-ray are produced by atomic excitations, gamma rays are emitted by transitions from excited states in the nucleus. An X-ray or gamma-ray photon is uncharged and creates no direct ionization or excitation on the material through which it passes. Only the fast electrons created in gamma-ray interactions provide any clue to the nature of the incident gamma rays. These electrons have a maximum energy equal to the energy of the incident gamma-ray photons and will slow down and lose their energy in the same manner as any other fast electron such as beta particle. In order to serve as a gamma-ray spectrometer a detector must carry out two distinct functions:

a) act as a conversion medium in which incident gamma rays have a reasonable probability of interacting to yield one or more fast electrons;

b) act as a conventional detector for these secondary electrons.

In gamma spectrometry between the various ways gamma rays can interact in matter, only three interaction mechanisms are significant: photoelectric absorption, Compton scattering and pair productions.

In the present work two different kinds of detector have been used to perform gamma spectrometry. Two Germanium semi-conductor detectors for in laboratory gamma spectrometry and a Sodium Iodide scintillator detector for *in situ* application.

3.4.1 Germanium semi-conductor detectors

The operation of Germanium detectors is briefly described. A large electric field is applied across the Ge-crystal so that it is totally depleted. When a photon interacts in the depleted region of the crystal, electron-hole pairs are created. The number of produced charge pairs is proportional to the energy deposited by the photon. The charge pairs drift to the electrodes of the detector under the influence of the electric field. The drift of charges produces an output pulse with an amplitude proportional to the energy deposited by the photon. Thus, the higher the energy deposited in the detector, the bigger the pulse height. Pulses from the preamplifier are then amplified once more and sorted according to their size by a multichannel analyzer. A spectrum is finally built by binning the pulses into different channels.
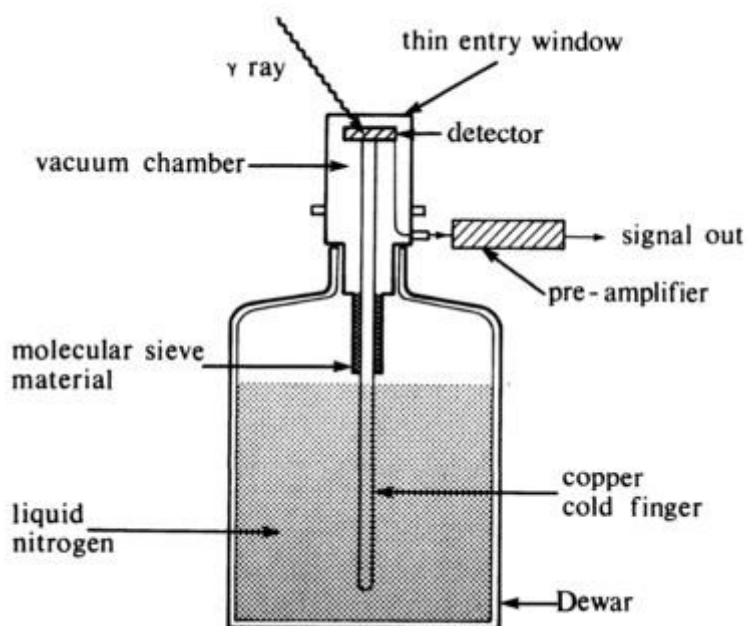

Fig. 3.8 HpGe Detector Schematic

Ge-detectors: a) allow non-destructive measurements, i.e. no radiochemical separations are necessary; b) provide information about both, the energy and rate of photons reaching the detector, i.e. they provide a spectrum, photons with different energy can be recorded simultaneously in the

same spectrum; c) their resolution are much better than other photon detectors such as scintillators, this allows differentiating photons with quite similar energies.

A disadvantage of the semiconductor detectors is the need to keep them cold, generally at liquid nitrogen temperature.

Laboratory Application

In the Laboratory of Environmental Radiochemistry of Bologna University gamma spectrometry measurements are carried out using two low background Hyper Pure Germanium crystal detectors (HPGe), a p-type coaxial and a planar (Fig. 3.9) respectively for higher and lower energy ranges (0-2000 keV and 0-900 keV). The first one has a relative efficiency of 38% and full width at half maximum of 1.8 keV at 1332 keV, whereas the second one has 1500 mm^2 and full width at half maximum of 0.73 keV at 122 keV. Spectra are processed with a specific software package GammaVision-32, (version 6.07, Ortec).

The activity of the sources can then be calculated from net number of counts registered under the photopeak, C, if the source-to-detector efficiency, Eff, is known:

$$A = \frac{C}{Eff * b * t} \qquad (1)$$

where b is the emission probability of the photons and t is the measurement time.

The systems were calibrated for energy and efficiency using a multiple nuclide source in a jar geometry (diameter 56 mm and thickness 10 mm). The calibration of Germanium detectors for laboratory application is a well known and routine operation in the Laboratory of Bologna. Certified reference materials (DH-1a and UTS-3, CANMET) are used to test the analytical quality control.

In the present work mostly materials such as rocks or soils have been analyzed by gamma spectrometry, in order to estimate the activity of natural radionuclides. The samples are crushed into fine grains, gauged with a scientific sieve of 2000 micro-mesh size and put in a jar geometry (diameter, 56 mm and thickness, 10 mm), following the same geometry used in the efficiency calibration (Fig. 3.10).

Our samples being characterized by low radioactivity levels, the counting time have to be increased to decrease the statistical errors of our measurements. Our samples are counted for more than 80000 s, about 1 day.

Fig. 3.9 Photograph of the two Germanium detectors (left-planar; right-coaxial) in the Laboratory of Environmental Radiochemistry of Bologna University

Fig. 3.10 Photograph of a sample crushed and put in the counting geometry.

3.4.2 Sodium Iodide scintillator detector

There are two types of scintillation detectors: solid crystals of inorganic material, and organic-based liquids and plastics. Their modes of excitation differ but the final result is the same. As charged particles pass through the material the energy that they lose is transferred into excitation energy of the inorganic crystals or molecular excitation of the organic molecules. The excitation energy is released in fluorescence, i.e., scintillation. The number of light photons emitted in any one event is proportional to the energy lost by the initial charged particle in that event.

A typical scintillator detector assembly consists of a hermetically sealed scintillation material optically mounted to the Photomultiplier tube (PMT). In a PMT the incident photons strike a photocathode thereby liberating photoelectrons. These photoelectrons are then accelerated towards another electrode at a higher potential where the energetic electrons impinging cause more electrons to be emitted. This electron multiplication process continues along a series of electrodes, each at

higher potential than the previous and, at each, the electron population is increased. The PMT can be considered a photon to electron amplifier. There is a preamplifier to produce a voltage pulse from the electrons collected at the last PMT electrode. By using this common configuration, the detector assembly is a stand-alone device that only requires an external voltage for the PMT and an external power supply for the preamplifier. Such an assembly is often called a *scintillation detector*. A gamma ray penetrating the scintillator material may give up its energy to the scintillator material through photoelectric interactions, Compton scattering and pair production reactions. If all of the incident gamma-ray energy is deposited in the scintillator material, the number of scintillation photons produced is proportional to the incident gamma-ray energy. Thus, by measuring the distribution of pulse sizes or the pulse height distribution produced by the scintillation detector, the energy distribution of the incident gamma rays can be determined. Thus, one of the most important applications of scintillation detectors is gamma-ray spectroscopy.

The most widely applied scintillators include the inorganic alkali halide crystal, of which sodium iodide is the commonest. In fact the crystalline sodium iodide in which a trace of thallium iodide - NaI(Tl) has been added in the melt produce an exceptionally large scintillation light output. It is hygroscopic, so it must be sealed in an air-tight container for normal use, it operates at room temperature. It is accepted as the standard scintillation material for routine gamma-ray spectrometry. NaI(Tl) detectors often have a higher efficiency for high energy gamma rays than germanium detectors, but a much poorer energy resolution. Sodium iodide (NaI) have limited abilities to resolve the gamma lines while high Purity Germanium (HPGe) has high resolution ability. Every radionuclide of concern in homeland security naturally emits a unique set of one or more gamma ray energies from which it can be uniquely identified. These energies are measured in units of electron volts (eV) or kiloelectron volts (keV) and most are found within the range of 30 KeV to 3000 KeV. They are not however uniformly spread across this range. Many are tightly spaced with only a few KeV or less between them. To make identifications accurately, one needs to be able to measure these energies to approximately 1/10th of 1 percent. HPGe detectors can provide this level of accuracy while NaI detectors provide only about 6 parts in 100. This problem is obvious when you look at the comparable spectra produced by NaI and HPGe detectors.The strong difference in the energy resolution between Na(Tl) and HpGe spectrometers is shown in Fig. 3.11.
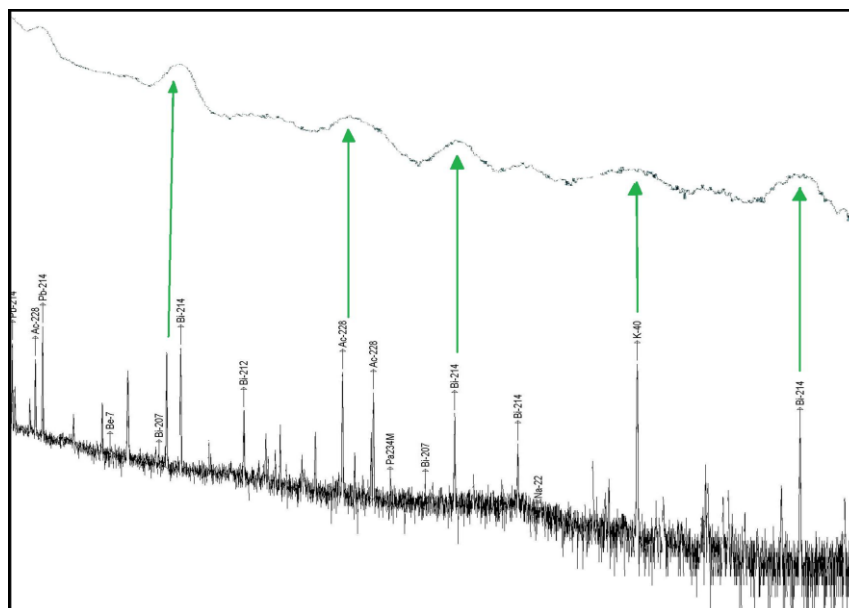
Fig. 3.11 Comparison of the energy resolution of HpGe and NaI(Tl) detector. The gamma ray source is a sample rock from Vulsini Volcanic District.

	Costs	Efficiency	Resolution	Acquisition Time	Applications
NaI	Low	High	Low	900 s	In situ
HpGe	High	Low	High	80000 s	In laboratory

Tab. 3.2 Comparison between NaI and HpGe detectors

In situ application

The term "*in situ* gamma-ray spectrometry" implies that a spectrum of the ambient gamma-ray flux would be collected at the site and analyzed to identify and quantify the radionuclides present. In fact the term in situ from Latin translates to "in the original place" (Miller and Shebell, 1993).

The power in the techniques of *in situ* gamma spectrometry lies in the fact that it gives a rapid identification of radionuclides in the environment. The techniques of *in situ* spectrometry had its origins during the time of atmospheric nuclear weapons testing and has been largely used during the Chernobyl accident. Applications of *in situ* gamma spectrometry in which our research is more interested are: measurements of natural radioactivity in the ground and in indoor building materials (Nucciatelli, 2008).

In comparison to taking samples of rock or soil from the field to analyze in a standard laboratory system, *in situ* technique is much faster and in much more economical. It is the most suitable method for rapid assessment of radiation exposure and identification of radionuclides. Moreover

indoor utilization of γ-spectrometry can be very interesting, providing information on building materials that in general cannot be sampled.

In the Laboratory of Environmental Radiochemistry of Bologna University a 75x75 mm thallium-activated sodium iodide NaI(Tl) scintillator detector, model 905-4 (Ortec) have been used to perform *in situ* gamma-spectrometry. The photomultiplier tube base used is **digiBASE (Ortec)** coupled with a Samsung netbook 12", in which the software Scintivision MCA (Ortec) is installed. The resolution is 46 keV at the ^{137}Cs peak (661 keV).

Calibration methods for *in situ* measurement with NaI(Tl) detector, have been developed and presented to perform *in situ* gamma spectrometry using three different configurations, NaI detector placed:

   a) one meter above the ground
   b) directly on the ground
   c) directly on the building materials for their characterization *in situ*.

Two different calibration methods have been applied based on:

   1. the use of calibration sources;
   2. Monte Carlo method.

3.5 Calibration using point sources: NaI placed one meter above the ground

The first approach to the calibration of the NaI detector for field spectrometry has been developed with detector at a height of 1 m according to Beck et al. (Beck et al., 1972).

The number of counts per second, N_f obtained under the photopeak due to a particular γ-energy, E, is related to the soil radioactivity concentration A (Bq/kg) of the radionuclide producing the peak according to the equation:

$$A = N_f \left[\left(\frac{N_0}{\Phi} \right) \cdot \left(\frac{N_f}{N_0} \right) \cdot \left(\frac{\Phi}{A} \right) \right]^{-1} \quad (2)$$

where:

$\frac{N_0}{\Phi}$ = the photopeak count rate per unit flux for a parallel beam of photons of energy E incident normally at the detector face;

$\frac{N_f}{N_o}$ = the correction factor for the detector response at γ-energy E to account for the fact that the flux from an extended source in the environment is not normal to the detector face but distributed across some range of angles;

$\frac{\Phi}{A}$ = the gamma flux per unit activity concentrations of the soil arriving at the detector unscattered (Tab. 3.3).

Parent Isotope	E_γ (keV)	ϕ/I $\left(\frac{\gamma' s/cm^2 -s}{\mu R/h}\right)$	Parent Isotope	E_γ (keV)	ϕ/I $\left(\frac{\gamma' s/cm^2 -s}{\mu R/h}\right)$
Uranium Series, I = 1.82 $\frac{\mu R/h}{pCi/g}$			Thorium Series, I = 2.82 $\frac{\mu R/h}{pCi/g}$		
^{226}Ra	186	2.52 (-3)	^{228}Ac	129	1.03 (-3)
^{214}Pb	242	5.71 (-3)		210	2.06 (-3)
	295	1.60 (-2)	^{212}Pb	239	2.57 (-2)
	352	3.30 (-2)	^{224}Ru	241	
^{214}Bi	609	5.18 (-2) } .0537	^{228}Ac	270	
	666	1.86 (-3)	^{208}Tl	277 }	3.62 (-3)
	768	6.43 (-3)	^{228}Ac	282	
	934	4.45 (-3)	^{212}Pb	301	1.96 (-3)
	1120	2.31 (-2)	^{228}Ac	338	7.73 (-3)
	1238	9.45 (-3)	Mixed	328-340	1.03 (-2)
	1378	8.19 (-3)	^{228}Ac	463	3.26 (-3)
	1401-08	6.87 (-3)	^{208}Tl	510	6.84 (-3)
	1510	3.91 (-3)	^{228}Tl	583	2.27 (-2)
	1730	5.60 (-3)	^{212}Bi, ^{228}Ac	727	6.60 (-3)
	1765	2.96 (-2) } .0395	^{228}Ac	755	9.57 (-4)
	1845	4.35 (-3)		772	1.45 (-3)
	2205	1.07 (-2)		795	4.25 (-3)
	2448	3.66 (-3)		830+835+840	3.33 (-3)
			^{208}Tl	860	4.18 (-3)
			^{228}Ac	911	2.68 (-2)
Potassium, I = 0.179 $\frac{\mu R/h}{pCi/g}$				965+969	2.17 (-2)
				1588	4.36 (-3)
^{40}K	1464	0.203	^{208}Tl	2615	5.92 (-2)

Table 3.3 Ratio of gamma-ray flux density to exposure rate from natural emitters in the soil (Beck, 1972).

The term Φ/A is characteristic of the source distribution in the soil and γ-energies. These terms can be obtained from earlier reported works (Beck et al., 1972; Miller and Shebell, 1993).

The hypothesis of normal incidence, N_f/N_o equal to 1, was made on the basis of literature data (Beck, 1972; Miller and Shebell, 1993; Jibiri, 2005). The possible error that can be made with the hypothesis of normal incidence can be accept in the measurements of the three radionuclides, ^{238}U, ^{232}Th and ^{40}K.

The factor N_o/Φ represents the response of the detector to photons at normal incidence. Its value at a particular γ energy was determined using three standard point sources of known strength at distance of 1 m from the detector face (Tab. 3.4).

Point Source	Activity (t_0) (Bq)	t_0	t_1	E_γ [keV]
^{133}Ba	1,0656 x 10^7	22/02/1979	12/05/2009	81 ; 356
^{60}Co	1,9080 x 10^5	26/05/1995	12/05/2009	1173 ; 1332
^{137}Cs	7,6960 x 10^6	28/03/1979	12/05/2009	662

Table 3.4 Standard point sources, γ-energies, their initial activity (t_0), data of spectra acquisition for calibration.

The sources were chosen because they span a wide energies range: 81-1332 keV.

The flux $\Phi_0(E)$ at the detector for a γ ray point sources was determined using the following expression:

$$\Phi_0(E) = \frac{A \times y}{4\pi R^2} \quad (3)$$

where A is the activity, y is the γ-yield for the specific energy and R is the source-detector distance (1 m). In order to account for attenuation effects due to air the flux $\Phi_0(E)$ has been corrected. For air attenuation, the following expression has been used:

$$\Phi_{00}(E) = \Phi_0(E) \exp(-\sigma \cdot R \cdot \rho) \quad (4)$$

where σ is the mass attenuation coefficient for air at a particular energy, R is the source detector distance (1 m) and ρ the density of air (0.0012 g/cm^3).

The experimental values of N_o/Φ at the energies in table 3.4 have been calculated by the spectra collected using the three sources. From these experimental data the best fitting was extrapolated, estimating N_o/Φ in the energy working range.

The curve obtained has the following expression:

$$\frac{N_o}{\varphi} = (0.029 + 6.26 * 10^{-8} * E_\gamma^2)^{-1} \quad (5)$$

and $r^2 = 0.981$.

3.5.1 Validation of calibration curve

In situ measurements using NaI detector, placed one meter above the ground, have been taken out in the Vulsini Volcanic District (Central Italy) (Fig. 3.12).

Fig. 3.12 Photograph of NaI detector placed one meter above the ground (sample V11).

The concentrations of U, Th and K using the NaI detector and the calibration approach described before have been compared with the concentration obtained from a sample of soil taken in the same area, and then analyzed using HPGe detectors in the laboratory. Data are reported in Table 3.5.

		ppm U	ppm Th	% K
V01	Ge	6.44 ± 1.01	31.08 ± 1.97	1.89 ± 0.14
	NaI	7.47 ± 1.75	43.65 ± 2.86	2.80 ± 0.09
V11	Ge	10.79 ± 1.31	48.72 ± 2.92	7.02 ± 0.41
	NaI	11.87 ± 2.44	63.56 ± 3.89	4.45 ± 0.13

Table 3.5 Comparison between concentrations from in situ measurement at 1 m above the ground and in laboratory measures.

There is acceptable agreement between data collected *in situ* using the NaI detector and those obtained on the HpGe detectors in the laboratory; the calculated calibration curve is an appropriate instrument for the use of NaI detector placed one meter above the ground. Even if the difference between the values obtained with the two detectors is relatively high (about 20% in some cases) the results could be considered good because of various factors. If *in situ* the area is not heterogeneous, the material sampled for laboratory analysis (HpGe) could not be completely representative of that area.

3.6. MCNP calibration for *in situ* application: NaI placed on the ground

For *in situ* gamma spectrometry to estimate natural radioactivity (^{40}K, ^{238}U and ^{232}Th) NaI detectors are usually calibrated by means of standard spectra acquired at three concrete pads enriched in ^{40}K, ^{238}U and ^{232}Th. These calibrations pads have a cost and may deteriorate over the years (Chiozzi, 2000).

The work described in this paragraph has the aim to use Monte Carlo–based calibration for in situ gamma spectrometry using NaI detector without the use of calibration pads.

The NaI detector is assumed directly placed on the ground. It has been assumed that: a) only natural radioactivity is present in the ground and b) these radionuclides are homogeneously distributed in it.

3.6.1. MCNP code

The MCNP4 Code (Shultis *et al.*,2004) used in the present work, has been developed and maintained by Los Alamos National Laboratory. It is the internationally recognized code for analyzing the transport of neutrons and gamma rays (hence NP for *neutral particles*) by the *Monte Carlo* method (hence MC). The code deals with transport of neutrons, gamma rays, and coupled transport, i.e., transport of secondary gamma rays resulting from neutron interactions. The MCNP code can also treat the transport of electrons, both primary source electrons and secondary electrons created in gamma-ray interactions.

3.6.2. Geometry of the NaI detector

The schematic representation of our detector is given in figure 12. The NaI(Tl) crystal has dimensions 75 x 75 mm, it is enclosed in a single integral unit with a photomultiplier tube. The aluminum cylinder that houses the crystal and the photomultiplier has a thickness of 0.05 cm. A thickness of glass of 0.5 cm is considered between the crystal and the photomultiplier: it is the sum of the thickness of the optical window and the glass that is on the top of the crystal (fig. 3.13).

The thickness of air between the aluminum and the crystal, the aluminum and the photomultiplier is 0.25 cm on the sides and 0.2 cm on the top and bottom. The dimensions of the integral unit housed in the aluminum cylinder are: 8.2 cm of diameter in the crystal part and 5.8 cm in the photomultiplier part, 22.35 cm of length. The photomultiplier tube base used is **digiBASE (Ortec)** with dimensions: 6.3 cm of diameter and 8.0 cm of length. Its density is given from the constructor and it is assumed by us to be entirely made of polystyrene. The input file is reported in Appendix I.
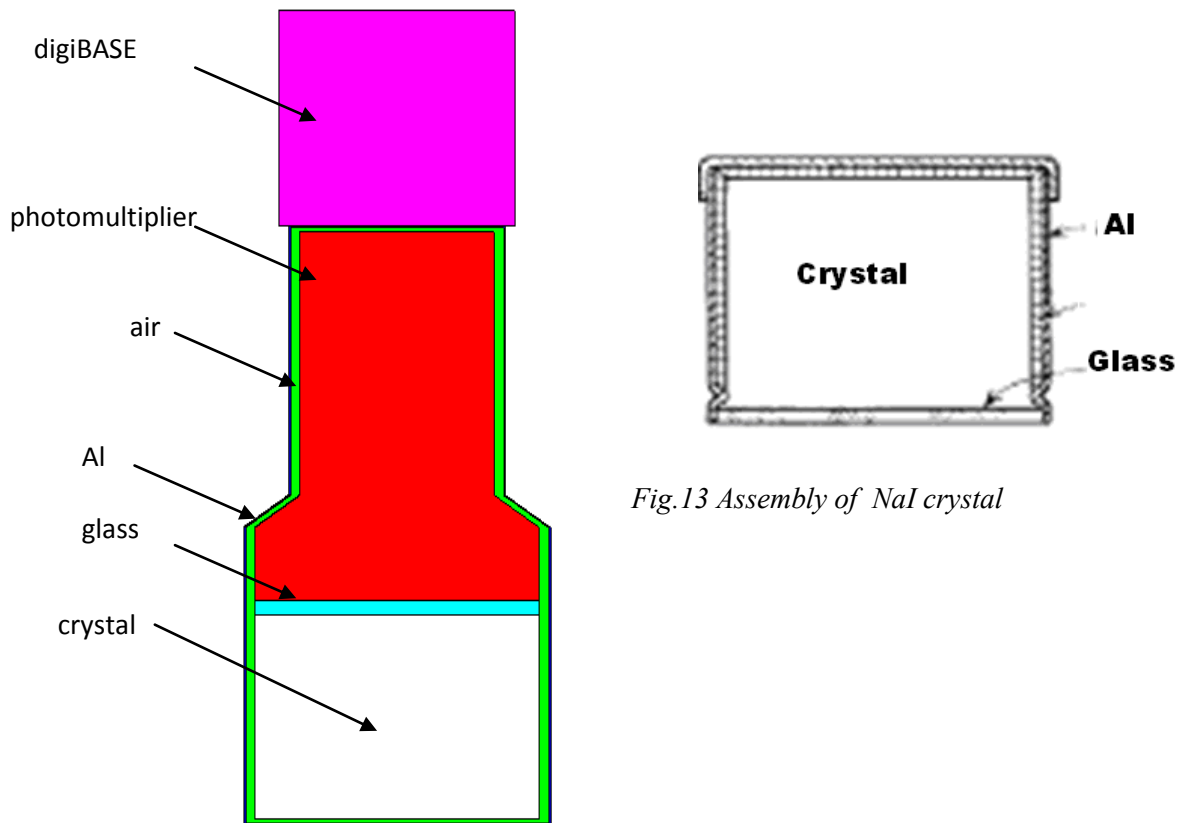
Fig.13 Assembly of NaI crystal

Fig. 3.13 Schematic structure of NaI detector

3.6.3 Definition of source data

In the first step source matrix data have to be studied. In particular you have to estimate the maximum volume (in which natural γ-emitters are homogeneously distributed) from which you can have contribution of radiations in the detector. As said before natural radioactivity in an uncontaminated environment natural gamma-emitters is due mainly to the primordial radionuclides, ^{238}U and ^{232}Th with their progenies and ^{40}K.

Composition and density of geological formation

For our volume the density and the composition of the geological formation have to be fixed.

Two different geological formations are considered: a soil and a rock. It is considered a soil (Fe3714) coming from Ferrara area (Po Plain, Italy) and a volcanic rock (V01), from the Vulsini District (North Latium, Italy). Both are considered to have homogenous compositions. The elemental composition of mineral soil and rock is carried out using X-ray fluorescence (XRF) technique using a Philips PW1480 WD-XRF (Wave Dispersion X Ray Fluorescence). The results

are shown in the table 3.6. A density of 1.3 g/cm^3 for the soil and of 2.0 g/cm^3 for the rock have been assumed.

	SiO$_2$	TiO$_2$	Al$_2$O$_3$	Fe$_2$O$_3$	MnO	MgO	CaO	Na$_2$O	K$_2$O	P$_2$O$_5$	LOI
Soil	45.28	0.58	14.94	5.6	0.15	4.13	9.01	0.88	2.32	0.15	16.96
Rock	46.31	0.7	15.72	6.6	0.16	4.06	7.12	0.85	2.83	0.52	15.13

Table 3.6 Major elements (in wt %) from X-ray fluorescence.

Estimation of the volume

To estimate the *maximum depth,* from which the detector samples the photon flux, a volume of soil or rock, in which a mono-energetic isotropic volumetric source exists (γ with energy 2.614 MeV), has been considered. The energy photon of ^{208}Tl (2.614 MeV) is chosen because it is the highest between the natural gamma emissions. In this phase of study only the crystal NaI and the can of Al around it have been taken into account, the photomultiplier and the DigiBASE have been neglected. The considered volume is a cylinder of 1m of radius in which we increase the height (Fig. 3.14).
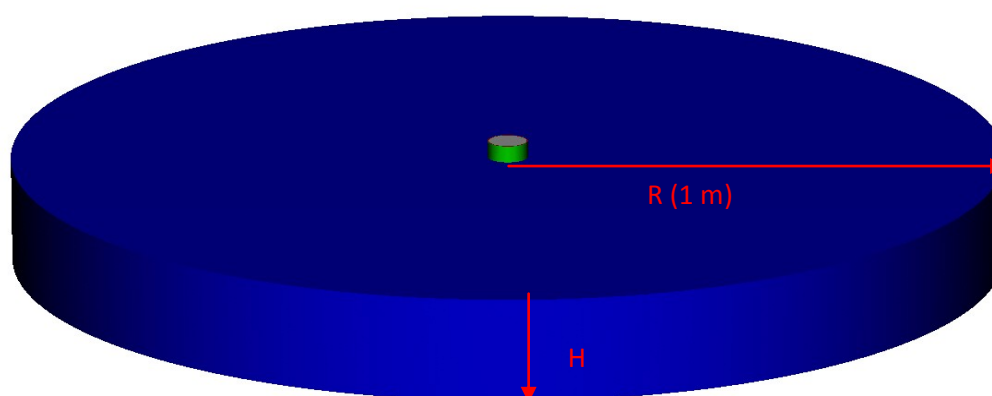

Fig. 3.14 Simplified detector above the volume of soil/rock in which the source is located.

The number of source particle histories per cubic meter has been taken constant (NPS/m^3 ~ 3x10^6). The total counting efficiency of the energy spectrum has been calculated, considering this value weighted on the thickness of cylinder (Tab. 3.7).

Soil				Rock			
Height (cm)	Total	% increase	cumulative	Height (cm)	Total	% increase	cumulative
10	2.31E-02	36.20%	0.44	5	1.24E-02	39.03%	0.35
20	3.62E-02	23.83%	0.69	10	2.03E-02	29.62%	0.58
40	4.75E-02	6.85%	0.90	20	2.88E-02	10.67%	0.83
60	5.10E-02	1.37%	0.97	30	3.23E-02	4.81%	0.92
70	5.17E-02	0.85%	0.98	40	3.39E-02	1.55%	0.97
80	5.21E-02	0.55%	0.99	50	3.44E-02	0.97%	0.99
90	5.24E-02	0.23%	1.00	60	3.48E-02	0.37%	1.00
100	5.25E-02		1.00	70	3.49E-02		1.00

Table 3.7 Total efficiency value varying the height, increase between two consecutive values and cumulative value.

When the increase of total counting efficiency between the volumes with thickness H_{i+1} and with H_i is less than 1%, the thickness H_i has been assumed as the maximum thickness from which you can have contribution of radiation in the detector.

Choosing therefore the 1% increase between two different values of thickness, for soil you can fix the maximum depth can be assessed at **70 cm**, and for rock at **50 cm**.

It can be seen that the 60% of the contribution is given in the first 15 cm for the soil and 10 cm for the rock. This difference is due more to the value of density that to the different composition between soil and rock.

To estimate the *maximum radius,* as above, a volume of soil or rock, in which a mono-energetic isotropic volumetric source exists (γ: 2.62 MeV), has been used. The volume considered is a cylinder with fixed height, same as the corresponding maximum thickness, explained above, in which the radius is increased (Fig. 3.15). Starting from a radius of 100 cm we increase it by steps of 25 cm. When the increase of total counting efficiency between the volumes with radius R_{i+1} and R_i is less than 1%, the radius R_i and the thickness are taken as the dimensions of the volume from which one can have contribution of radiations in the detector (Tab. 3.8).
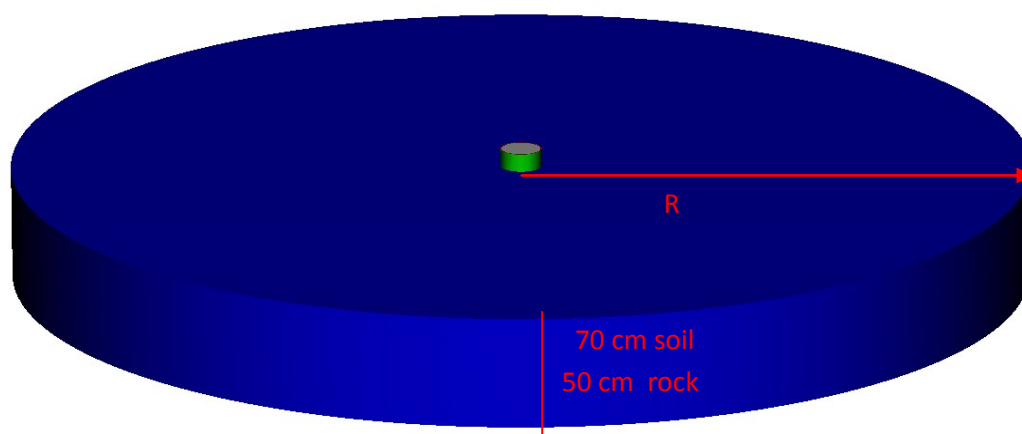
Fig. 3.15 Simplified detector above the volume of soil/rock in which the source is located.

Soil (thickness=70 cm)				Rock (thickness=50 cm)			
Radius (cm)	Total	% increase	Cumulative	Radius (cm)	Total	% increase	Cumulative
100	7.38	1.75	0.959	100	6.89	1.95	0.976
125	7.51	1.40	0.976	125	6.97	1.04	0.988
150	7.62	0.66	0.990	150	7.03	0.47	0.995
175	7.67	0.32	0.997	175	7.04	0.21	0.998
200	7.69		1.000	200	7.06		1.000

Table. 3.8 Total counting efficiency varying the radius, increase between two consecutive values and cumulative value of total contribution.

We can fix the maximum radius at 150 cm for the soil and at 125 cm for the rock.

The volume of the cylinder, with dimensions summed in table 3.9, represents the effective volume of soil/rock that the NaI detector, placed on the ground, samples.

	Soil	Rock
Radius (cm)	150	125
Thickness (cm)	70	50

Table 3.9 Summary of the dimensions of the cylinder assumed as maximum volume.

3.6.4 Calibration Procedure

As said in the previous paragraphs and chapters, in the study of natural radioactivity of soil/ rock usually ^{238}U, ^{232}Th and ^{40}K are investigated. In *in situ* measurements usually the determination of

uranium and thorium activity are based on measurements of γ radiation from the decay of ^{214}Bi (1.76 MeV) in the ^{238}U decay series and from ^{208}Tl (2.62 MeV) in the ^{232}Th series. The primary decay of potassium ^{40}K (1.46 MeV) is directly measured. For the determination of these elements, three energy windows, called regions of interest (ROI 1, ROI 2 and ROI 3), are investigated. Table 10 reports ROI widths utilized in general for data processing.

	Radionuclides	Main peak energy (Mev)	Window width (MeV)
ROI 1	^{40}K	1.46	0.20
ROI 2	^{214}Bi	1.76	0.24
ROI 3	^{208}Tl	2.62	0.30

Table 3.10 γ-ray spectrometry energy windows.

As discussed already portable instruments are usually calibrated by means of standard spectra acquired at three concrete pads enriched in K, U and Th. These sources are cylindrical, 2-3 m in diameter and 0.3-0.5 m thick. Practically, the calibration procedure consists of measuring the net count rate of each ROI at each pad. However, the calibration pads have finite dimensions, and furthermore, even though the instrument is set at a few centimeters from the surface, in such conditions the count rates are lower than those expected for a 2π infinite geometry (Chiozzi, 2000). Our goal is to have an accurate calibrations using Monte Carlo methods, without the use of the calibration pads. The first positive aspect of these approach is connected with the spatial response of the detector. In the Monte Carlo approach you can calibrate using the maximum volume of soil-rock from which photons can reach the detector. So you are closer to the real condition.

Considering:

- the complete detector, with the photomultiplier and its tube base DigiBase;
- the device placed on the ground;
- the rock (or soil) volume is the cylinder with dimensions estimated using the procedure explained above.

We simulated three different kinds of rock in which respectively there is:

a) a mono-energetic isotropic volumetric source: ^{40}K (1.46 Mev)

b) a mono-energetic isotropic volumetric source: ^{208}Tl (2.64 Mev)

c) isotopic volumetric source with 6 discrete energies: ^{214}Bi.

For the last situation, ^{214}Bi, the estimation of the frequency of each energy has been done normalizing the values of the probability of emission considering the energy that we decided to take into account (Tab.3.11).

Energy (keV)	1509.217	1729.64	1764	1847.42	2204.071	2447.673
Frequency	0.07	0.10	0.53	0.07	0.17	0.06

Table 3.11 Energies and frequency of the most important γ emissions of ^{214}Bi.

In figure 3.16 the three spectra for the three types of rock (1-2-3) from Monte Carlo simulations are shown. The counting efficiency is estimated in each ROI and the results are shown in table 3.12 for rock and table 3.13 for soil.
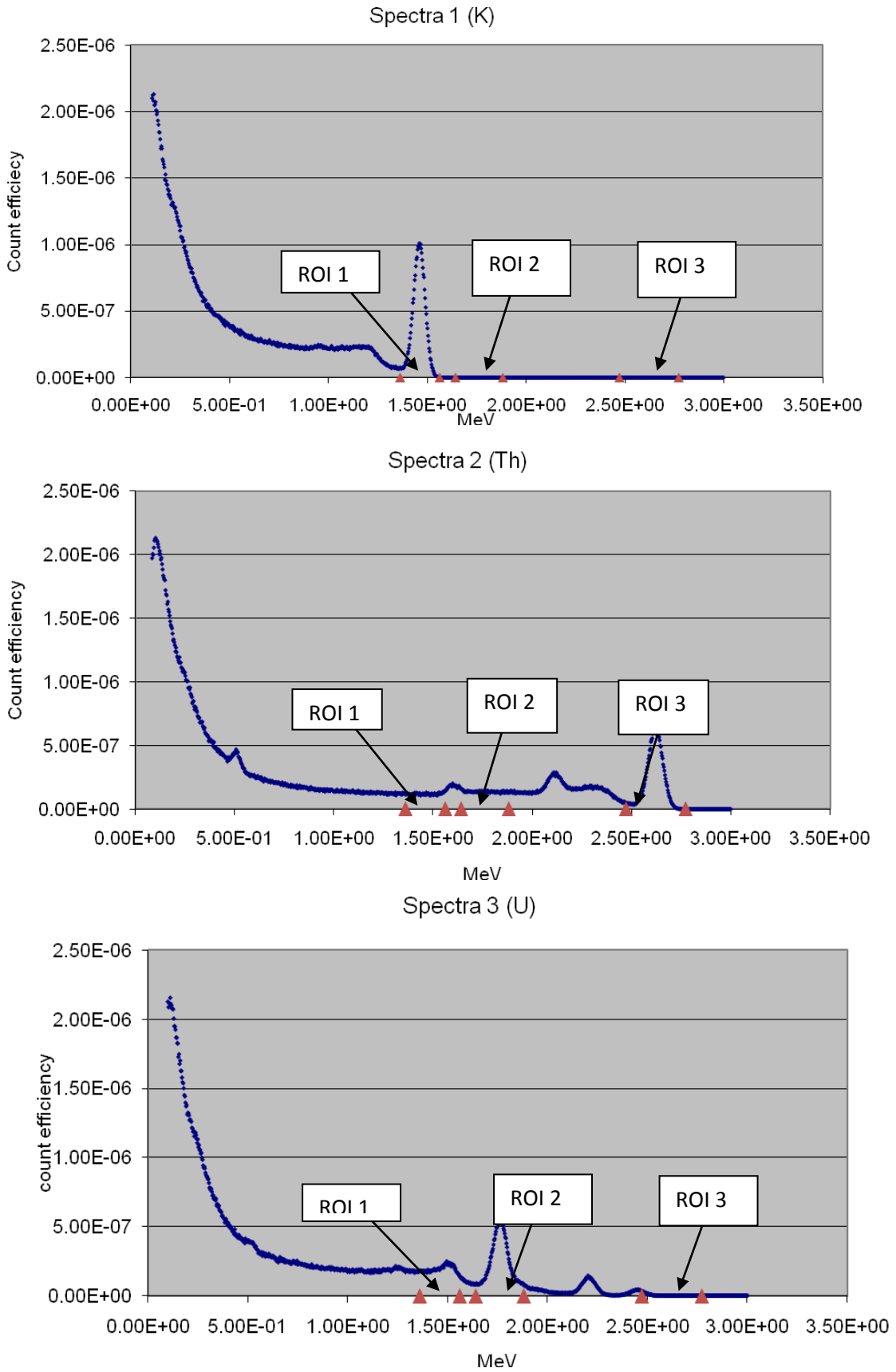
Fig. 3.16 Efficiency energy spectrum of the three kinds of soil respectively 1,2,3.

Rock	1.(K)	2.(Th)	3.(U)
ROI 1	2.60E-05	8.73E-06	2.6E-05
ROI 3	0.00E+00	2.07E-05	7.39E-07
ROI 2	0.00E+00	1.18E-05	3.84E-05

*Tab. 3.12 **Cps / γ** emitted in each ROI for the three different kinds of rock.*

Soil	1.(K)	2.(Th)	3.(U)
ROI 1	1.97E-05	6.67E-06	1.99E-05
ROI 3	0±0	1.57E-05	5.62E-07
ROI 2	0±0	8.92E-06	2.91E-05

*Tab. 3.13 **Cps / γ** emitted in each ROI for the three different kinds of soil.*

The counting efficiency represents the counts per second (cps) for each γ emitted. In fact the efficiency in MCNP represents the efficiency of a single photon, so considering the probability of emission and the weight of the soil that we are sampling, the specific activity in each standard rock is shown in table 3.14 and in each standard soil in table 3.15.

Rock	1.(K)	2.(Th)	3.(U)
K	1.91E-03	0	0
Th	0	5.68E-04	0
U	0	0	2.53E-03

Tab. 3.14 Specific Activity (Bq/kg) of the K, Th and U in the three different rocks.

Soil	1.(K)	2.(Th)	3.(U)
K	1.46E-03	0	0
Th	0	4.34E-04	0
U	0	0	1.93E-03

Tab. 3.15 Specific Activity (Bq/kg) of the K, Th and U in the three different soils.

Applying the following expression:

$$E_{ij} = \sum_{n=1}^{3} \alpha_{in} A_{nj} \qquad \begin{array}{ll} \forall i: & i = 1,2,3 \\ \forall j: & j = 1,2,3 \end{array} \qquad (6)$$

where: E_{ij} is the cps / γ emitted in the ith ROI in rock j

A_{nj} is the specific activity of the nuclide n (n=1,2 ,3 for K, Th, U) in the rock j,

α_{in} is the instrument sensitivity to a unit concentration of a radioelement n in a given ROI i.

The matrix of instrument sensitivities, $\boldsymbol{\alpha_{in}}$, has been calculated; named Rc (Rock Contact) for rock and Sc (Soil contact) for soil.

$$\text{Rc} \quad \begin{pmatrix} 0.013592 & 0.015355 & 0.010291 \\ 0 & 0.036242 & 2.91\text{E-}04 \\ 0 & 0.020756 & 0.015152 \end{pmatrix}$$

$$\text{Sc} \quad \begin{pmatrix} 0.01353 & 0.015378 & 0.010291 \\ 0 & 0.036242 & 2.91\text{E-}04 \\ 0 & 0.020559 & 0.015071 \end{pmatrix}$$

According as the soil has a high density (rock) or low density (soil), using the inverse of the calibration matrix and the number of counts per second in the ith ROI (E), the specific activity in (Bq/kg) of the three nuclides, K, Th and U can be estimated.

$$A= \text{Inv(Rc)} \cdot \text{(E)} \qquad (7) \qquad\qquad A= \text{Inv(Sc)} \cdot \text{(E)} \qquad (8)$$

We easy can calculate the concentration of the tree elements applying these conversion factors (D. C. STROMSWOLD) : $1\%K = 309.7$ *Bq/ kg*

$1ppmU = 12.35$ *Bq/ kg*

$1ppmTh = 4.072$ *Bq/ kg.*

Statistics Produced by MCNP

MCNP produces a wealth of information about a simulation to assess the *precision* (not the accuracy) of the result. While much of the detailed assessment performed by an experienced user depends on careful examination of the many output tables, the initial focus should be on the ten statistical indices calculated by MCNP. In our simulations no one of the 10 statistical tests are failed.

3.6.5 Propagation of errors

The output file in MCNP gives the value of R, called relative error.
Considering this definition :

$$\frac{N_i \pm \sqrt{N_i}}{N} = \varepsilon_i \left(1 \pm \frac{1}{\sqrt{N_i}}\right) = \varepsilon_i + \sigma_{\varepsilon_i} \quad (9)$$

where: N is the total number of particles considered (NPS)

ε_i is the MCNP efficiency in the ith channel energy

$N_i = N * \varepsilon_i$

the R for each ith energy channel is equal to:

$$R_i = \frac{1}{\sqrt{N_i}}$$

so

$$\sigma_{\varepsilon i} = \varepsilon_i \cdot R_i$$

The estimated relative error can be used to form confidence intervals about the estimated efficiency, and to make statements about what the true result is. The Central Limit Theorem states that as N approaches infinity there is a 68% chance that the true result will be in the range $\overline{\varepsilon_i}(1 \pm R)$ and a 95% chance in the range $\overline{\varepsilon_i}(1 \pm 2R)$. It is extremely important to note that these confidence statements refer only to the precision of the Monte Carlo calculation itself and not to the accuracy of the result compared to the true physical value.

To estimate the error σ in the ith ROI (energy window table 8) this relation is used:

$$\varepsilon_{ROI} \left(1 \pm \frac{1}{\sqrt{\sum \varepsilon_i \cdot N}}\right) = \varepsilon_{ROI} \pm \sigma_{\varepsilon_{ROI}} \quad (10)$$

The uncertainties for the *i*th ROI for the tree different kinds of rock/soil are calculated and reported in table 3.16 for rock and table 3.17 for soil.

Rock	1.(K) cps/γ ±σ	2.(Th) cps/γ ±σ	3.(U) cps/γ ±σ
ROI 1	2.6E-05±7.21E-08	8.73E-06±4.18E-08	2.6E-05±9.9E-08
ROI 3	0±0	2.07E-05±6.43E-08	7.39E-07±1.67E-08
ROI 2	0±0	1.18E-05±4.86E-08	3.84E-05±1.2E-07

*Table 3.16 **Cps / γ** emitted and their uncertainties in each ROI for the three different kinds of rock.*

Soil	1.(K) cps/γ ±σ	2.(Th) cps/γ ±σ	3.(U) cps/γ ±σ
ROI 1	1.97E-05±6.28E-08	6.67E-06±3.65E-08	1.99E-05±8.67E-08
ROI 3	0±0	1.57E-05±5.61E-08	5.62E-07±1.46E-08
ROI 2	0±0	8.92E-06±4.22E-08	2.91E-05±1.05E-07

*Table 3.17 **Cps / γ** emitted and their uncertainties in each ROI for the three different kinds of soil.*

The propagation of error, that is the effect of the uncertainties in variables on the uncertainty of a function based on them, have been studied (Bevington, 1969).

Given a formula $y = f(x)$ with an absolute error in x of dx, the absolute error is dy. The relative error is dy / y. If $x = f(u, v...)$, u and v are uncorrelated (covariance = 0) the sample variance is given by:

$$s_x^2 = s_u^2 \left(\frac{\partial x}{\partial u} \right)^2 + s_v^2 \left(\frac{\partial x}{\partial v} \right)^2 \tag{11}$$

where

$$s_u^2 = \frac{1}{N-1} \sum_{i=1}^{N} (u_i - \bar{u})^2 \tag{12}$$

$$s_v^2 = \frac{1}{N-1} \sum_{i=1}^{N} (v_i - \bar{v})^2 \tag{13}$$

The matrix Rc and Sc with errors are respectively Rc' and Sc'.

Rc'
$$\begin{pmatrix} 0.013592\pm3.77\text{E-}05 & 0.015355\pm7.35\text{E-}05 & 0.010259\pm3.91\text{E-}05 \\ 0\pm0 & 0.036393\pm0.000113 & 0.000292\pm6.59\text{E-}06 \\ 0\pm0 & 0.020756\pm8.55\text{E-}05 & 0.015152\pm4.75\text{E-}05 \end{pmatrix}$$

Sc'
$$\begin{pmatrix} 0.01353\pm4.31\text{E-}5 & 0.015378\pm8.42\text{E-}05 & 0.010291\pm4.48\text{E-}05 \\ 0\pm0 & 0.036242\pm0.000129 & 2.91\text{E-}04\pm7.53\text{E-}06 \\ 0\pm0 & 0.020559\pm9.74\text{E-}05 & 0.015071\pm5.42\text{E-}05 \end{pmatrix}$$

3.6.6 Validation of calibration method

Five spectra (A, B, C, D and E) are acquired at different sites. The spectra A, B and C have been acquired at two concrete pads enriched respectively in U and Th and the third with low radioactive material to measure the background counts rate (Table 3.18).

These standard calibration pads are located in the Polytechnic Faculty of Mons (Belgium), their diameter is 2 m and the depths are reported in table 3.18.

Pads	Concentration (ppm)	Depth (cm)
A(^{238}U)	36	115
B(^{232}Th)	102	65
C	-	65

Tab. 3.18 Composition and depth of the standard pads

The concentrations of the three radionuclides of interest (table 3.19) are calculated using the net count rates (subtracting the count rate of pad C) and the MCNP calibration matrices.

Pads	Standard concentration (ppm)	*In situ* (MCNP matrix) High density	Relative error (%)	*In situ* (MCNP matrix) Low density	Relative error (%)
A(^{238}U)	36	38.14	5.94	38.35	6.52
B(^{232}Th)	102	95.00	6.86	95.40	6.47

Tab. 3.19 Comparison between the concentration in situ using the matrix for high density soil and the standard concentration.

The relative errors are always less than 10%, very satisfactory results.

The spectra D and C have been acquired at two different kind of clay in Castel San Pietro, Emilia Romagna (Italy). At each sites, soil samples were collected. Aliquots of soil sample were analyzed to evaluate K, U and Th content, using pre-calibrated measurement geometries using a lead-shield HPGe. The values of U, Th and K concentration in the soil using the gamma-spectrometry in laboratory and *in situ* are show in tables 3.20 and 3.21.

Sample/ Site	K(%)		238U (ppm)		232Th (ppm)	
	HPGe	*In situ*	HPGe	*In situ*	HPGe	*In situ*
D	1.56±0.10	1.04±0.05	<1.09	0±0.83	6.71±0.64	7.50±0.41
E	2.10±0.14	1.68±0.06	<1.99	0±0.89	7.16±0.95	7.65±0.48

Tab. 3.20 Comparison between the concentrations from in situ using the matrix for high density (rock) and in laboratory measures.

Sample/ Site	K(%)		238U (ppm)		232Th (ppm)	
	HPGe	*In situ*	HPGe	*In situ*	HPGe	*In situ*
D	1.56±0.10	1.05±0.05	<1.09	0±0.83	6.71±0.64	7.53±0.41
E	2.10±0.14	1.68±0.06	<1.99	0±0.89	7.16±0.95	7.68±0.48

Tab. 3.21 Comparison between the concentrations from in situ using the matrix for low density (soil) and in laboratory measures.

The comparison between the *in situ* and laboratory measurements of clays shows a good agreement, even if there can be noticed a light underestimation of K and overestimation of Th, about U the value are so small that the results can be considered satisfactory.

3.7. Limits of Detectability

The aim of the present work is to quantify the minimum detectable amount (MDA) of activity of ^{238}U, ^{232}Th and ^{40}K for NaI detector for *in situ* measurement, in other words to estimate the smallest signal that can be detected reliably in order to set a "detection limit" for the counting system.

The theory part taken from the Chapter 3- Limits of Detectability of the book Radiation Detection and Measurement (Knoll, 2000).

Let N_T be the number of counts recorded with un unknown sample and N_B be the number of recorded counts when a blank sample is substituted to determine the back-ground level. The net counts resulting from the unknown are then calculated:

$$N_S = N_T - N_B \quad (14)$$

To establish if the sample contains activity, N_S is compared with a Critical Level L_C:

If $N_S < L_C$ the sample does not contain activity

If $N_S > L_C$ the sample contain activity.

In the absence of statistical fluctuation L_C could to set at 0.

In any counting measurement the statistical fluctuations are inevitable, however some positive N_S could be observed even for samples with no activity. One would therefore like to choose a value of L_C that is high enough to minimize the likelihood of such *false positive*, while keeping it low to reduce the possibility of missing real activity when some is actually present (*false negative*).

We assume that the counting time is long enough so that the total number of counts recorded in each of these measurements is large (>30) and N_T and N_B follow Gaussian distributions. The net counts follow also a Gaussian whose mean is the true net number of counts and whose standard deviation can be predicted using:

$$\sigma_{N_S}^2 = \sigma_{N_T}^2 + \sigma_{N_B}^2 \qquad (15)$$

No real activity is present

N_S is 0, under these conditions $\sigma_{N_T} = \sigma_{N_B}$, the standard deviation of the Gaussian distribution for N_S is:

$$\sigma_{N_S} = \sqrt{2\sigma_{N_B}^2} = \sqrt{2}\ \sigma_{N_B} \quad (16)$$

If the only significant fluctuations are from counting statistics then: $\sigma_{N_B} = \sqrt{N_B}$ and $\sigma_{N_S} = \sqrt{2N_B}$. Since no true activity is present any positive indication will be a false positive. We set L_C high enough to ensure that the probability that a particular measurement of N_S exceed L_C is acceptability small. If we consider the mean $\pm 1.645\ \sigma$, considering in this case only the positive part of the distribution, we have the 95% of probability that a random sample will lie below the mean+1.645 σ

setting : $LC = 1.645\ \sigma_{N_S} = 1.645\ \sqrt{2}\ \sigma_{N_B} = 2.326\ \sigma_{N_B}$ (17)

ensure that a false positive probability will be no larger than 5%.

Real activity is present

The MDA of activity is defined the source strength necessary to produce a mean value of N_S that is high enough to reduce the false negative rate to the level of 5%. The N_D represents the minimum value of N_S that permit to reach the criterion of MDA.

$N_D = L_C + 1.645 \, \sigma_{N_D}$ (18)

$N_D \ll N_B$ then $\sigma_{N_D} \cong \sqrt{2} \, \sigma_{N_B}$ and

$N_D = L_c + 1.645\sqrt{2} \, \sigma_{N_B}$

$N_D = L_c + 2.326 \, \sigma_{N_B}$ (19)

using the equation calculated before for Lc

$N_D = 2.326 \, \sigma_{N_B} + 2.326 \, \sigma_{N_B} = 4.653 \, \sigma_{N_B}$ (20)

considering only statistical fluctuations $\sigma_{N_B} = \sqrt{N_B}$.

The assumption that the width of the net distribution of N_S with activity is the same as the width without activity is made. Because of the small real signal these widths are not exactly the same, and a more rigorous derivation is $\sigma_{N_D} \cong \sqrt{(2N_B + N_D)}$ expanding for $N_D \ll N_B$

$$\sigma_{N_D} = \sqrt{2N_B}\left(1 + \frac{N_D}{4N_B}\right)$$

Using the previous approximation

$$\sigma_{N_D} = \sqrt{2N_B}\left(1 + \frac{4.653 \, \sigma_{N_B}}{4N_B}\right)$$ (21)

Assuming all variances are from counting statistics

$\sigma_{N_D} = \sqrt{2} \, \sigma_{N_B} + 1.645$ (22)

from $N_D = L_C + 1.645 \, \sigma_{N_D}$ using the value Lc and σ_{N_D}

$N_D = 4.653 \, \sigma_{N_B} + 2.706$ (23)

This is frequently quoted Currie Equation.

To convert N_D in counts to minimum detectable activity additional factors have to been considered as radiation yield per disintegration (f) and the absolute detection efficiency (ε).

3.7.1 MDA estimation

The background radiation was evaluated collecting spectra using the same configuration for *in situ* measurement: NaI detector positioned directly on the ground.

The site (44° 10' 32.6'' N, 9 °35' 09.4'' E) chosen to collect spectra of background radiation is in Bonassola (SP, Italy). The geology of this area is essentially formed by dunite, serpentinite and gabbro outcrops (Fig. 3.17). These three rock types may be considered virtually free of uranium and thorium (Chiozzi, 2000), and with a negligible amount (less than 0.03%) of potassium. Samples (approx. 2 kg each) of dunite, serpentinite and gabbro were taken in the same place were *in situ* gamma spectrometry measurement were carried out. After collection, the rock samples collected in bulk amounts were crushed into fine grains and sieved at 2000 micro-mesh size. Samples were analyzed by γ-spectrometry with Hyper Pure Germanium crystal detectors (HPGe) in the Laboratory of Radiochemistry of the Bologna University. Secular equilibrium was assumed between ^{214}Bi and ^{238}U and between ^{228}Ac and ^{232}Th.

Fig. 3.17a Photograph of the NaI detector on dunite outcrop.

Fig. 3.17b Photograph of the NaI detector on gabbro outcrop.

The results of gamma spectrometry for the three radionuclides of interest (^{238}U, ^{232}Th, ^{40}K) are reported in the table 3.22 in term of specific activities and concentrations.

	Code	Counting Time (s)	^{238}U (Bq/kg)	^{232}Th (Bq/kg)	^{40}K (Bq/kg)	^{238}U (ppm)	^{232}Th (ppm)	^{40}K (%)
Dunite	**Bon3**	244283	<9.05	<3.51	<25.16	<0.72	<0.86	<0.08
Serpentinite	**Bon4**	86998	<13.91	<5.80	<41.40	<1.10	<1.43	<0.13
Gabbro	**Bon5**	169822	<10.44	<3.67	<28.10	<0.83	<0.90	<0.09

Table 3.22 Specific activities and concentrations of ^{238}U, ^{232}Th and ^{40}K in the three sampled rocks and counting times using HPGe detector.

In situ the detector has been positioned directly on the rock, where it was sure to have rock homogeneity in a cylindrical volume of about 1.5 m of radius and 50 cm height (dimensions estimated above for rock).Three different spectra of more 900 s has been collected on the three different rocks. The counts per second in the ROIs described widely before are reported in table 3.23.

Rock Type	Code	Counting Time (s)	ROI1(cps)	ROI2(cps)	ROI3 (cps)
Dunite	Bon3	903	0.03	0.12	0.07
Serpentinite	Bon4	969	0.12	0.09	0
Gabbro	Bon5	912	0.13	0.02	0.03

Table 3.23 Counting times and counts per second in the ROI's of interest for $^{40}K(1)$, $^{238}U(2)$, $^{232}Th(3)$ in the three spectra collected with NaI.

The results of gamma spectrometry indicate that the dunite rocks are the most suitable to estimate the background radiation. therefore to calculate the detection limits of the instrument.

By adopting the dunite spectrum as background radiation for *in situ* measurement, for a measurement time of 900 s, the minimum detectable amount of activity are :

2.48 Bq/kg for ^{40}K (0.01 % K);

1.34 Bq/kg for ^{232}Th (0.33 ppm ^{232}Th);

2.44 Bq/kg for ^{238}U(0.20 ppm ^{238}U).

3.8 *In situ* Application

The NaI detector for *in situ* measurements has been used to estimate concentrations of ^{238}U, ^{232}Th and ^{40}K in different matrixes. The measures have been carried out placing the instrument directly on the ground/building material and using MCNP calibration matrixes.

In outdoor ambient γ-spectrometry has been carried out in two sites: the beach of the Bolsena Lake and the soil of the Archaeological Excavation of Volsinii (Nord of the Bolsena centre) (figure 3.18).
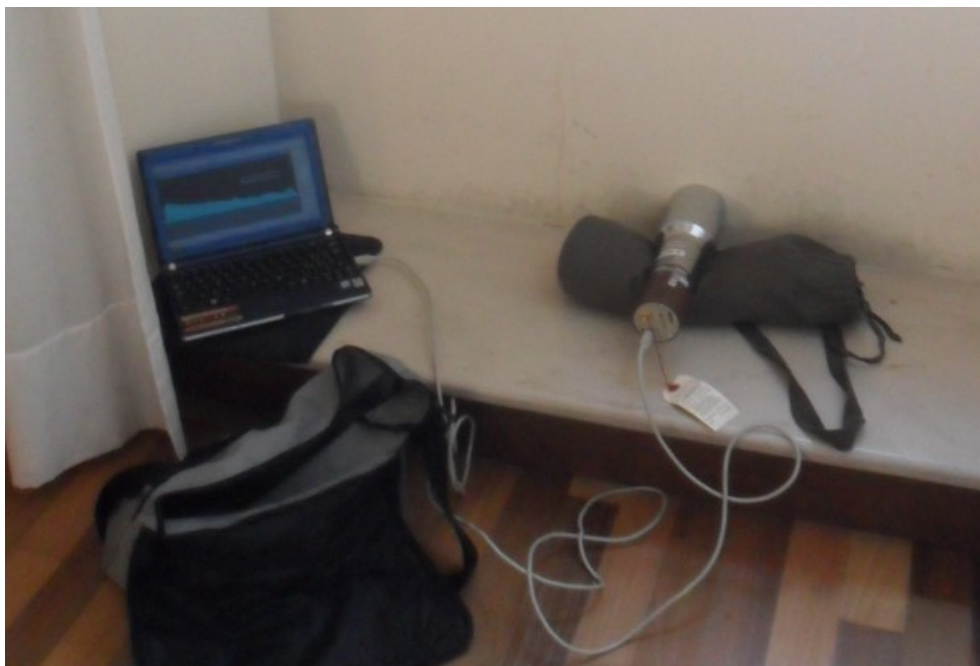

Fig. 3.18 Photograph of NaI detector in the Archaeological Excavation of Volsinii.

Indoor *in situ* γ-spectrometry has been carried out in the Territorial Museum of Lake Bolsena that is in the Fortress of Monaldeschi Cervara (fig. 3.19) and inside a building made of concrete (fig. 3.20).

Fig. 3.19 Photograph of NaI detector used in indoor ambient, in the Fortress of Monaldeschi Cervara (on the top-left), particular of its external wall (on the top- right).

Fig. 3.20 Photograph of NaI detector used indoor ambient in the hotel room.

For outdoor measurements the calibration matrix for soil has been used, while for indoor the calibration matrix for rock (high density). Moreover in indoor applications the assumption that the walls have thickness at least of 50 cm has been done. The walls of the fortress, built until 1451 AD using a mix of local volcanic rocks, have thickness larger than 50 cm.

	K %	^{232}Th (ppm)	^{238}U
Lake Beach	2.71 ± 0.08	30.48 ± 0.92	11.27 ± 1.13
Archaeological Site	1.29 ± 0.06	28.00 ± 0.85	3.20 ± 0.82
Territorial Museum	4.51 ± 0.10	67.37 ± 1.31	10.13 ± 1.31
Building	1.15 ± 0.08	33.29 ± 1.18	1.96 ± 1.26

Table 3.24 Results of in situ γ-spectrometry, concentration of K (%), 238U (ppm) and ^{232}Th (ppm) with errors.

The results show radionuclide contents that are similar to that found by γ-spectrometry in laboratory on the sampled rock and soil, values presented in chapters 4 and 5.

References

Bevington, P.R., *Data Reduction and Error Analysis for the Physical Sciences*, McGraw-Hill Book Company, 336 pp.

Briesmeister,J.F.,1993, *MCNP-4A: A Monte Carlo N-Particle Transport Code*, LA-12625-M, Los Alamos National Laboratory.

Chiozzi, P., Pasquale, V., Verdoya, M., De Felice, P., 2000. *Practical applicability of field γ-ray scintillation spectrometry in geophysical surveys*. Applied Radiation and Isotopes 53, 215–220.

Gilmore G., 2008, *Practical Gamma-Ray Spectrometry*, John Wiley & Sons.387 pp.

Field, R.W., Jenkins, P. and Steck, D., 2011. *Radon Measurement*, <u>Encyclopedia of Environmental Health</u>, Pages 754-767.

Jigiri, N.N, Farai, I.P., 2005, *Application of in-situ gamma-ray spectrometry in the determination of activity concentrations of 40K, 238U and 232Th and mean annual effective dose rate levels in southeastern cities in Nigeria*, Radioprotection 2005, Vol. 40, n° 4, 489-501

KNOLL, G.F., *Radiation Detection and Measurement,* 3rd ed., Wiley, New York, 2000.

McGregor, D.S., 2007. *"Chapter 8, Detection and Measurement of Radiation," in Fundamentals of Nuclear Science and Engineering*, 2nd Ed., by J.K. Shultis and R.E. Faw (CRC Press, Boca Raton, 2007).

Miller K M and Shebell P 1993 *In-situ gamma-ray spectrometry-a tutorial for environmental radiation scientists Report EML-557* (Environmental Measurements Laboratory, US Department of Energy)

Nuccetelli, C., 2008. *In situ gamma spectrometry in environmental research and monitoring*, Applied Radiation and Isotopes 66, 1615-1618.

Suárez, Francisco Javier Hernández. 2002. *Optimization of the Environmental Gamma Spectrometry Using Monte Carlo Methods*, PhD thesis.

RAD ELEC E-PERM, 2008, Sistema per la misura del gas Radon, Manuale d'uso, mi.am s.r.l

RAD7 Radon Detector ,2009, User Manual, Durrige Company Inc.

Shultis, J. K., and R. E. Faw, 2004. *An MCNP Primer*. Rep. Manhattan: Kansas State University.

Chapter 4 - Natural radioactivity in the quaternary Vulsini Volcanic District (Central Italy): evaluation of potential indoor radiological risk[2]

4.1 Introduction

Natural ionizing radiation is considered the largest contributor to the collective effective dose received by the world population (UNSCEAR, 1993; Agnesod, 2005). The human population is continuously exposed to ionizing radiation from several natural sources that can be classified in two broad categories: high-energy cosmic rays incident on the Earth's atmosphere and releasing secondary radiation (cosmic contribution); radioactive nuclides generated during the formation of the Earth and still present in the Earth's crust (terrestrial contribution). Terrestrial radioactivity is mostly provided by ^{238}U, ^{235}U, ^{232}Th radioactive families together with ^{40}K, which is a long lived radioactive isotope of the elemental potassium. In most circumstances ^{222}Rn, produced in the radioactive decay of the ^{238}U progeny, is the major contributor to the total dose. Both the International Agency for Research on Cancer (IARC), an agency of the WHO (World Health Organization), and the US National Toxicology Program, have classified radon as a human carcinogen (http://www.who.int/ionizing_radiation/env/radon/en/index.html). Recent epidemiological indoor studies show that radon in homes causes about 20000 lung cancer deaths every year in the European Union, therefore representing the second cause of lung cancer after smoking (Dubois, 2005).

Radon is a noble gas, released from the solid mineral grains to the filled pores, and subsequent transported through the pores of the material into the atmosphere by two basic mechanisms: molecular diffusion, and advection. In open atmosphere, it is rapidly diluted in a large volume of air and its concentration rarely becomes a problem. But if radon enters a building, the volume of air available for dilution may be much smaller and high concentrations become possible.

Radon hazard is affected by several factors which have been widely studied for many decades (Nazaroff, 1998). One of the most determining factor is the level of specific activity of radon

---

[2] This chapter consists of a paper by Capaccioni,B., Cinelli, G., Mostacci, D, Tositti, L. *Natural radioactivity in the quaternary Vulsini Volcanic District (Central Italy): evaluation of potential indoor radiological risk*. Journal of Volcanology and Geothermal Research, under revision.

precursors in the rock matrix, therefore the local geology and construction habits play a determining role.

Besides the radiation protection issues, investigation of natural radionuclides is of primary importance in the Earth Sciences. Radioactivity is the major heat sources driving the geological evolution of the Earth (Bao, 2007). Radionuclides are widely used in geochronology and cosmochronology, and they can be very efficient markers for various geochemical and petrological processes (Ivanovich, 1992; Lanzo, 2010; Chiozzi, 2002 ; Sato, 1977). Processes of magma genesis and evolution can determine a strong enrichment of natural radionuclides, up to tens of times with respect to the mean crustal concentration. A particularly strong enrichment of radionuclides occurs in the potassic magmas emitted during the quaternary age in the Vulsini Volcanic District, a large volcanic area located between northern Latium and southern Tuscany (Central Italy). In this context, subduction-related metasomatic enrichment of incompatible elements in the mantle source coupled with magma differentiation within the upper crust has given rise to U, Th and K enriched melts.

In central Italy use of volcanic rocks as building material has been reported throughout centuries, from as far back as the Etruscan civilization continuously until present. According to De Rita (2006) the ancient town of Rome has been built mostly with volcanic rocks from the Sabatini volcanic District. Almost every ancient village and town located in the northern part of Latium (Bolsena, Montefiascone, Gradoli, Pitigliano, Sovana etc.) has been built with volcanic rocks pertaining to the Vulsini Volcanic District. Among them, Bolsena is one of the most important, located on the shore of the homonymous lake, along the ancient "Francigena" road (historically connecting the northern Europe with the city of Rome) and with remarkable architectural and archeological features. In this area volcanic stones have been widely used to build walls and graves during the Etruscan period, amphitheater and walls during Roman dominion and private and public buildings through Middle Age and Renaissance. Nowadays, concrete and bricks have largely replaced natural materials.

The extensive use of tuffs as building material is due to their intrinsic properties. In fact tuffs are easy to cut and fit into blocks of almost any shape and size, they are resistant to weathering but, at the same time, with densities lower than most other stones; moreover tuffs are also efficient thermal insulators. All these properties make tuffs a rather attractive building material (Funiciello et al., 2006).

However, alongside the qualities mentioned above, tuffs are known for their radioactivity usually higher than other rocks, leading to higher exposures to population in this part of Italy (Righi, 2006; Unscear, 2000).

The radionuclide distribution data presented in this work together with direct indoor measurements provide new data and evaluation of the radiological risk associated with buildings made of volcanic products and built on volcanic rock substrates.

The mechanisms of enrichment of the main radionuclides in volcanic rocks are a complex matter being the result of a combination of magma genesis and evolution, alteration and depositional processes and will not be investigated in the present work.

4.2. Geological and volcanological setting

4.2.1 The quaternary volcanism of central Italy

Products of the quaternary potassic and ultrapotassic volcanism are widespread along the Thyrrenian side of the Italian peninsula, from the southern Tuscany to Latium (Conticelli and Peccerillo, 1992). This area includes four large volcanic districts (Vulsini, Vico, Sabatini and Colli Albani), each covering an area of more than 1000 km^2.

Although the volcanic activity started more or less contemporaneously in a period between 600 and 500 ka ago, the last recorded eruptive events span from 127 ka ago in the Vulsini to the Holocene age in the Colli Albani District. Explosive volcanic activities prevail in all the districts, invariably associated with volcanic or volcano-tectonic collapses and development of large caldera structures, often occupied by lacustrine basins (Bolsena, Vico, Bracciano and Albano lakes) which are a typical feature of the regional landscape. Products of ignimbrite-forming eruptions are usually represented by yellowish to orange colored blocks and ash tuffs, usually deposited by progressive aggradations during the passage of a sustained pyroclastic flow (Capaccioni et al., 2001). Lithification may occur by secondary mineralization or primary welding.

4.2.2. The Vulsini Volcanic District

The Vulsini Volcanic District, active during the period 590 – 127 ka (Gillot et al., 1991, Nappi et al., 1995), is the northernmost of the Italian potassic quaternary volcanic areas. Its eruptive products, mainly pyroclastics, cover an area of ~2000 km^2, between northern Latium and southern Tuscany, and radially distributed all around the Bolsena lake. On the basis of temporal and spatial distribution of the eruptive activity, it has been subdivided into four volcanic complexes: Paleobolsena, Bolsena, Latera and Montefiascone (Nappi et al., 1991). The volcanic complexes display similar eruptive styles, characterized by ignimbrite-forming events preceded and followed by effusive and strombolian activities, usually taking place along peripheral circum-calderic fault

systems. The oldest Paleobolsena complex produced a series of grayish welded pyroclastic deposits ("Nenfro" auct.; Civitella d'Agliano formation, Nappi et al., 1991) cropping out in the peripheral belt of the district and directly overlying the sedimentary substratum. These paroxistic explosive activities, originally taking place from a central vent, probably triggered a first structurally-controlled, vertical collapse, giving rise to a trap-door like, asymmetric volcano-tectonic depression now occupied by the Bolsena lake. Nowadays, due to their mechanical properties, these tuffs are extensively quarried and used as floor tiles, baseboards and steps.

The north-eastern faulted sector of the Bolsena caldera became the site of a new period of eruptive activity, producing tens of cinder and spatter cones as well as lava flows. This fissural monogenic activity was followed by at least two paroxistic eruptions, respectively producing a plinian fall and pyroclastic flow deposits. The last of these, dated at 333 ka, is represented by a latitic ignimbrite, highly lithified by means of secondary mineralization known as Orvieto-Bagnoregio ignimbrite (Capaccioni and Sarocchi, 1996, Nappi et al., 1994a and b). This tuff as well has been excavated for galleries and cellars and extensively quarried for building material even during the 20th century.

In the western sector of the Vulsini Volcanic District, the eruptive activity started later (~280 ka) and lasted for almost 120 ka, with a series of large, ignimbrite-forming eruptions, producing at least four yellowish to orange lithified pyroclastic deposits, preceded and followed by effusive and strombolian eruptions, and finally resulting into the formation of a polygenic caldera (Latera caldera; Sparks, 1975; Metzeltin and Vezzoli, 1983; Barberi et al., 1984, Conticelli et al., 1987). Nowadays the fine-grained and homogeneous "D" ignimbrite (Sparks, 1975) is quarried for blocks.

The youngest activity occurred in the south-eastern side of the Vulsini District and gave rise to the development of a polygenic, relatively small Montefiascone volcano (Marini and Nappi, 1986). The mechanical properties of pyroclastics pertaining to the Montefiascone volcano lack suitable characteristics to be extensively quarried.

4.3. Instruments and Methods

4.3.1. Sampling

Twenty two rock samples (approx. 0.7 kg each) were collected at different sites between Latera and Bolsena volcanic complexes (Fig. 4.1). The rock samples investigated include both lavas and pyroclastic rocks, representing different volcanic units (Table 4.2) erupted at different times from Latera and Bolsena volcanoes (Nappi, 1969; Sparks, 1975). A concrete block (M01) used in the area as building material has also been sampled and analyzed.
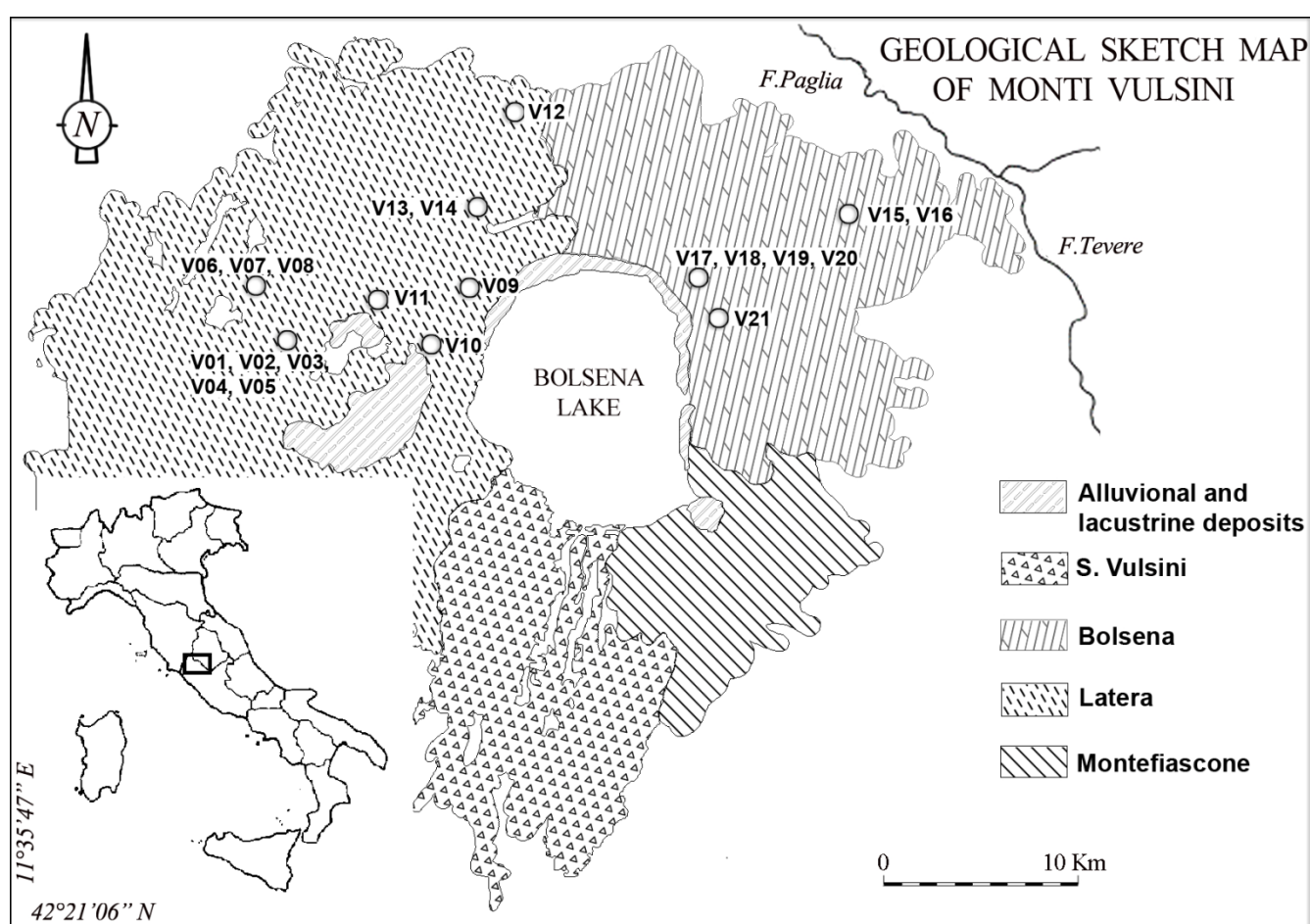

Fig.4.1 Geological sketch map of the Vulsini Volcanic District (after Vezzoli et al, 1987, modified) with location of the sampling site.

4.3.2. High resolution γ spectrometry

Bulk rocks and concrete samples, crushed and sieved at 2000 μm-mesh, were analyzed by γ-spectrometry with a p-type coaxial Hyper Pure Germanium crystal detectors (HPGe), with an

energy range 0-2000 keV. The detector has a relative efficiency of 38% and a resolution (FWHM) of 1.8 keV at 1330 keV respectively. The system was calibrated for energy and efficiency using a multiple nuclide source (QCY48, Amersham) in a jar geometry (diameter: 56 mm; thickness:10 mm). Spectra were analysed with the GammaVision-32 software (version 6.07, Ortec). Quantitative analysis on samples was carried out by subtracting the spectrum of water in the same geometry, while uncertainty on peaks (k = 1, 68% level of confidence) was calculated propagating the combined error over the efficiency fit previously determined with the counting error. Minimum detectable activity was calculated making use of the Traditional ORTEC method with a peak cut-off limit of 40%.

^{238}U and ^{232}Th were determined using the emissions of their radioactive descendents ^{226}Ra and ^{228}Ac. The intensity of the ^{226}Ra peak was evaluated at 186 keV and corrected for the contribution of ^{235}U with the hypothesis of natural ^{235}U/^{238}U isotopic ratio (Gilmore, 2008). Assuming a secular equilibrium, the activities of ^{226}Ra and ^{228}Ac will be equal to those of ^{238}U and ^{232}Th, respectively. ^{226}Ra has been also cross-checked by ^{234}Th emission at 63 keV, including overlap of measurement uncertainty intervals. Conversion from specific activity (Bq/kg) to bulk elemental weight fraction was obtained with the following conversion factors (Stromswold,1995):

1% K= 309.7 Bq/kg

1 ppm U= 12.35 Bq/kg

1 ppm Th = 4.072 Bq/kg.

To reach appropriate counting statistics samples were counted for 80000 s. Certified reference materials (DH-1a and UTS-3, CANMET) were used to verify the quality of the measurements.

All samples were pressed into pellets (diameter of 25 mm) on a boric acid support and analyzed for both major and trace elements with a Philips PW1480 WD-XRF (Wave Dispersion X Ray Fluorescence), while crystallization water and other volatile compounds were determined as Loss on Ignition (LOI).

4.3.3. Indoor Radon measurements

A campaign of indoor radon measurements has been carried out in the Bolsena village during the period 2010-2011. The locations of the investigated buildings are reported in Fig. 4.2. To have the largest number of possible typologies, buildings differing in location, age, number of floors, structure and building material were chosen (Tab. 4.1). Older constructions (dating back at 1200-1500 AD), located in the old centre of Bolsena village and entirely built with local volcanic rocks

were considered (public buildings A and B, house G and Church house) as well as modern houses, built around the 70's (houses A,B, C, D, E, and F; public building C; hostel and hotel). An ancient cellar artificially carved in a welded tuff in the old centre of Bolsena (Fig. 4.2) was also investigated. Measurements were taken in the inner part of the cellar, about 30 m away from the external access to minimize air exchange and radon dilution. The use of cellars carved in tuff deposits to store high quality wine, grapes and other foodstuff is a common practice in central Italy since very ancient times.

Direct indoor radon measurements were made with both a *femto*-TECH, INC CRM 510 Continuous Radon Monitor and an E-Perm system. The *Femto*-TECH radon monitor system is based on an ionization chamber device: after filtration to remove Radon progeny associated to aerosol particles, ambient air Radon is collected and measured by means of passive diffusion into an ionization chamber. The apparatus is equipped with temperature, pressure and relative humidity sensors, whose measurements are stored together with radon activity concentrations in a memory buffer. The instrument has been calibrated at the radon chamber of the Department of Energy, Radioprotection Lab-Radon sector of the Polytechnic University of Milan. The E-Perm system consists of a very stable electrically charged Teflon disk (Electret) mounted inside a small chamber made of electrically conducting plastic. The electret serves both as a source of electrostatic field and as a sensor. Radon gas diffuses passively into the chamber through filtrating inlets so that once entered the alpha particles emitted by the decay process ionize air molecules. Ions produced inside the chamber are collected onto the electret, causing a reduction of its surface charge. The charge reduction is a function of the total ionization produced during a given exposure time and can be related to ambient radon activity concentration once the chamber volume and the characteristics of the electrets are known.

Radon activity in air is usually expressed in becquerels per cubic meter (Bq/m^3). Radon exposure is given by the decay of radon gas and of its decay products. The overall contribution of radon + progeny to airborne radioactivity is quantified by the so called "working level" parameter, (WL; Nazaroff, 1988). 1 WL equals any combination of short-lived ^{222}Rn progeny (^{218}Po, ^{214}Pb, ^{214}Bi, and ^{214}Po) in 1 liter of air that releases 1.3×10^5 MeV of potential alpha Energy; one WL is equivalent to 2.08×10^{-5} joules per cubic meter of air (J/m^3). One WL is defined also as the potential alpha particle energy released by short-lived radon daughters in radioactive equilibrium with 3700 Bq/m^3 of ^{222}Rn. Ordinarily these equilibrium conditions are not fulfilled in homes, and the equilibrium factor (empirically assumed at 0.4; EPA, 2003) has to be considered.

Occupational exposure to radon daughters is expressed in working level month (WLM) which is the exposure at an average concentration of 1 WL for 170 working hours.

To assess the potential radon contribution of building materials the Radon Emanating Power (REP-ε) is used, that is the fraction of radon atoms released into the inter-granular spaces from a radium-bearing particle (Nero, 1988). This value is calculated using the ratio between the mean specific activity of radon decay products ^{214}Pb and ^{214}Bi w.r.t. the parent ^{226}Ra (Nuccetelli, 2008).

Site	Building Type	Floor	Building Material	Average Indoor Radon Activity (Bq/m^3)	Lifetime Radon Risk (10^{-2})
					EPA-Male/Female ES/NS
	Collected with continuous radon monitor: Femto-Tech				
1	Hotel	3	Concrete Block	307	5
2	Hostel	2	Tuff + Plaster	243	4
3	Public Building A	3	Tuff	3152	16**
		3	Tuff	3269	16**
4	House A	1	Tuff + Plaster	688	12
5	Public Building B	0	Tuff + Plaster	761	4**
6	Church House	2	Tuff+ Plaster	407	7
7	House B	1	Concrete Block	46	1
		0	Tuff	611	11
8	House C	1	Concrete Block	142	3
9	House D	1	Concrete Block	63	1
	Collected with electrets E-Perm				
10	Tuff cellar	underground	Tuff	30000	28*
11	Public Building C	0	Concrete Block	190	3
12	House E	1	Concrete Block	283	5
		0	Concrete Block	332	6
13	House F	1	Concrete Block	93	2
		0	Concrete Block	158	3
14	Apartment G	3	Tuff	1140	20
		2	Tuff	1139	20
		1	Tuff	1277	23
		0	Tuff	2513	45
		-1	Tuff	2662	2*

*considering one hour each day (i.e.0.04 indoor fraction)
**considering 2000 hours per years

Tab. 4.1 Average indoor Radon Activity (Bq/m^3) and estimation of radon risk for ever/never smoker population measured in the Bolsena village are reported (locations of the measured buildings are reported in Fig. 4.2).
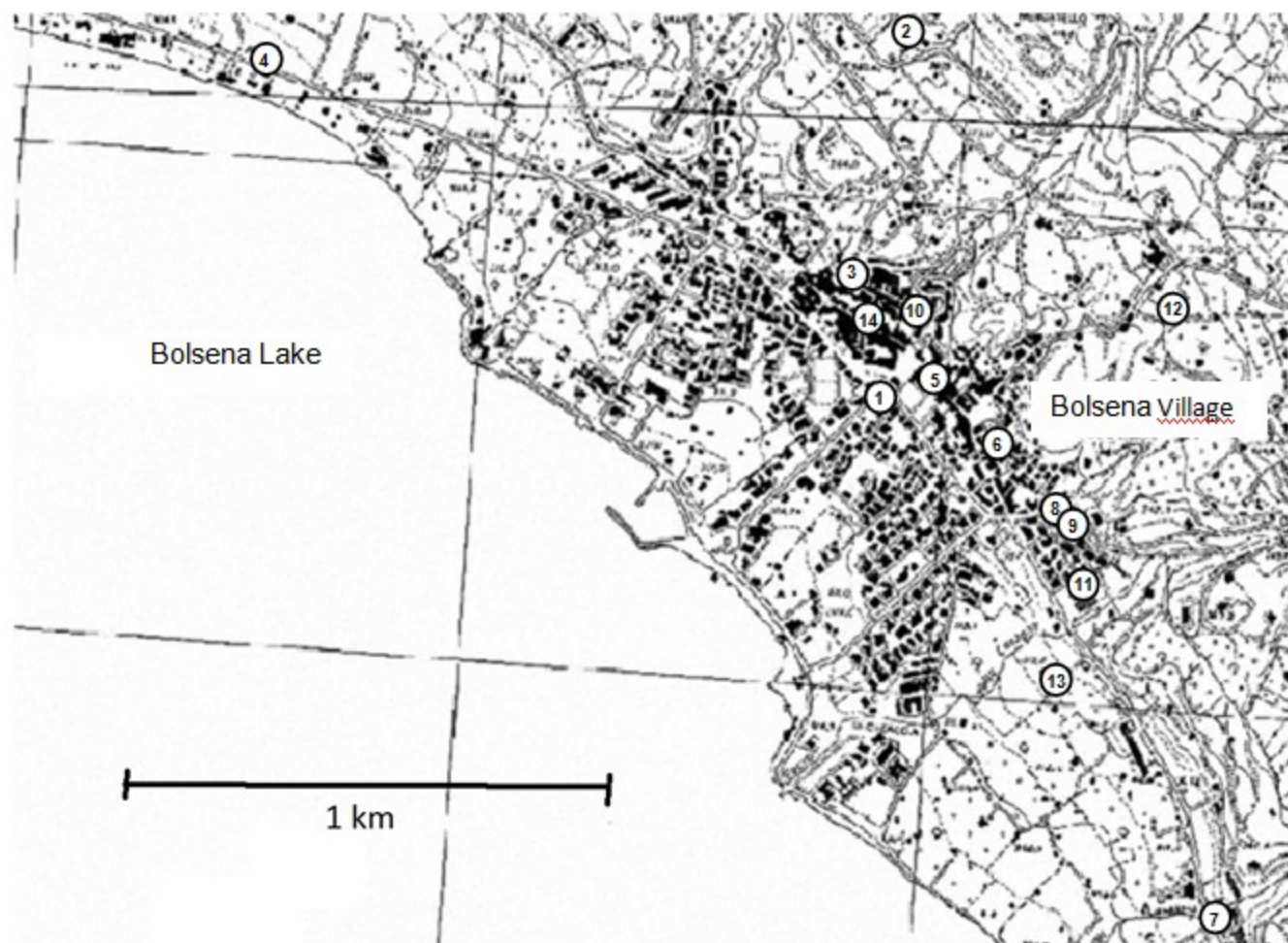
Fig. 4.2 Locations of the indoor radon measurements in the Bolsena village (open circles numbered with reference to Tab. 1)

4.3.4 Estimation of dose and risk assessment

Health effects on a human body after exposure to ionizing radiation are assessed by means of the quantity "effective dose", a measure of the energy deposited by ionization, weighted over the type of radiation and the organs affected to give an overall effect on the entire body. The international system unit for the effective doses is the Sievert (Sv).

Exposure to natural ionizing radiation can be external, due to exposure through the external surface of a human body, or internal, as a consequence of the inhalation or ingestion of terrestrial radionuclides. Concerning the internal exposure due to inhalation, the dominant contribution is given by the short-lived decay products of ^{222}Rn and ^{220}Rn, respectively produced by the decay series of ^{238}U (Radium series) and ^{232}Th.

In the present work, the internal and external doses due to natural radioactivity from building material have been evaluated by using the RESidual RADioactivity in BUILDings (RESRAD-BUILD) code (DOE, 2003). The RESRAD-BUILD code considers the exposure to radioactive material released from walls, floor and roof according to mechanisms such as diffusion, mechanical removal or erosion. Specifically:

For external exposure: a) radiations emitted directly from walls, roof and floor; b) radiations from deposited particles directly coming from the mechanical alteration of walls, roof and floor; c) radiations from suspended particles.

For internal exposure: d) inhalation of suspended particles; e) inhalation of suspended radon decay products; f) inadvertent ingestion of suspended and deposited particles.

The RESRAD-BUILD code provides the "effective dose" absorbed by an individual living in a simulated "standard room" for given specific occupancy factor, building material (with a defined content of natural radionuclides, ^{238}U, ^{232}Th and ^{40}K), air exchange rate and so forth. The code assumes a person positioned in the centre of a standard room having width, length and height respectively of 4, 5 and 2.8 m. The "reference point", i.e., the point where the dose is calculated, is the middle of the body, 1 m above the floor. The standard room is assumed to be delimited by homogeneous walls 20 cm thick and with a bulk density of 2.35 g/cm^3. The input data includes: REP-ε values calculated for each rock samples (Table 4.3); occupancy factor (the fraction of time spent within the room yearly, set at 0.8); air exchange rate (the fraction of the indoor air volume hourly exchanged, set at 0.25); wall erosion (the amount of material removed from walls per unit time, set at $2.4*10^{-8}$ cm/d); air released fraction (fraction of the walls erosion that is released into the air as suspended particles, set at 0.1); wall porosity (set at 0.2) and radon diffusion coefficient (set as 0.00002 m^2/s). The code uses dose conversion factors taken from different standard libraries: the EPA's (US Environmental Protection Agency's) Federal Guidance Report No.11 for inhalation and ingestion (FGR11, Eckerman et al., 1988) and the EPA's Federal Guidance Report No. 12 for external exposure (FGR12, Eckerman and Ryman 1993).

The risk for radiogenic cancer morbidity due to indoor natural radioactivity has been also evaluated by means of the RESRAD-BUILD code coupled with the EPA's model "Risks from Radon in Homes" (EPA, 2003) (http://www.epa.gov/radon/pubs/citguide.html). The RESRAD-BUILD code provides external and internal exposure scenarios using activity concentration data on building material and risk coefficients given by the EPA's Federal Guidance Report No. 13 (FGR13, Eckerman et al. 1999). Conversely, the EPA's model "Risks from Radon in Homes" (EPA, 2003) considers the inhalation of Radon and its products and provides the probability of a fatal lung cancer per WLM unit, which, in turn, is calculated from both the empirical indoor radon

measurements (Table 4.1) and the theoretical indoor radon production (Table 4.5). In the calculations the occupancy factor is set at 0.8 for homes, 0.2 for working place and 0.03 for cellars. The EPA model also considers the synergistic effects of radon inhalation and smoking.

EPA's model suggests the following risk estimate per WLM unit:

$9.68*10^{-4}$ per WLM for ever smokers (ES)

$1.67*10^{-4}$ per WLM for never smokers (NS)

$5.38*10^{-4}$ per WLM for a mixed population (ES-NS).

The ES-NS category includes 53% of males and 41% of females pertaining to the ES category.

The cumulative radon risk has been calculated using 74.2 and 76.4 years of expected life for ES and NS respectively (Table 4.5). The results of the cumulative risks are reported on Tables 4.1 and 4.5.

The dose –response relationship for radiation-induced cancer in humans have the best estimation in the range from about 0,1 to 2,5 Gy, thanks to atomic-bomb data. Below and above this range considerable uncertainty exists. The linear no-threshold assumption has been adopted in the present work, as recommended by standards organization, such as the International Commission on Radiological Protection or National Council on Radiation Protection and Measurements (Hall et al., 2006). However knowing that this understanding is incomplete and that therefore the evidence for this assumption is not conclusive (EPA, 2003).

4.4. Results and Discussions

4.4.1. Chemical composition and radionuclides distribution in volcanic rocks from Vulsini Volcanic District

Twenty one rock samples were collected and analyzed through high resolution γ-ray spectrometry, XRF and LOI (Loss of Ignition) analysis for the determination of radionuclide distribution and chemical composition. The results are reported in Table 4.2.

Sample	V04	V07	V08	V03	V05	V06	V01	V02	V09	V13	V14 (z)	V11	V10 (h)	V12	V15	V16 (z)	V17	V18	V19	V20	V21	M01
Volcanic Complex	Latera														Bolsena							
Formation	Canino	Canino	Canino	Sovana	Sorano	Sorano	Grotte di Castro	Grotte di Castro	Onano	Onano	Onano	Pitigliano	Pitigliano	Acquapendente	Bagnoregio-Orvieto	Bagnoregio-Orvieto	Bolsena	Bolsena	Bolsena	Bolsena	Bolsena	Bolsena
SiO_2	49.04	58.05	57.75	57.44	51.06	51.73	46.31	45	46.26	50.01	46.42	53.05	76.18	56.65	54.19	53.03	58.42	58.86	58.83	60.11	47.79	41.84
TiO_2	0.55	0.44	0.44	0.54	0.58	0.53	0.7	0.57	0.8	0.83	0.8	0.6	0.73	0.47	0.62	0.49	0.58	0.51	0.49	0.53	0.67	0.82
Al_2O_3	18.96	18.29	18.15	18.26	18.71	16.28	15.72	15.24	18.07	17.82	17.5	19.64	8.26	20.32	19.25	17.83	18.54	18.48	18.34	18.13	19.19	13.70
Fe_2O_3	4.24	3.01	2.99	3.97	3.74	3.57	6.6	5.65	8.67	8.88	7.68	5.81	0.35	3.53	6.03	3.83	4.57	4.04	4.14	4.16	7.62	7.18
MnO	0.13	0.15	0.14	0.14	0.14	0.14	0.16	0.14	0.11	0.17	0.15	0.15	0.06	0.15	0.15	0.14	0.13	0.13	0.14	0.13	0.19	0.19
MgO	1.29	0.97	1.21	0.99	1.19	1.49	4.06	2.56	2.37	3.22	3.57	1.48	0.23	0.71	1.85	1.4	1.32	1.09	1.11	1.28	2.63	4.09
CaO	7.49	2.17	2.12	3.5	5.59	5.08	7.12	6.78	6.26	8.02	7.77	6.29	0.59	3.35	5.28	4.1	4.16	3.52	3.78	3.21	9.27	16.94
Na_2O	1.55	2.47	2.57	3.19	1.82	0.62	0.85	0.56	1.33	6.33	1.12	2.81	0.71	3.9	2.97	0.91	2.92	2.55	2.76	2.99	3.27	1.37
K_2O	4.91	6.64	6.7	9.46	5.54	5.88	2.83	3.47	1.38	1.16	2.84	8.05	4.24	9.26	6.89	6.39	7.94	8.59	8.35	8.77	7.61	4.66
P_2O_5	0.15	0.12	0.12	0.2	0.14	0.2	0.52	0.39	0.58	0.43	0.39	0.3	0.19	0.12	0.21	0.11	0.30	0.24	0.26	0.28	0.55	0.22
LOI	11.69	7.69	7.79	2.31	11.49	14.50	15.13	19.64	14.17	3.13	11.75	1.81	8.47	1.53	2.57	12.76	1.11	2.00	1.80	0.40	1.20	9.01
Rb	265	337	360	263	356	298	242	263	54	624	237	369	42	209	403	221	344	475	319	419	380	407
Sr	813	242	298	960	709	1149	3369	4389	990	974	1044	1318	1060	1098	1163	1633	997	1078	1028	954	1950	978
Zr	283	419	422	186	384	221			166	156	115	150	403	343	231	220	446	533	430	427	305	314

(h) Hydrotermalizated; (z) Zeolitizatated

Tab. 4.2 Major (in wt.%) and trace elements (in ppm) in the whole rocks from the Vulsini Volcanic District.

		^{214}Bi (Bq/kg)	σ %	^{214}Pb (Bq/kg)	σ %	^{226}Ra (Bq/kg)	σ %	^{228}Ac (Bq/kg)	σ %	^{40}K (Bq/kg)	σ %	REP ε	U (ppm)	Th (ppm)	K (%)	Th/U	K/U 10^3	K/Th 10^3
V04	Lat-A	102	7	115	6	122	15	240	6	1490	6	0.11	10	59	4.8	5.9	4.9	0.8
V07	Lat-A	166	6	174	6	220	10	309	6	1559	6	0.23	18	76	5.0	4.2	2.8	0.7
V08	Lat-A	150	6	149	6	201	14	272	6	1724	6	0.25	16	67	5.6	4.1	3.4	0.8
V03	Lat-C	132	6	131	6	157	12	208	6	2325	6	0.16	13	51	7.5	4.0	5.9	1.5
V05	Lat-D	170	6	180	6	215	10	322	6	1564	6	0.19	17	79	5.0	4.5	2.9	0.6
V06	Lat-D	82	6	83	6	133	8	232	6	1668	6	0.38	11	57	5.4	5.3	5.0	0.9
V01	Lat-E	60	8	45	8	80	16	126	6	586	7	0.34	6	31	1.9	4.8	2.9	0.6
V02	Lat-E	56	8	61	7	86	11	151	2	808	7	0.32	7	37	2.6	5.4	3.8	0.7
V09	Lat-F	75	7	66	7	92	15	150	6	260	10	0.23	7	37	0.8	4.9	1.1	0.2
V13	Lat-F	99	7	105	6	112	9	180	6	227	12	0.09	9	44	0.7	4.9	0.8	0.17
V14(z)	Lat-F	79	7	80	7	95	15	155	6	769	7	0.16	8	38	2.5	4.9	3.2	0.65
V11	Lat-Pit	113	6	118	6	133	12	197	6	2175	6	0.13	11	48	7.0	4.5	6.5	1.45
V10(h)	Lat-Pit	235	6	250	6	262	9	333	6	1218	6	0.08	21	82	3.9	3.9	1.9	0.48
V15	Bols	175	6	186	6	234	10	306	6	1855	6	0.23	19	75	6.0	4.0	3.2	0.80
V16(z)	Bols	144	6	147	6	228	8	327	6	1694	6	0.36	18	80	5.5	4.3	3.0	0.68
V17	Bols	140	6	151	6	199	9	240	6	2377	6	0.27	16	59	7.7	3.7	4.8	1.3
V18	Bols	197	8	206	6	232	9	278	6	2289	6	0.13	19	68	7.4	3.6	3.9	1.1
V19	Bols	64	7	73	7	177	16	273	7	2472	6	0.55	14	67	8.0	4.7	5.6	1.2
V20	Bols	125	6	124	7	141	13	256	6	2487	7	0.12	11	63	8.0	5.5	7.0	1.3
V21	Bols	214	6	217	6	293	8	335	6	2106	6	0.27	24	82	6.8	3.5	2.9	0.8
V12	Lat	319	6	320	6	394	7	487	6	2443	6	0.19	32	120	7.9	3.8	2.5	0.7
M01		101	6	108	6	148	12	167	6	1441	6	0.29	12	41	4.7	3.4	3.9	1.1
M02*		-	-	-	-	53	-	86	-	543	-	0.05	4	21	1.8	-	-	-
Max		319		320		394		487		2487		0.55						
Min		56		45		80		126		227		0.08						

	Reguar soil[a]	Median/Range		Median/Range		Median/Range	
		35 (17-60)		30 (11-64)		400 (140-850)	

[a] UNSCEAR 2000; (h) Hydrotermalizated; (z) Zeolitizatated
*data from Nuccetelli (2008)

Tab. 4.3 Activity concentrations (Bq/kg) of natural radionuclides in the whole rocks from Vulsini Volcanic District. Radon Emanation Power (REP), expressed as one minus the ratio between the mean specific activity of radon decay products ^{214}Pb and ^{214}Bi w.r.t. the parent ^{226}Ra, is also reported.

The rock samples investigated represent lithified pyroclastic material (tuffs) from phonolitic/trachitic to shoshonitic/latitic composition of the juvenile fractions (V01 to 09 and V15 to 20 and M01) and lavas of phonolitic to tephritic composition (samples V10 to V14 and V21). The LOI displays a large variability from 0.40% (V20 sample) to 19.64% (V02 sample) by weight, clearly testifying variable degrees of hydration due to weathering and/or hydrothermal alteration.

Table 3 reports the specific activities of ^{226}Ra, ^{214}Pb and ^{214}Bi for the Uranium Series, ^{228}Ac for the Thorium Series and ^{40}K, the corresponding values of Radon Emanation Power (REP-ε) and the calculated concentration of the three parent elements with their concentration ratios (Th/U, K/Th and K/U). For comparison the values of a concrete sample M02 (Nuccetelli, 2008) and the average activity concentrations observed in worldwide rocks (Paschoa,A.S. and Steinhäuscer, 2010) are also reported. ^{238}U, ^{232}Th and ^{40}K contents range respectively from 6 to 32 ppm, from 31 to 120 ppm and from 0.7 to 8 % by weight (as total K).

The highest concentrations of U and Th are displayed by the phonolitic lava V12 (32 and 120 ppm respectively), with specific activities of ^{226}Ra and ^{228}Ac ten times those of regular soil, while the highest concentration of total K (8.77%) is displayed by sample V20. More than half the samples analyzed contain specific activities of ^{226}Ra higher than 150 Bq/kg and of ^{228}Ac higher than 250 Bq/kg. These are significantly higher than the average activity concentrations in granite samples (Pavlidou, 2006; Righi, 2006) while similar to those reported by Marocchi (Marocchi, 2011) for volcanic rocks like trachyte, tephriphonolite, etc. Similar values of U contents are reported by Gomes (Gomes et al., 2011), while lower Th contents.

In Fig. 4.3 concentrations of U are reported against Th for all the samples analyzed. U and Th concentrations for basaltic lavas and rhyolitic obsidians pertaining to Iceland and Aeolian islands (Italy), granites, trachites, rhyolites and high grade metamorphic rocks (Pavlidou, 2006; Marocchi, 2011) are also reported. Volcanic rocks from Iceland show the lowest concentration of U and Th with rhyolitic obsidians significantly enriched with respect to basaltic lavas. Higher contents of U and Th are displayed by the rhyolitic obsidians from the Aeolian island, while granites show a large variability, mainly due to different processes of magma genesis and source composition. Trachites and phonolites from the Vulsini Volcanic District display the highest U concentration while Th contents are similar to those of radionuclide-rich granites. Samples from Vulsini display the largest variability with a significant positive correlation among the two elements This correlation is due to their common incompatible behavior during processes of magma evolution: both elements tend to concentrate into evolved melts during crystal fractionation (Conticelli and Peccerillo, 1992). In

addition to factors such as source composition, magma genesis and evolution, volcanic rocks usually also suffer post-depositional weathering and can be subject to variable degrees of hydrothermal alteration. Samples V10 and V11 are fresh and strongly hydrothermalized tephritic lavas of the Pitigliano formation (130 ka, Nappi et al. 1991). The relevant depletion in FeO, MnO, MgO, CaO, Na2O and K2O, together with a severe enrichment of amorphous silica and water, likely reflect the effect of acid hydrothermal alteration. This type of alteration leads to a remarkable enrichment in ^{238}U and ^{232}Th accompanied by a severe decrease of ^{40}K activity.
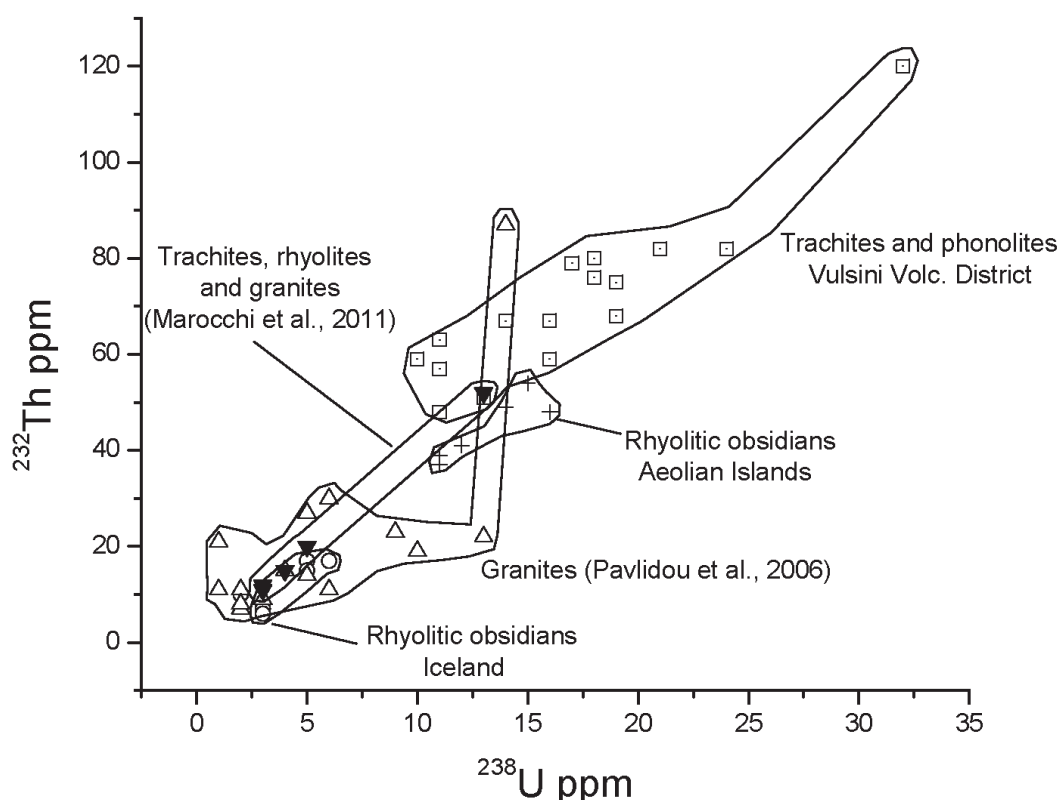
Fig. 4.3 Correlation between the concentrations of ^{238}U and ^{232}Th measured by gamma spectrometry in samples from Vulsini Volcanic District, rhyolitic obsidians from Iceland* and Aeolian*Islands (* unpublished data), granites from different origin (after Pavlidou, 2006), trachites, rhyolites and granites from different origin (after Marocchi et al., 2011).

According to Aiello and Colella (1975) and Hay (1986) usually tuffs result from post-depositional lithification of tephra due to interaction of fresh volcanic glass with neutral to alkaline waters which gives rise to secondary minerals, such as chabasite and phillipsite. On the basis of macroscopic observations (degree of lithification, colour, texture etc.), samples V14 and V13 (Onano formation; Nappi, 1969) can be considered respectively as zeolitizated (tuff) and almost unlithified (tephra)

equivalents. The zeolitizated sample displays similar ^{238}U and ^{232}Th concentrations w.r.t. the tephra equivalent but with a significant enrichment of ^{40}K (Table 4.3). A further example of tuff and tephra equivalent is given by samples V16 and V15, pertaining to the Orvieto-Bagnoregio pyroclastic formation (Capaccioni and Sarocchi, 1996, Nappi et al., 1994). The strong lithified sample (V16) does not provide significant variation of ^{238}U, ^{232}Th and ^{40}K concentrations w.r.t. the other (V15).

4.4.2 Indoor radon measurements and risk assessment

Direct indoor radon measurements have been made in 14 homes using the radon instrument described in the previous paragraph: E-perm and *Femto*-TECH. The values obtained are reported in Table 1 together with the main characteristics of the buildings (cf. Fig.2 for their locations). Indoor radon activity varies from 243 to 3152 Bq/m^3. Values measured in buildings made of tuff are mostly above 1000 Bq/m^3, while in those built with concrete bricks they fall in the range 46-332 Bq/m^3 (Table 4.1). Radon activity measured at the Hotel (site n° 1) yields a relatively high value on the third floor (307 Bq/m^3), despite the fact that this building is entirely made of concrete blocks. This value is also significantly higher than the 243 Bq/m^3 measured at the hostel second floor, entirely made of tuff. In House B (cf. Table 4.1) an extremely large difference between the ground (made of tuff: 611 Bq/m^3) and first floor (made of concrete blocks: 46 Bq/m3) was registered, possibly testifying the combined effect of the radon-emitting building material and of radon leaking into the ground floor from the basement. The apparently anomalous large radon activity measured on the third floor of the Hotel (site n° 1) is clearly explained by the contents of ^{40}K, ^{238}U and ^{232}Th observed for a concrete block sample (M01; Table 4.3) of the type the building has been built with, also analyzed together with the rock samples collected. These values are not very different from those directly measured in natural volcanic materials because the concrete block sample turned out to be composed by an inert skeleton of coarse lapilli-sized black scoriae of volcanic origin.

An extremely high value of radon activity has been recorded in a cellar located in the old centre of Bolsena, directly carved into the tuff deposits (30000 Bq/m^3, Table 4.1). The exceptional radon indoor activity is due to the joint effect of the whole structure being excavated in the tuff radioactive rock and of the air exchange rate being practically null.
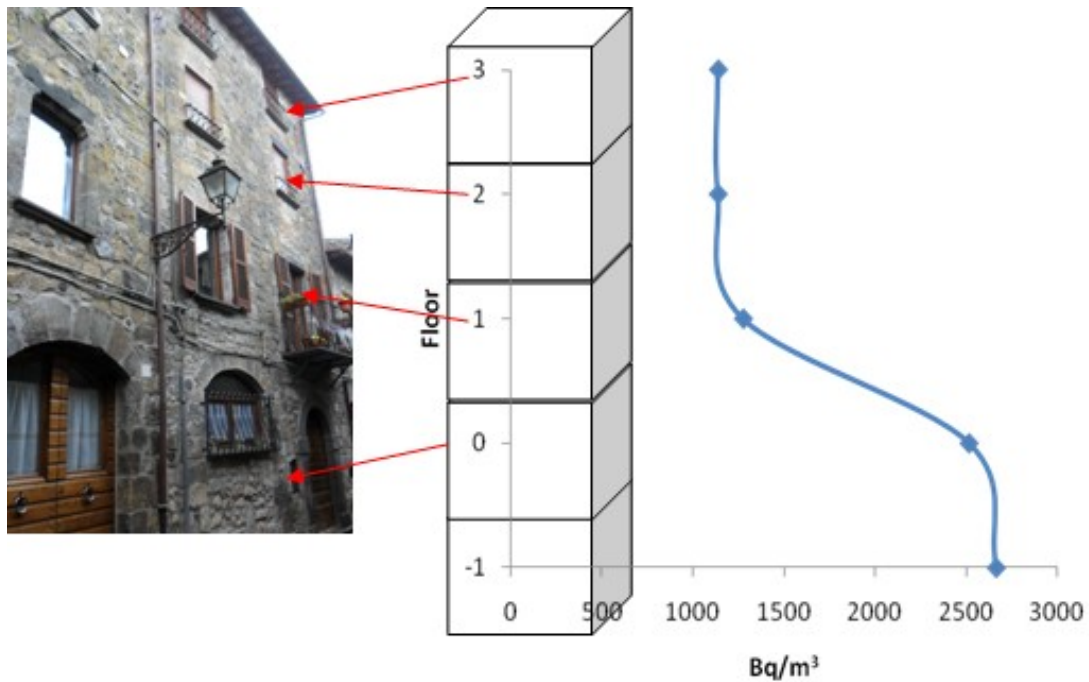
Fig. 4.4 Activity concentrations of radon measured at different floors in the Private House G.

Fig. 4.4 reports the results of radon activity measurements in a five-story house (G, cf. Fig. 4.2), representing a typical example of medieval housing in the old centre of the Bolsena village. The measurements were carried out on the different floors, starting from the underground (-1). The two lower floors (-1 and 0) display values exceeding 2500 Bq/m^3, more than 10 times the threshold value recommended by the European Commission (EC, 1990). The activity decreases to 1277 Bq/m^3 on the first floor (1) and reaches an almost constant value (~1140 Bq/m^3) on the second (2) and third floors (3). The higher radon activities measured in the underground (-1) and at the ground floor (0) reflect significant radon contributions from the basement, while the constant values recorded on the second and third floors can be almost entirely attributed to the building material.

Table 4.1 reports the radiological risk in terms of probability of a fatal lung cancer for an expected lifetime of 75.4 y due to radon exposure, calculated using EPA coefficients (EPA, 2003) and the indoor radon activities measured. The values estimated show that the risk of lung cancer is extremely high, ranging from 20 to 40 % in houses entirely constructed with local tuffs and above a volcanic basement, as is the case in the ancient centre of Bolsena. Conversely, the highest risk for houses entirely built with concrete block does not exceed 6 %. In public buildings (A, B and C, Table 1), assuming a lower occupancy factor of 0.2, the highest estimated risk is 17 %.

4.4.3 Estimation of dose and risk assessment in a simulated "standard room"

The expected dose and related radiological risk for a person living in a simulated "standard room" assumed built with the different volcanic rocks of the samples investigated, are evaluated using the RESRAD-BUILD code. It is assumed that building materials as the only source of radon and the contribution of thoron (^{220}Rn, from ^{232}Th decay chain) can be considered negligible. The annual effective doses predicted are reported in Table 4.4. The external dose ranges between 1.34 and 5.62 mSv/y, with more than 50% of the values >3 mSv/y. The dose due to radon inhalation ranges between 0.93 and 8.68 mSv/y, with 45% of values >4 mSv/y. Doses from particle inhalation, submersion, ingestion and deposited particles can be neglected, being 2 to 9 orders of magnitude lower. The sum of the external and radon inhalation doses often exceed the total annual dose averages estimated for Italy and worldwide (4.5 and 3.5 mSv/y respectively; Dionisi et al, 2005; UNSCEAR, 2008).

The lifetime risk of lung cancer due to radon inhalation and the cancer risk from the other pathways have been estimated also for the simulated standard rooms (Table 4.5). As expected, external exposure and radon inhalation are the dominant contributions to the total risk, the others being negligible. The probability of radiogenic cancer morbidity due to external doses ranges from 0.77 to 3.22 %, while that of fatal lung cancer due to radon inhalation ranges from 0.88 to 8.20 % for ever smokers and from 0.16 to 1.46 % for never smokers.

	Effective Dose (mSv/y)					
	Direct External	Exposure of Deposited Material	Immersion	Inhalation	Radon Inhalation	Inadverted Ingestion
V04	2.57	1.19E-06	1.54E-08	9.68E-03	1.20	8.56E-05
V07	3.44	1.63E-06	2.08E-08	1.27E-02	4.51	1.24E-04
V08	3.19	1.53E-06	1.97E-08	1.12E-02	4.48	1.11E-04
V03	2.86	1.42E-06	1.83E-08	8.54E-03	2.24	8.66E-05
V05	3.50	1.64E-06	2.10E-08	1.31E-02	3.64	1.26E-04
V06	2.64	1.25E-06	1.61E-08	9.40E-03	4.51	8.64E-05
V01	1.34	6.20E-07	7.95E-09	5.12E-03	2.42	4.83E-05
V02	1.61	7.47E-07	9.58E-09	6.11E-03	2.45	5.57E-05
V09	1.42	6.32E-07	8.08E-09	6.10E-03	1.89	5.62E-05
V13	1.67	8.14E-07	1.03E-08	8.14E-03	0.93	7.50E-05
V14	1.66	8.46E-07	1.08E-08	7.02E-03	1.41	6.51E-05
V11	2.63	1.43E-06	1.84E-08	8.96E-03	1.60	8.72E-05
V10	3.64	1.88E-06	2.40E-08	1.53E-02	1.94	1.53E-04
V15	3.61	1.90E-06	2.44E-08	1.40E-02	4.98	1.40E-04
V16	3.64	1.89E-06	2.42E-08	1.49E-02	7.60	1.44E-04
V17	3.25	1.62E-06	2.07E-08	9.90E-03	4.79	1.03E-04
V18	3.59	1.77E-06	2.27E-08	1.15E-02	2.69	1.20E-04
V19	3.40	1.65E-06	2.12E-08	1.11E-02	8.68	1.07E-04
V20	3.15	1.52E-06	1.95E-08	1.03E-02	1.51	9.46E-05
V21	4.14	2.01E-06	2.57E-08	1.39E-02	7.05	1.47E-04
V12	5.62	2.69E-06	3.44E-08	2.01E-02	6.67	2.06E-04
M01	2.22	1.10E-06	1.41E-08	6.91E-03	3.82	7.41E-05
M02	0.96	4.56E-07	5.84E-09	3.49E-03	0.24	3.27E-05

Table 4.4 Annual Effective doses (mSv/y) for different scenarios calculated using the RESRAD-BUILD code considering a standard room. The specific activity of the building materials is the same of the sampled.

Lifetime Risk from Radon in homes (10^{-2})			Lifetime Risk from other scenarios (10^{-2})							LifetimeTotal Risk (10^{-2})
EPA (2003) Male-Female			RESRADBUILD FGR13 morbidity							
ES	NS	ES-NS	Direct External	Exposure of Deposited Material	Immersion	Inhalation	Radon External Exposure	Inadverted Ingestion	ES-NS	
Expected Life (years) 74.2	76.4	75.4	75.4	75.4	75.4	75.4	75.4	75.4	75.4	
V04 1.13	0.20	0.64	1.48	6.86E-07	8.82E-09	6.74E-04	1.00E-02	2.23E-05	2.13	
V07 4.26	0.76	2.41	1.97	9.33E-07	1.19E-08	9.26E-04	3.78E-02	3.12E-05	4.42	
V08 4.23	0.75	2.39	1.84	8.81E-07	1.13E-08	8.23E-04	3.75E-02	2.84E-05	4.26	
V03 2.12	0.38	1.19	1.64	8.17E-07	1.05E-08	6.38E-04	1.87E-02	2.34E-05	2.85	
V05 3.44	0.61	1.94	2.01	9.41E-07	1.21E-08	9.50E-04	3.05E-02	3.17E-05	3.98	
V06 4.26	0.76	2.41	1.52	7.18E-07	9.24E-09	6.65E-04	3.77E-02	2.26E-05	3.96	
V01 2.29	0.41	1.29	0.77	3.55E-07	4.56E-09	3.68E-04	2.03E-02	1.21E-05	2.08	
V02 2.32	0.41	1.31	0.92	4.29E-07	5.50E-09	4.32E-04	2.05E-02	1.43E-05	2.25	
V09 1.78	0.32	1.01	0.81	3.62E-07	4.63E-09	4.33E-04	1.58E-02	1.37E-05	1.83	
V13 0.88	0.16	0.50	0.96	4.66E-07	5.93E-09	5.67E-04	8.19E-03	1.79E-05	1.46	
V14 1.33	0.24	0.75	0.95	4.85E-07	6.23E-09	4.89E-04	1.24E-02	1.63E-05	1.71	
V11 1.51	0.27	0.85	1.51	8.22E-07	1.06E-08	6.39E-04	1.41E-02	2.34E-05	2.38	
V10 1.83	0.33	1.03	2.09	1.08E-06	1.38E-08	1.11E-03	1.70E-02	3.75E-05	3.14	
V15 4.70	0.84	2.66	2.07	1.09E-06	1.40E-08	1.02E-03	4.37E-02	3.54E-05	4.77	
V16 7.18	1.28	4.06	2.09	1.08E-06	1.39E-08	1.06E-03	6.68E-02	3.61E-05	6.21	
V17 4.53	0.80	2.56	1.87	9.29E-07	1.19E-08	7.49E-04	4.01E-02	2.74E-05	4.47	
V18 2.54	0.45	1.43	2.06	1.01E-06	1.30E-08	8.69E-04	2.25E-02	3.11E-05	3.52	
V19 8.20	1.46	4.63	1.95	9.46E-07	1.22E-08	8.04E-04	7.25E-02	2.84E-05	6.66	
V20 1.43	0.25	0.81	1.80	8.72E-07	1.12E-08	7.31E-04	1.26E-02	2.56E-05	2.62	
V21 6.66	1.18	3.76	2.37	1.16E-06	1.48E-08	1.06E-03	5.89E-02	3.71E-05	6.19	
V12 6.31	1.12	3.56	3.22	1.54E-06	1.97E-08	1.50E-03	5.59E-02	5.15E-05	6.84	
M01 3.61	0.64	2.04	1.27	6.32E-07	8.08E-09	5.31E-04	3.20E-02	1.92E-05	3.35	
M02 0.22	0.04	0.12	0.55	2.62E-07	3.36E-09	2.50E-04	1.98E-03	8.44E-06	0.68	

Table 5.5 Radon risk calculated using EPA risk coefficients and doses from RESRAD-BUILD code. Internal and external risks calculated with the RESRAD-BUILD code using the risk coefficients given by the EPA's FGR13: for explanation see text.

4.4.4 Effects of air exchange rate for doses and related risks in a simulated "standard room"

As stated above, Radon, usually being the major contributor to the total dose, produces the highest radiological risk. Being a noble gas, Radon can easily diffuse into closed spaces and accumulate therein. As a consequence, the indoor air exchange rate becomes a critical parameter to prevent or minimize dangerous radon accumulation. Starting from the radionuclide concentrations detected in the V05 tuff sample (largely used as building material in the Bolsena area) and fixing all the other parameters, doses have been estimated at different air exchange rate (from 0.01 to 0.9 1/h). Following the considerations previously described (Table 4), only radon and external exposure are considered and the results are reported in Fig. 5.
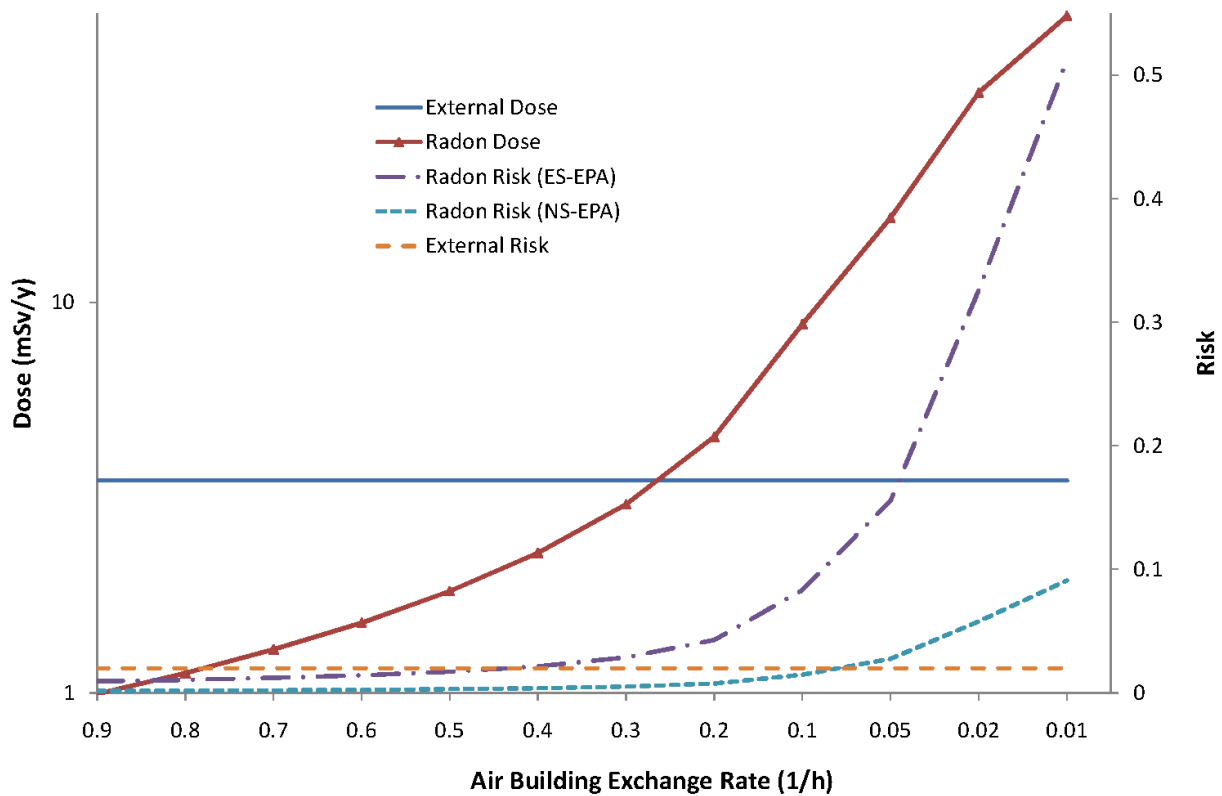
Fig. 4.5 Dose and risk (10^{-2}) due to external and radon exposures vs Air Building Exchange Rate (h^{-1}) in a RESRAD-BUILD standard room in which sample V05 from Vulsini Volcanic District is taken as building material.

At relatively high air exchange rates (>0.3 h^{-1}) the contribution from direct external exposures dominates over radon inhalation. This relationships progressively changes as the air exchange rate is lowered. At values below 0.3 h^{-1}, (a situation potentially encountered in the cold season) radon becomes the dominant contributor. For very low air exchange rates (0.01 h^{-1}) the dose from radon

increases exponentially, reaching extremely high values (up to 50 mSv/y), which, as reported on Fig. 4.5, produces a radiological risk of 50% for an ever smoker and 8% for a never smoker.

4.5 Conclusions

The widely distributed volcanic products of the quaternary Vulsini Volcanic District, mostly consisting of lithified pyroclastic deposits (ignimbrites, auct.), have been largely used as building material since a very early age. They have been used to produce buildings blocks, cellars, tombs and amphitheaters, directly carved into the lithified pyroclastic deposits. Moreover, during the Middle age, their upper almost flat surface coupled with their overlooking position and stability have promoted the development of villages on top of the pyroclastic plateaux. Houses made of tuffs together with their location on volcanic basement have produced remarkable high external and internal indoor exposure for population living in the area.

The chemical compositions of tuffs and lavas appear to be characterized by an exceptional enrichment in natural radionuclides, such as ^{238}U, ^{232}Th and ^{40}K, possibly due to a coupled effect of source composition and magma evolution at shallow levels. Lithification due to glass $\rightarrow$ zeolites conversion does not provide significant enrichment/depletion of ^{238}U and ^{232}Th, whereas volcanic rocks appear to undergo a remarkable enrichment during acid hydrothermal alteration.

Simulations of a "standard room" built with the different tuffs collected in the Latera and Bolsena areas, suggest that exposures to external radiation and radon inhalation represent by far the dominant contributions to dose from natural radioactivity. Exposure to radon activity becomes the prevailing contributor if air exchange rate in the "standard room" is lowered below 0.3 1/h.

The contribution of indoor radon exposure to the risk of developing a lung cancer in this area in a 74 year lifetime is estimated from numerical simulations to about 8% for ever smokers and 1.5% for never smokers. These values have to be added to cancer risk due to other causes, including smoking (without radon contribution, lifetime lung cancer risk for a regular smoker in Italy is estimated at 13.8%; ISS, 2004). Apart from building materials, doses due to indoor radon inhalation appear strongly influenced by the air exchange rate. Low to very low exchange rates give rise to severe build up of radon and consequently to a dramatic increase of risk associated to lung cancer. This conditions presumably dominate in homes and public buildings of the old centre of Bolsena village. Here, the cumulative risk of developing a lung cancer reaches extremely high values, in the range 20-40%. Extremely low air exchange rates are possibly reached in cellars directly carved into the pyroclastic deposits (typically with scarce or no ventilation). In this case radon activity reaches well

above safety limits and, even with a low occupancy factor, provides a risk of lung cancer >20%, so that access should be avoided or, at least, limited or increase air exchange rates.

In Italy the cumulative risk (within 74 years) of developing a cancer is 33.12% among men and 24.19% among women, while the cumulative risk of a lethal cancer is 16.52 % among men and 8.97 % among women (AIRTUM register). Therefore, the cumulative radiological risk of developing a cancer estimated in this work for the Vulsini Vulcanic District cannot be considered negligible and precautionary actions should be foreseen by the local community.

References

Agnesod G., Dionisi M., Falcone M., Fontani S., Magro L., Menna G., Ocone R., Parisi D., Salierno C., Salvi F., Sogni R., Sotgiu A.M., Torri G., Zeppa P., Wells J., Apat, 2005, *Enviromental Data Yearbook (cap. 11 Radiazioni Ionizzanti),* 897-931.

Aiello, R. and Colella, C., 1975. Sintesi idrotermale di zeoliti da vetro riolitico in presenza di basi miste sodico-potassiche. Rend. Soc. Miner. Petrol., 31, 641-652.

Bao, X., Zhang, A., 1998. Geochemistry of U and Th ant its influence on the origin and evolution of the crust of earth and the biological evolution. Acta Petrologica et Mineralogica 17, 160-172.

Barberi, F., Innocenti, F., Landi, P., Rossi, U., Saitta, M., Santacroce, R. and Villa, I.M., 1994. *The evolution of Latera caldera (central Italy), in the light of the subsurface data.* Bull. Volcanol., 47(1), 125-141

Capaccioni, B. and Sarocchi, D., 1996. *Computer-assisted image analysis on clast shape fabric from the Orvieto-Bagnoregio ignimbrite (Vulsini District, central Italy): implications on the emplacement mechanisms.* Journal of Volcanology and Geothermal Research 70, 75-90.

Capaccioni, B., Nappi, G. and Valentini, L., 2001. *Directional fabric measurements: an investigative approach to transport and depositional mechanisms in pyroclastic flows.* Journal of Volcanology and Geothermal Research 107, 275-292.

Conticelli, S.,Francalanci, L., Manetti, P., Peccerillo, A., 1987, *Evolution of Latera Volcano, Vulsinian district (Central Italy): stratigraphical and petrological data*, Per.Mineral., 56, 175-199

Conticelli, S., Peccerillo, A., 1992, *Petrology and geochemistry of potassic and ultrapotassic volcanism in central Italy: petrogenesis and inferences on the evolution of the mantle sources*. Lithos, 28, 221-240.

De Rita, D., Ciriaco, G., 2006*, A case study - Ancient Rome was built with volcanic stone from the Roman land,* Cap VI, Tuffs-Their Proprieties, Uses, Hydrology and Resources. The Geological Society of America.127-131.

Dionisi, Fontani, Innocenzi, Menna, Parisi, Salierno, Torri, Zeppa, Wells. 2005, APAT. *Enviromental Data Yearbook*.

DOE, U.S. Department of Energy, 2003. User's Manual for RESRAD-BUILD Version 3.318 pp.

Dubois, G. (2005), *"An overview of radon surveys in Europe"* Radioactivity Environmental Monitoring Emissions and Health Unit Institute for Environment and Sustainability JRC - European Commission. EUR 21892 EN, EC.168 pp.

EC (European Commission), 1990. Commission recommendation 90/143/Euratom of 21 February 1990 on the protection of the public against indoor exposure to radon. Official Journal L-80 of 27/03/90. European Commission, Bruxelles.2 pp.

EC (European Commission), 1990. Council Directive 96/29/Euratom of 13 May 1996 laying down basic safety standards for the protection of the health of workers and the general public against the dangers arising from ionizing radiation. Official Journal L-159 of 27/06/96. European Commission, Bruxelles.29 pp.

EC (European Commission), 1999. Radiation protection 112, report on radiological protection principles concerning the natural radioactivity of building materials.16 pp.

Eckerman, K.F., et al., 1988, *Limiting Values of Radionuclide Intake and Air Concentration and Dose Conversion Factors for Inhalation, Submersion, and Ingestion,* EPA-520/1-88-020, Federal Guidance Report No. 11, prepared by Oak Ridge National Laboratory, Oak Ridge, Tenn., for U.S. Environmental Protection Agency, Office of Radiation Programs, Washington, D.C.224 pp.

Eckerman, K.F., and J.C. Ryman, 1993, *External Exposure to Radionuclides in Air, Water, and Soil, Exposure to Dose Coefficients for General Application, Based on the 1987 Federal Radiation Protection Guidance,* EPA 402-R-93-076, Federal Guidance Report No. 12, prepared by Oak Ridge National Laboratory, Oak Ridge, Tenn., for U.S. Environmental Protection Agency, Office of Radiation and Indoor Air, Washington, D.C.238 pp.

Eckerman, K.F., et al., 1999, *Cancer Risk Coefficients for Environmental Exposure to Radionuclides*, EPA 402-R-99-001, Federal Guidance Report No. 13, prepared by Oak Ridge National Laboratory, Oak Ridge, Tenn., for U.S. Environmental Protection Agency, Office of Radiation and Indoor Air, Washington, D.C.335 pp.

Environmental Protection Agency-EPA, 2003. *EPA assessment of risks from radon in homes*. Office of Radiation and Indoor Air. Washington DC, 98 pp.

Funiciello, R, Heiken, G., Levich, R., Obenholzner J., Petrov V., 2006, *Construction in regions with tuff deposits*, Tuffs-Their Proprieties, Uses, Hydrology and Resources. The Geological Society of America.119-126.

Gillot, P.Y., Nappi, G., Santi, P. and Renzulli, A., 1991. *Space-time evolution of the Vulsini Volcanic Complexes, central Italy*. EUG VI, Strasburg, 24-28 March 1991. Terra Abstract, 3-1, 446.

Gilmore G., 2008, Practical Gamma-Ray Spectrometry, John Wiley & Sons.387 pp.

Gomes, M.E.P., Neves, L.J.P.F., Coelho, F., Carvalho, A., Sousa, M., Pereira, A.J.S.C., 2011. *Geochemistry of granites and metasediments of the urban area of Vila Real (northen Portugal) and correlative radon risk*. Environ Earth Sci, 64, 497-502.

Hay, R.L. 1986. *Geological occurrence of zeolites. In: Sand LB, Mumpton FA (eds) Natural Zeolites, Occurrence, Properties, Use*. Pergamon Press, Oxford, 135-143.

Istituto Superiore di Sanità - ISS, 2004, *Fumo e Patologie Respiratorie, Le carte del Rischio per Broncopneumopatia Cronica Ostruttiva e Tumore al Polmone*, Report.35 pp.

Ivanovich, M.,Harmon, R.S.,1992. *Uranium-series Disequilibrium, Applications to Earth, Marine, and Environmental Sciences.* Oxford Science Publications. 910 pp.

Lanzo,G., Basile, S., Brai, M., Rizzo, S., 2010. *Volcanic products of Lipari (Aeolian islands, Italy): Multivariate analysis of petrographic and radiometric data*. Radiation Measurements 45, 816-822.

Marini, A., Nappi, G., 1986. *Origin and evolution of the Montefiascone caldera (Vulsini Volcanoes)*.Mem Soc Geol Ital 35, 657-665.

Marocchi, M., Righi, S., Bargossi, G.M., Gasparotto, G. , 2011. *Natural radionuclides content and radiological hazard of commercial ornamental stones: An integrated radiometric and mineralogical-petrographic study*, Radiation Measurements 46, 538-545.

Metzeltin S. and Vezzoli, L., 1983. *Contributi alla geologia del volcano di Latera (Monti Vulsini, Toscana Meridionale – Lazio Settendrionale)*. Mem. Soc. Geol. Ital., 25, 247-27.

Nazaroff, W.W., and Nero, A.V., Jr., Eds., 1988, *Radon and its decay products in indoor air*. New York, John Wiley and Sons, Inc., 518 p.

Nappi, G., 1969, *Stratigrafia e petrografia dei Vulsini sud-occidentali (caldera di Latera)*, Boll.Soc.Geol.It., 88, 171-181

Nappi, G., Renzulli, A. and Santi, P., 1991. *Evidence of incremental growth in the vulsinian calderas (Central Italy)*. J. Volcanol. Geotherm. Res. 47, 13–31.

Nappi G., Capaccioni B., Mancini E., Mattioli M., Valentini L. 1994a. *Plinian fall deposits from Vulsini Volcanic District (Central Italy)*. Bull. Volcanol., 56, 502-515.

Nappi, G., Capaccioni, B., Renzulli, A., Santi, P. and Valentini, L., 1994b. *Stratigraphy of the Orvieto-Bagnoregio Ignimbrite eruption (Eastern Vulsini District, Central Italy)*, Mem. Descript. Carta Geol. Ital. 49, 241–254.

Nappi, G., Renzulli A., Santi, P. and Gillot, Y.P. 1995. *Geological evolution and geochronology of the Vulsini volcanic district (central Italy)*. Bollettino della Società Geologica Italiana, v.114, 599-613.

Nero, A.V.Jr,1998, Radon and its decay products in indoor air, John Wiley & Sons.518 pp.

Nuccetelli, C., 2008. *In situ gamma spectrometry in environmental research and monitoring*, Applied Radiation and Isotopes 66, 1615-1618.

Palladino, D., Simei, S., 2005, *The Latera volcanic complex (Vulsini, Central Italy): eruptive activity and caldera evolution*, Acta Vulcanologia 17 (1-2), 75-80.

Paschoa A.S., Steinhäuscer, F., 2010, *Terrestrial, Atmospheric, and Aquatic Natural Radioactivity*, Radioactivity in the Environment, Volume 17, 29-85.

Pavlidou, S., Koroneos, A., Papastefanou, C., Christofides, G., Stoulos, S., Vavelides, M., 2006. *Natural radioactivity of granites used as building materials*. Journal of Environmental Radioactivity 89, 48-60.

Righi, S., Bruzzi, L., 2006. *Natural radioactivity and Radon exhalation in building materials used in Italian dwellings*. Journal of Environmental Radioactivity 88, 158-170.

Santi, P., 1990. *New geochronological data of the Vulsini Volcanic District (Cental Italy). Proceedings of SIMP Congress on Genesi e differenziazione del magmatismo potassico del bordo tirrenico*, Ischia, 15-18 Ottobre, abstract.

Sato, J., Sato, K., 1997. *Gamma-ray spectrometric characterization of volcanic magmas*. Geochem.J.,11, 261-266.

Schon, J.H., 1998. Physical proprieties of rocks. Pergamon, 583 pp.

Sparks, R.S.J, 1975, *Stratigraphy and geology of the ignimbrites of Vulsini volcano, Central Italy.* Geologische Rundshau, 64, 497-523.

United Nations Scientific Committee on the effects of Atomic Radiation (UNSCEAR), 1993. Sources and Effects of Ionizing Radiation. Report to General Assembly, Annex A, United Nations, New York, NY.89 pp.

United Nations Scientific Committee on the effects of Atomic Radiation (UNSCEAR), 2000. Sources and Effects of Ionizing Radiation. Report to General Assembly, Annex B, United Nations, New York, NY. 156 pp.

United Nations Scientific Committee on the effects of Atomic Radiation (UNSCEAR), 2008. Sources and Effects of Ionizing Radiation. Report to General Assembly, Annex B, United Nations, New York, NY.245 pp.

Vezzoli, L., Conticelli, S., Innocenti, F., Landi, P., Manetti, P., Palladino D.M. and Triglia, R., 1987. *Stratigraphy of the Latera Volcanic Complex: proposals for a new nomenclature*. Per. Min., 56, 89-110.

Chapter 5 - Radon soil gas measurements and development of a radon risk map in an urbanized area: the village of Bolsena (Vulsini Volcanic District, Central Italy)[3]

5.1 Introduction

Radon is a radioactive noble gas, naturally occurring in three isotopic forms: ^{219}Rn (actinon), ^{220}Rn (thoron) and ^{222}Rn (radon), as members of the primordial ^{235}U, ^{232}Th and ^{238}U series respectively. The parent atoms of these series can be found in all natural materials, so all the three radon isotopes are released from the surface of rocks, soils or building materials. Outdoor radon exhalation from the earth's surface or other materials is rapidly dispersed into the atmosphere, while when it occurs indoor, such as within houses and underground mines, its concentration can increases up to dangerous levels. Because of short half-life of ^{219}Rn and ^{220}Rn, their indoor activity concentrations are much less than that of ^{222}Rn.

Recent studies on indoor radon and lung cancer in Europe, North America and Asia provide strong evidences that radon causes a substantial number of lung cancers in the general population, for which represents the second cause of lung cancer, after smoking. Current estimates of the proportion of radon-induced lung cancers range from 3 to 14%, depending on the average radon concentration in the country and the calculation methods (Zeeb and Shannoun, 2009). The analyses indicate that the lung cancer risk increases proportionally with increasing radon exposure. As many people are exposed to low and moderate radon concentrations, the majority of lung cancers related to radon are caused by these long-lasting exposure levels rather than by higher concentrations. Most of the radon-induced lung cancer cases occur among smokers due to a strong combined effect of smoking and radon (Zeeb and Shannoun, 2009).

The international commission for radiological protection (ICRP) and the EU Council Directive 96/29/EURATOM (1996) give recommendations concerning the identification of areas, where an increased number of houses are likely to have high indoor radon risk and thus should be considered as ''radon prone''. To further identify regions susceptible to high indoor radon levels, different approaches for the survey techniques, classification system and mapping procedures are used worldwide. In Europe a large heterogeneity of the used approach for choosing the measured

---

[3] Manuscript in praparation

variable and a method for presenting radon levels exists (Dubois, 2005). Two main strategies for geographically defining the indoor radon exposure have been encountered: a) indirect evaluation of radon-prone areas by means of geological mapping and soil-gas measurements; b) direct measurements of indoor radon concentration (Dubois and Bossew, 2006). For instance maps based on indoor radon measurements and integrating geological information, are used in Great Britain (Miles and Appleton, 2005) and Belgium (Cinelli et al., 2010), whereas maps based on soil-gas measurements have been developed in Germany (Kemsky et al, 2009) and Czech Republic (Barnet et al, 2008).

A previous study on the natural radioactivity in the Vulsini Volcanic District (Lazio, Italy) has been carried out (ref.) reporting the amounts of natural radionuclides (^{238}U, ^{232}Th and ^{40}K) in volcanic products, used as bulding material, and indoor radon measurements obtained from different buildings in the Bolsena village. According to the relatively high measured concentrations of ^{226}Ra (the direct precursor or ^{222}Rn) in volcanic products, radon concentrations in soil-gas can be expected higher than in other geological situations.

Since a significant fraction of the indoor radon is expected to originate from foundations (Kemski et al., 1996; Barnet, 2008), in order to estimate the potential for indoor radon accumulation in buildings, a campaign of soil-gas radon measurements have been carried out in Bolsena village.

The collected data have been treated using statistical and geostatistical techniques and compared with geological information. A radon risk map has been finally provided.

5.2 Geological Setting

The Vulsini Volcanic District, exhaustively described in the previous chapter, is located at the northern end of the Quaternary potassic volcanic belt and belong to the Roman Magmatic province form southern Tuscany and Campania (Central-South Italy). Four volcanic complexes have been recognized in the evolution of the district: Paleobolsena, Bolsena, Latera and Montefiascone (Nappi et al., 1991). They developed with alternating effusive and explosive eruptions, with Strombolian, Plinian and Ignimbrite-forming phases. Volcanic products are characterized by a wide range of compositions belonging to the leucite, basanite and shoshonite magmatic suites (Nappi and Valentini, 2005).

The Bolsena volcanic complex mainly tool place in the eastern part of the Vulsini District (see Chap.4, fig. 4.1) after an extensive phase of the subsidence which affected the final activity of the Paleo-Bolsena complex, responsible for a thick sequence of volcano-lacustrine deposits (Nappi

et al., 2005). The Bolsena complex developed during two eruptive cycles (Nappi and Marini, 1986). The first one is characterized by an initial effusive and/or Strombolian phase and a short-time final explosive and effusive phase. On the contrary the second cycle is made up of a moderate initial effusive and/or Strombolian phase and a paroxysmal final explosive activity. The oldest products of Bolsena complex are represented by leucite-bearing lava flows outcropping in the N and E sectors. The final phase of the first cycle is characterized by pyroclastic falls, small scale pyroclastic flows, welded tuffs and several outward and inward trachytic lava flows. Phases of volcanic-tectonic collapses took place after this moderate explosive to effusive activity and part of the NE Bolsena caldera was outlined by complex-faulting. N-S and NNW-SSE lines of weakness formed throughout the E side of the present Bolsena Caldera and High Potassic Series magmas were tapped. The leucite-bearing lava flows and scoria cones associated to this activity can be considered the initial phase of the second Bolsena cycle. On the contrary the final stage of the Bolsena complex give rise to the Orvieto-Bagnoregio Ignimbrite pyroclastic sequence (see Chap.4).

The detailed geological formations present around Bolsena village are shown in figure 1.

5.3 Instruments and Methods

A campaign of soil radon concentration measurements was performed in Bolsena village on march 2011 using a continuous radon monitor system (RAD 7, Durridge Co.). Sixty-three measurements have been carried out in an area of about 2 km^2 around the Bolsena's downtown, with a density of about 30 measurements per squared kilometer (Fig. 5.2). Eight soil samples (about 1 kg each), taken as representatives of the whole area, were collected to estimate their permeability and porosity. The measured points have been referenced in the WGS 84 (UTM 32T) geographic coordinate system (Fig. 5.3).
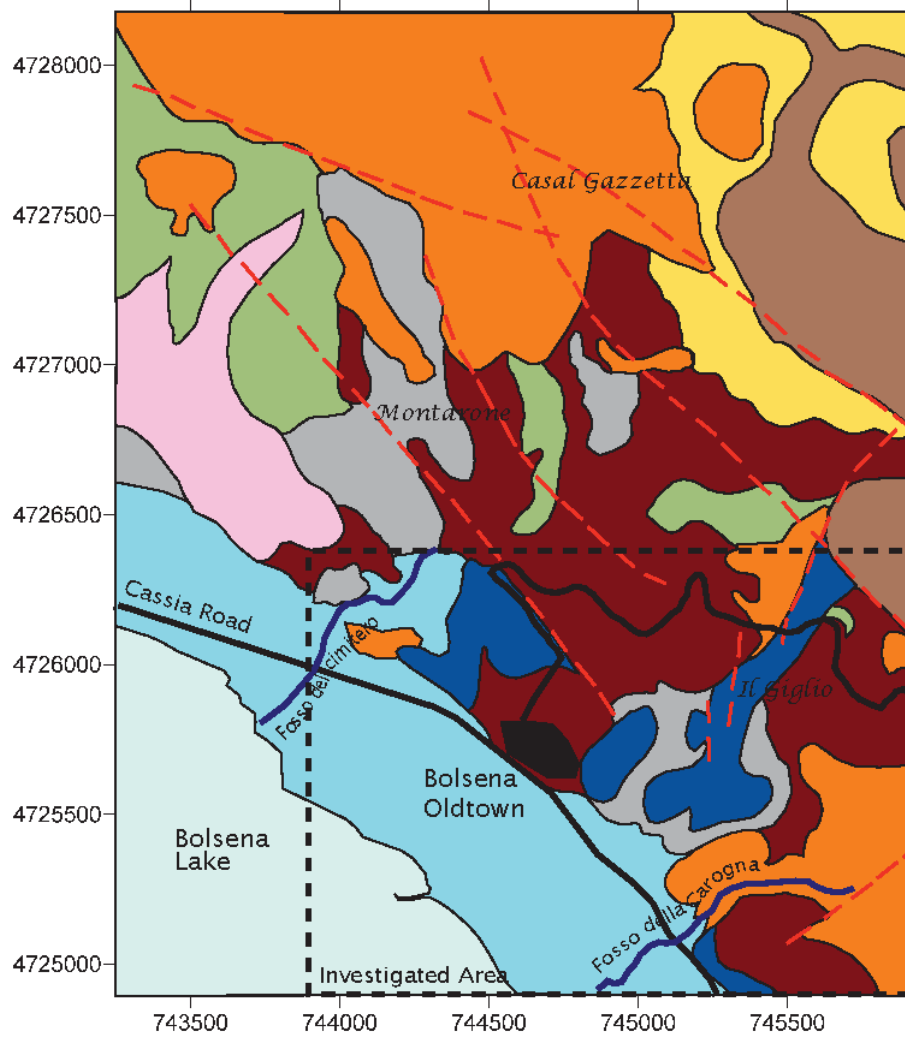
Fig.5.1 Geological sketch map of the area around Bolsena Village (after Renzulli 1988, modified).
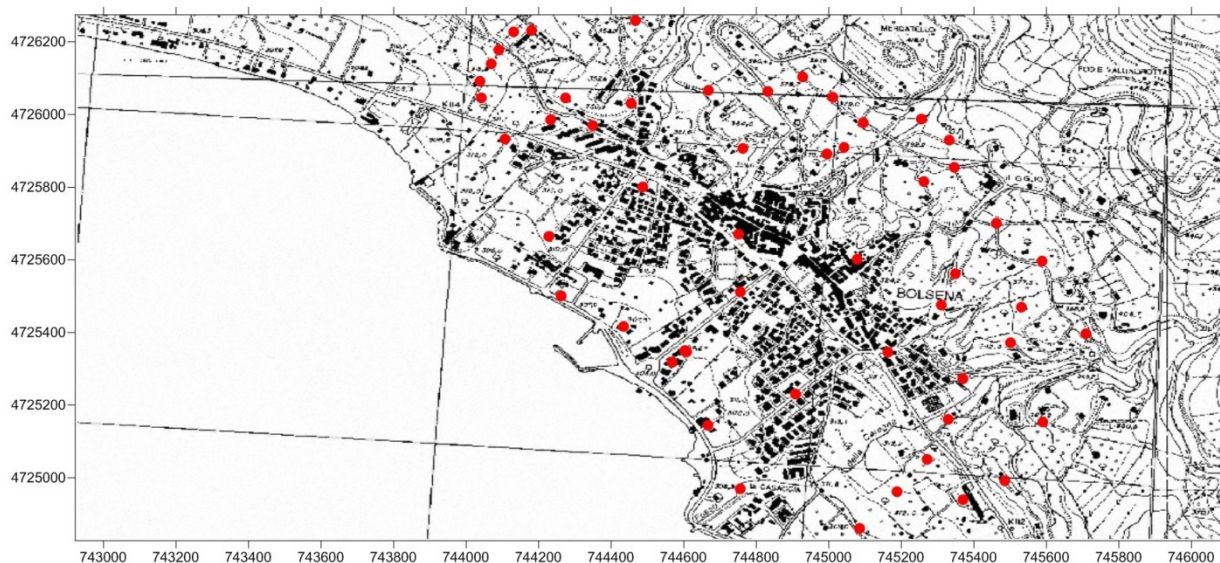
Fig. 5.2 Locations where soil gas radon concentrations have been measured in the city of Bolsena. the measurement points in red.

5.3.1 Sampling and Determination of soil gas radon concentration

The soil gas probe (Durridge), made of stainless steel, is 120 cm long, 1.6 cm outside diameter and 0.8 cm inside diameter. It was inserted to about 60-70 cm depth, checking for a reasonable seal between the probe shaft and the surrounding soil, so that the ambient air did not descend around the probe to dilute gas sample. The pilot rod, 120 cm long and 1.27 cm diameter, was used to make a pilot hole for the probe. A drying unit were connected between the probe head and the continuous radon monitor (RAD 7, Durridge Co.) to keep relative humidity below 10 %. The instrument pumps air from soil, through the desiccant (drierite) and an inlet filter, into the measurement chamber. The filtered air decays inside the chamber, producing detectable alpha emitting progeny, particularly the polonium isotopes. A high voltage of 2500V is applied to the chamber walls. The solid state silicon detector converts alpha radiation directly to an electrical signal discriminating the electrical pulses generated by α-particles from the polonium isotopes of ^{218}Po and ^{214}Po of 6.0 and 7.7MeV, respectively. Using only the ^{218}Po peak for ^{222}Rn, the equilibrium between ^{218}Po and ^{222}Rn is achieved in about 15 min .Using this approach a single measurement has an average duration of 25-30 minutes, with partial reading every five minutes (cycle), and ends when the relative difference between the last two cycles is lower than 15%. The final result is the average of the last two readings.

5.3.2 Permeability of soil

The gas permeability of soils and rocks is one of the most important physical characteristics of soil pertinent to indoor radon. For instance in case of high permeability of soil in the contact between the building and the soil even low soil gas concentrations can cause significant indoor radon concentrations. This parameter is fundamental in the determination of radon risk classification of building sites.

The permeability was derived from the weight percentage of fine fraction (< 0.063 mm). Soil with the weight percentage of the fine fraction < 15 % were designed as high permeable soils, in the range 15-65 % as medium permeable and in the case of the fine fraction above 65 % as low permeable ones (Barnet, 2008). Using this method of classification others factor influencing the permeability (mainly natural moisture, density, effective porosity etc) were not taken into consideration.

5.3.3 Study of data distribution and Mapping Method

Before the construction of a radon risk map is fundamental to study the best distribution to model our data. Different methods has been used to test if our data are normally distributed: histograms, coefficient of Skewness and Kurtosis, Shapiro-Wilk test and quantile-quantile plots.

The *t*-test was applied to test the comparability between different geological groups. The significance level was chosen arbitrarily to be 0.05 both for the normality test and t-test.

"Geostatistics offers a way of describing the spatial continuity of natural phenomena and provides adaptations of classical regression techniques to take advantage of this continuity" (Isaaks and Srivastava, 1989). At the difference of conventional statistics, whatever the complexity and the irregularity of the real phenomenon, geostatistics search to exhibit a structure of spatial correlation. This accounts for the intuitive idea that points close in the space should be likely close in values. What makes geostatistics powerful is its capability to characterize by means of a consistent probabilistic model the spatial structure. This spatial structure is characterized by the variogram.

Because of its probabilistic framework, the geostatistical approach is claiming that the descriptions of the reality are subject to uncertainty, which can be quantified and provide efficient decision tools for practitioners and managers.

Each time experiments are made in a defined space (i.e. data with coordinates and values), a geostatistical approach can be used.

Geostatistics originated from the mining industries where it found acceptance through successful applications to problems where decisions concerning large-investment operations are based on

interpretations of limited and sparse data. Because of the large variety of domains and the related specific problems, many methods are now proposed in literature and software.

Also to analyze the spatial structure of soil-gas radon concentration Geostatistics offers helpful methods and tools (Dubois and Bossew 2006).

Variograms has been studied using isotropic standardized variograms in Surfer8 (Surfer8).

The methodological approach used in this study to construct a map of soil radon concentration and a radon risk map based on soil gas radon measurements and geological information consists of :

(a) Division of the region in cells of 0.01 square kilometer;

(b) Association of geological information to each cell;

(c) Application of geostatistical techniques to calculate mean radon concentration and association with each cell of the corresponding value of mean;

(c) Estimate in each cell the radon index (RI).

The area is divided in cells of 100 m constructing a square grid. Each cell is characterized by a coordinate couple that represents the center of the cell.

The geological map (Fig. 5.1) have been geo-referenced and geology for each cell is determined; the geology at the center of each cell is assigned to the cell.

Using the code Surfer, the predicted mean at one node (cell center) is evaluated using an exact interpolator and a smoothing interpolator applied to the radon concentration. Inverse Distance to Power has been chosen as exact interpolator using 2 as weighting power. Instead as smoothing interpolator has been applied Kriging considering only the nugget effect in the variagram model, which makes Kriging equivalent to the simple moving average (Tondeur, 2006), called hereafter Moving Average interpolator.

The following values are considered:

• 15: the maximum number of data to use; this value limits the total number of points used when calculating a grid node.

• 10: the minimum number of data; node is doubtful if fewer.

• 500 m: the distance (radius) from the grid node that Surfer looks up to find data points when calculating the mean at the grid nodes.

The radon risk classification (table 5.1) has been based on a modified version of the method used in Czech Republic (Barnet, 2008).

Radon Index (RI) category	Soil gas radon concentration c(kBq/m3)		
Low	c < 30	c < 20	c < 10
Medium	30 ≤ c < 100	20 ≤ c < 70	10 ≤ c < 30
High	c ≥ 100	c ≥ 70	c ≥ 30
	Low	**Medium**	**High**
	Permeability		

Table 5.1 Radon index (risk) assessment (Barnet, 2008).

To estimate the radon index the soil gas radon concentration considered was the third quartile and the value for which the cumulative probability of the distribution (chosen to best fit our data) is 0.75, so the equivalent of the third percentile using observed data.

In addition the percentage of high Radon Index has been estimated. This percentage above the chosen threshold (CL), which depends on soil permeability, has been calculated assuming normal distribution using the following expression:

$$\% \, highRI = \int_{CL}^{\infty} \exp\left(-\frac{(x-\bar{x})^2}{2 \times \sigma_g^2}\right) \times \frac{1}{\sigma_g \times \sqrt{2\pi}} \, \delta x \quad (4)$$

Where $\bar{x}$ is the mean of soil gas concentration and σ is the standard deviation of the considered group of data.

5.4 Results and Discussion

5.4.1 Simplified radon concentration profile in soil

The following general equation describes the radon concentration in the pore air in a differential volume of soil considering the transport of radon by molecular diffusion and forced convection and the production and removal of radon by radioactive decay (Nero, 1988):

$$\frac{\partial C}{\partial t} = \nabla \cdot \left(D_e \nabla C + C \frac{k}{\varepsilon \cdot \mu} \nabla P\right) - \lambda_{Rn} C + G \qquad (1)$$

where C is the radon concentration in pores (Bq/m^3), D$_e$ the effective diffusion coefficient (m^2/s), k the permeability, ε the porosity, μ the viscosity of air, P the pressure, λ_{Rn} the radioactive constant of radon and G is the volumetric radon generation rate in the soil pores (Bq·m^{-3}·s^{-1}) defined by the equation (2):

$$G = A_{Ra} \cdot \rho \cdot f \cdot \lambda_{Rn} \cdot \left(\frac{1 - \varepsilon}{\varepsilon}\right) \qquad (2)$$

where A_{Ra} is the activity concentration (Bq/kg) of ^{226}Ra and f the emanation factor, defined as the ratio between the radon activity emanating in the air-filled pores to the total radon production in the material. The equation 1 should be solved numerically to study realistic solutions, coupled with an air flow model. However, a precise knowledge of the relevant parameters D_e, k, ε, G in every point is often impossible to achieve. A general trend may be shown in a schematic approach considering the soil a semi-infinite, homogeneous, isotropic, steady state system and transport is limited to one-dimensional diffusion toward the surface. Under these conditions, considering the concentration in the atmosphere C(z=0) = 0 and C(-∞) = G/λ_{Rn} at equilibrium:

$$C(z) \approx \left(1 - e^{z\sqrt{\lambda_{Rn}/D_e}}\right) \cdot C(-\infty) \quad (3)$$

The density ρ was set at 2650 kg/m^3, the porosity ε at 0.434, the coefficient of diffusion D_e at $2\cdot10^{-6}$ m^2/s for normal soil, $5\cdot10^{-6}$ m^2/s for dry soil and $2\cdot10^{-5}$ m^2/s for wet soil. The calculated diffusion profile in an ideal soil is reported in fig. 3. In the first case (fig.3a) the ^{226}Ra activity and emanation coefficient was fixed at 221 Bq/kg and 0.23 respectively. These values are the average of these related to Bolsena formation reported in the previous chapter. In the second case (fig.3b) the ^{226}Ra activity was fixed at 142 Bq/kg and the emanation coefficient 0.33 on the basis of gamma spectrometry analysis carried out on two samples of soil collected in the site point C60 and C41.
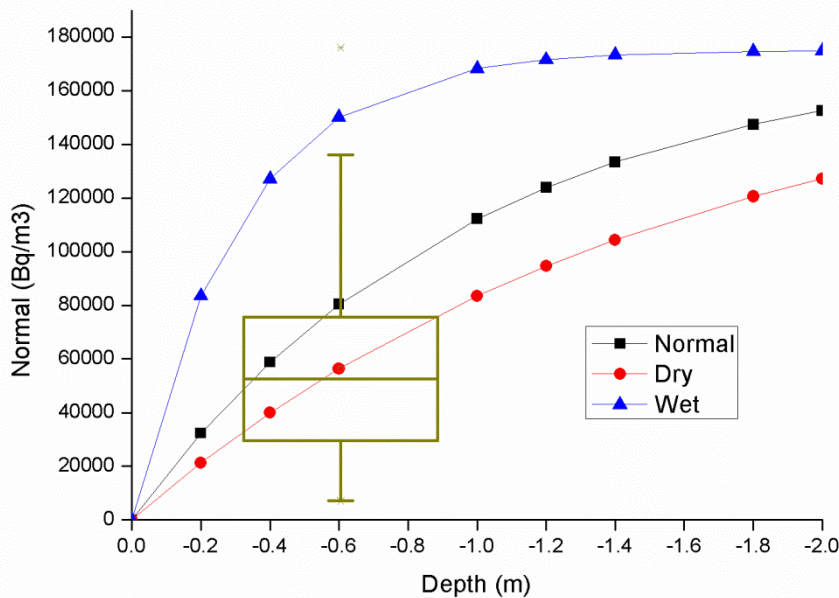
a)
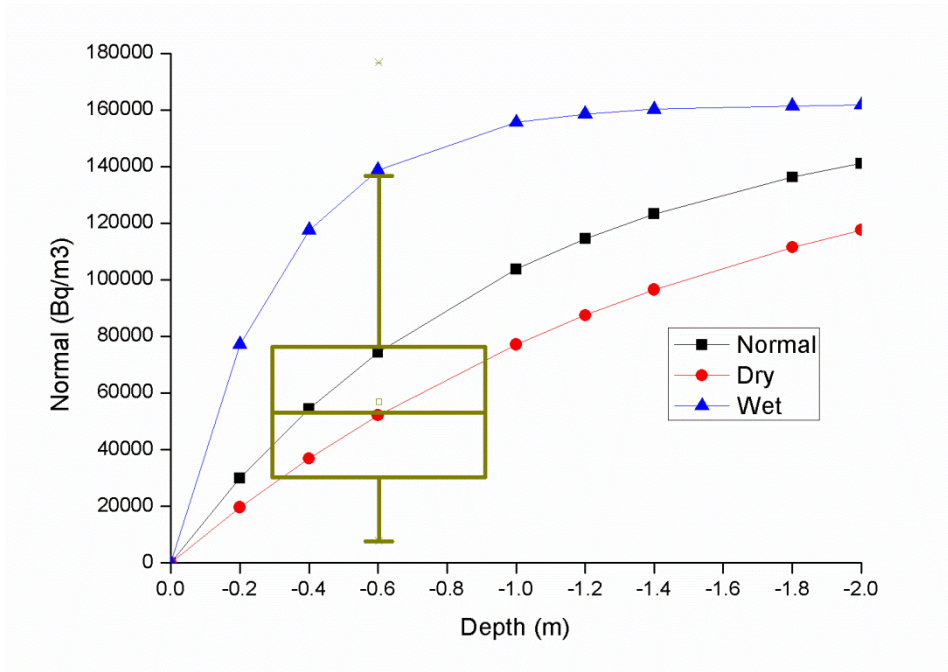
b)

Fig. 5.3 Calculated diffusive profile in an ideal soil, having soil proprieties specified above, using ^{226}Ra activity and emanation coefficient from rock samples (a) and from soil samples (b). Box- whisker plot using soil gas measurements: the box ranges between 25/75th percentiles and the whisker coefficient is 1.5, outliers are indicated with crosses.

The values of concentration of the ideal cases for normal soil, in which only the diffusive transport is considered, at depth of 60-70 cm (Fig. 5.4a-Fig. 5.4b), are similar to the average of the collected data that is about 56 kBq/m^3 considering the full database (Table 5.2). The soil radon gas concentration ranges between 7 kBq/m^3 and 176 kBq/m^3.

The histogram for the full database (in blue in Fig. 5.4) presents two peaks, the first at about 30 kBq/m^3 and the second at 60 kBq/m^3. These peaks can be explained by the presence of two different groups of data belong to two distinct geological areas (fig. 5.1). In fact as suggested also by Nappi (1982) the map in Figure 5.1 can be simplified considering only two main formations: alluvial and volcanic products. The latter groups all lithologies that have a direct volcanic origin. So data are organized in these two geological groups (Table 5.1).

	Total	Volcanic Products	Alluvial
Valid N	63	36	27
Mean	56.2	66.9	42.0
Median	52.4	66.2	36.9
Minimum	7.0	9.3	7.0
Maximum	176.0	176.0	90.9
1.Quartile	29.6	42.9	24.2
3.Quartile	75.6	86.3	63.2
Std.Dev.	33.5	35.6	24.6
Skewness	0.93	0.81	0.49
Kurtosis	1.47	1.27	-0.73
p-value S-W test	0.0084	0.1886	0.1257
p-value t-test		0.0028	

Table 5.2 Main statistics parameters of soil gas radon concentrations (kBq/m^3) considering the full database and the geological groups separately. The p-value of the Shapiro-Wilk test and t-test are reported.
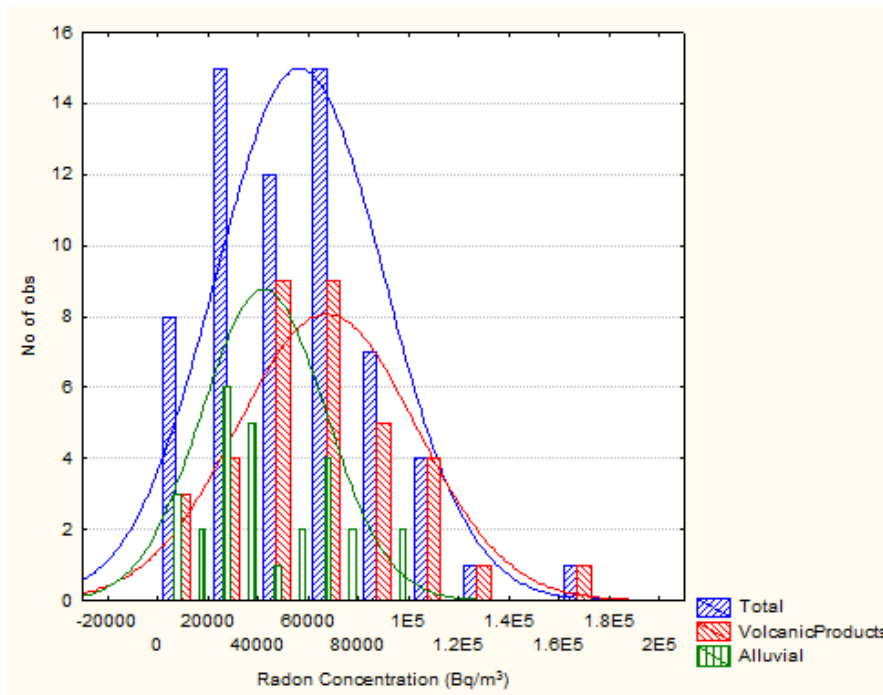
Fig. 5.4 Histogram and normal distribution fit (continue line) considering total database (blu) and the two geological groups separately (green-alluvial, red-volcanic).

The histogram of alluvial data (green in Fig. 5.4) shows a peak in correspondence of the first peak of the total histogram, while the volcanic data (red in Fig. 5.4) of the second one.

Observing our histograms a normal distributions have been assumed to model our data (Fig. 5.5). The hypothesis of normality has been verified for the total database and for the data coming from the two geological groups using the Shapiro-Wilk test (Table 5.2). Only for the full database the hypothesis of normality is rejected at the 0.05 level, while considering the two geological groups separately it is retained (tab. 5.1). Observing the histograms and the quantile-quantile plots (Fig. 5.5) the normal distribution seems to fit our data.
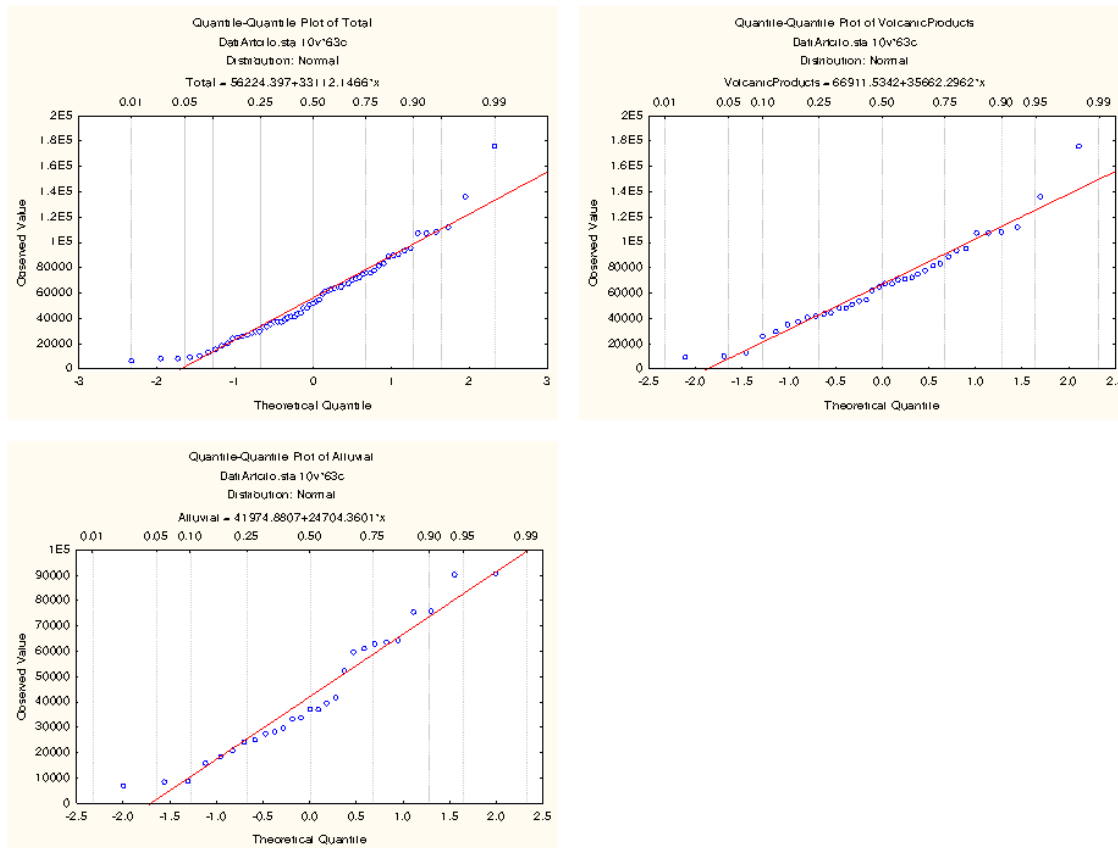
Fig. 5.5 Normal quantile-quantile plots for the total data and for volcanic products and alluvial geological groups.

In table 5.1 statistical parameters are reported for radon measurements considering also the two different geological groups. The t-test shows that these two groups of data are not statistically compatible ($p < 0.05$). At the present time the available information are not enough to establish which parameters most affect the radon soil concentrations such as to determine the difference between the two groups.

The Skewness values are all positive, and they are significantly greater than zero, it indicates that the distributions of data are thus positively skewed, i.e. the high concentration tail is probably stronger than with the normal distribution.

The kurtosis are greater than zero (normal distribution), apart for the alluvial geological group, so they can be described as leptokurtic.

Table 5.3 reports the comparison between our data and reference statistics obtained from literature.

^{222}Rn (kBq/m^3)	Min	Max	Mean	Median	LQ	UQ	SD
Italy[a]	0.4	1200	26.6	13.7	5.5	32.6	39.5
Bolsena Total	7.0	176.0	56.2	52.4	29.6	75.6	33.5
Ciampino-Marino	1.5	367.3	52.0	30.5	23.3	64.8	47.2
Volcanic areas(Italy)[a]	0.4	393.3	43.4	28.5	12.2	59.9	45.0
Czech Republic[b]	1	1663.9	28.1	-	-	-	40.4
Protezozoic-Paleozoic volcanites[c]	-	233.8	28.5	21.7	10.9	37.1	28.7
Terziary volcanites[c]	-	197.20	21.14	16.20	6.90	26.0	25.8

[a]Beaubien et all, 2003; [b]Dubois, 2005; [c]Barnet, 2008

Table 5.3 Comparison of soil gas radon concentration in Italy and in Czech Republic.

The mean of our data is doubtless higher than that using all Italian data, but also higher than that of volcanic areas and Czech data.

The comparison with the Ciampino-Marino data is of significant importance. In fact the Ciampino and Marino Districts are located in the Alban Hills, the most southerly of the Quaternary Volcanic complex, characterized by the same potassic and ultrapotassic volcanism. Data collected in Bolsena (Volsini Volcanic District) present a mean slightly higher, a standard deviation slightly lower and a median much higher (similar to the mean) than the Ciampino-Marino. It means that Bolsena data, as confirmed by the histogram, quantile-quantile plot and normality test, present a distribution almost symmetric around the median. This kind of distribution and the maximum value not so high in comparison to Ciampino-marino can suggest that in Bolsena area the surface component, i.e.^{222}Rn

activity induced by ^{238}U content in the rocks is dominant compared to the deep component, i.e.^{222}Rn activity induced by rapid geogas uprising through faults. (Etiope and Lombardi, 1994).

The variograms have been studied for the full database and considering separately the two geological groups. They present important statistical fluctuations, and the best model to apply is not clearly visible (Fig. 5.6) observing the isotropic variograms. In addition also anisotropic experimental variograms has been calculated using an angular tolerance of 30° but they don't show any different variability in different directions.
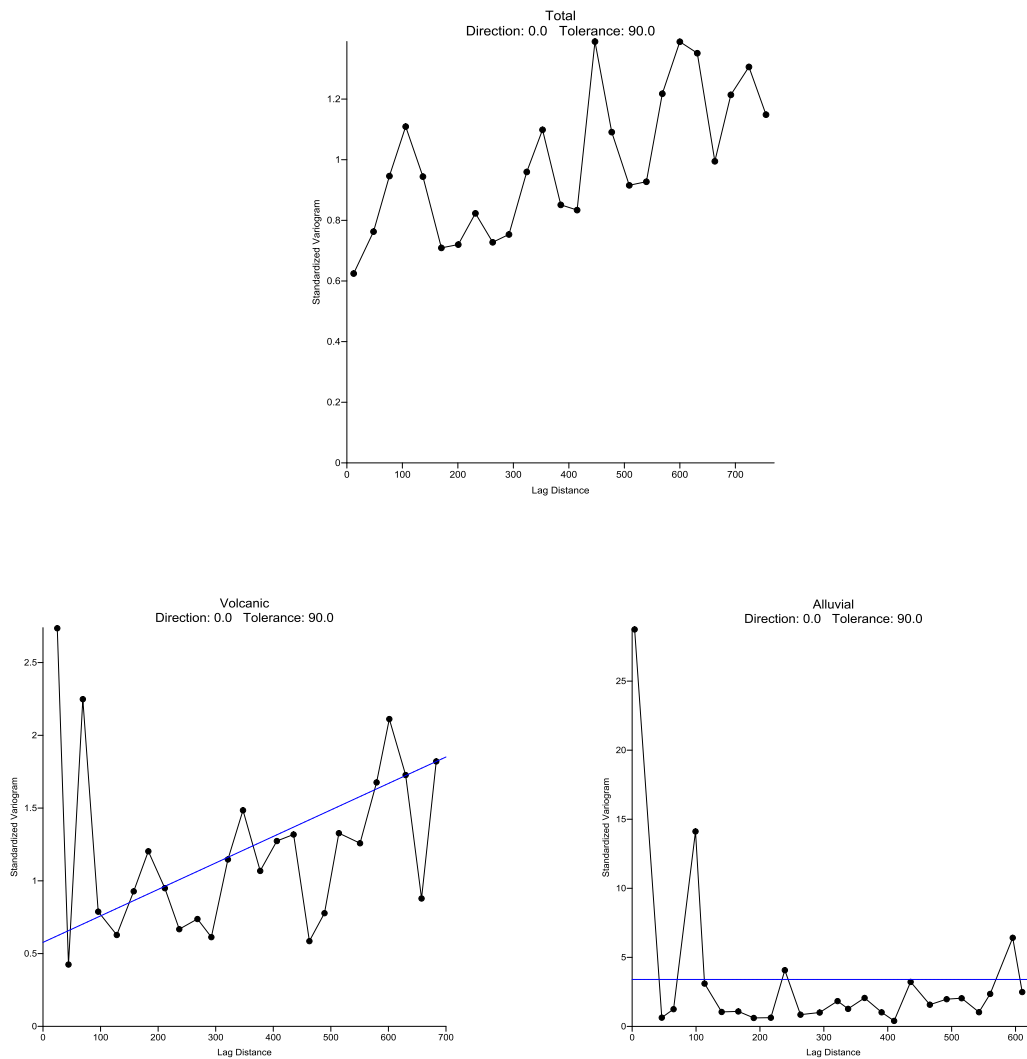
Fig. 5. 6 Variograms of the total database and considering the two geological groups.

5.4.2 Mapping of mean radon concentration

The maps of radon soil gas concentration has been constructed separately for each geological units and with the methods and parameters previously described assuming that the data are normally distributed. In each cell the mean radon soil concentration is reported.

The two maps, the first using Inverse Distance to Power (Fig. 5.7a) interpolator and the second using the moving average (Fig. 5.7b) are reported. It can be noticed that the first map presents some cells with high concentration (120 kBq/m^3) and low concentration (10 kBq/m^3), while in the second the values are spread in a restricted range (30 kBq/m^3 - 85 kBq/m^3). This is due to the different methods of interpolation, in fact the moving average being a smoothing interpolator tend to smooth the data while the Inverse Distance to Power present the generation of " bull's-eyes" surrounding the position of observations within the gridded area.
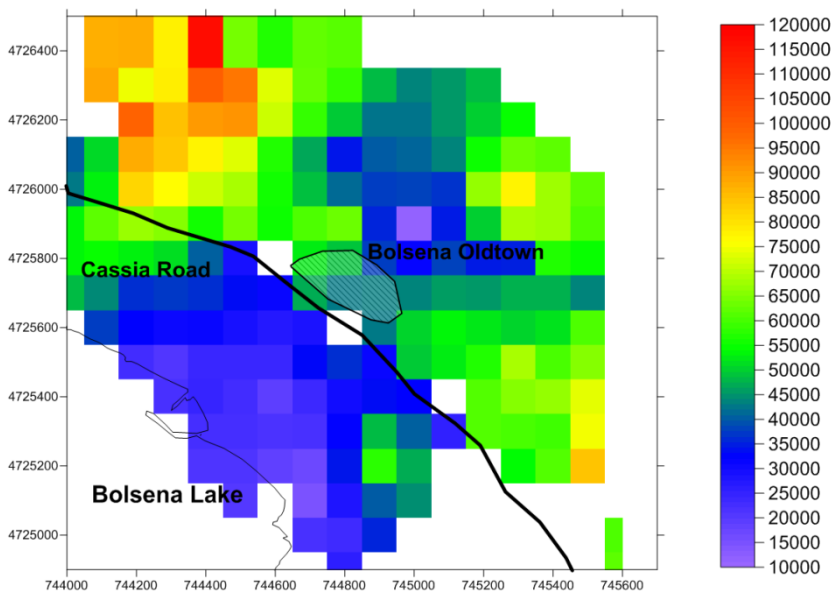
a)
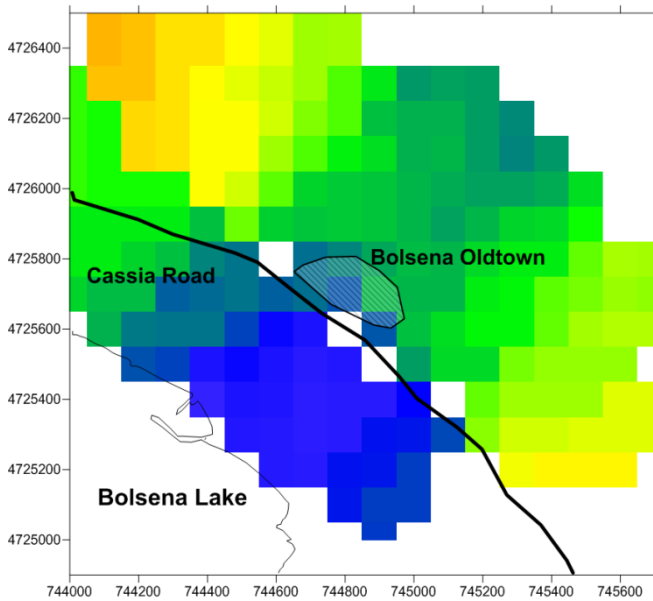
b)

Fig. 5.7 Map of radon soil concentrations in Bq/m³ based on geology and soil gas measurements, using a) Inverse Distance to Power interpolator, b) Moving Average.

5.4.2 Radon Risk Assessment

Permeability, derived from the particle size distribution for all soil samples, are medium, so the whole area can be assumed as medium permeable soil.

In the first analysis, taking in account the total database and the geological groups separately, the third quartile for the soil radon concentration data has been considered for the risk classification (Tab. 5.1). The assumption of normal distribution of data allow to use also the value for which the cumulative probability of the distribution is 0.75. The values using observed data and normal distributions for the total and the two geological groups are similar; the choice of normality for our data is confirmed. The percentage of high radon index, considering the threshold (CL in equation 4) fixed at 70 kBq/m³ (medium permeability) for the total database and the two geological groups are reported in table 5.3.

The total database shows a percentage of 34% for high radon risk with an high Radon Index. Considering instead the two geological groups separately the alluvial presents a medium Radon Index with a percentage of 13 versus the higher 47 of volcanic.

The maps of the radon index estimated in each cell using the value of 75% cumulative are reported in Figures 8 a and b for the two different interpolative methods.

Using the Inverse to Distance Power interpolator the 53% of the cells can be classified as an high radon risk area, while using the Moving Average interpolator the 64% of the cells can be classified as an high radon risk area.

^{222}Rn(Bq/m^3)	Using Observed Data		Using Normal Distribution		
	Third Quartile	Radon Index	Cumulative probability 0.75	Radon Index	% high Radon Index
Total	75567	High	78846	High	34
VolcanicProducts	86284	High	90949	High	47
Alluvial	63208	Medium	58547	Medium	13

Table 5.3 Comparison between the third quartile of observed data and the value corresponding to 0.75 cumulative probability, percentage of high radon index considering the entire database and the two geological groups separately.

a)   b)
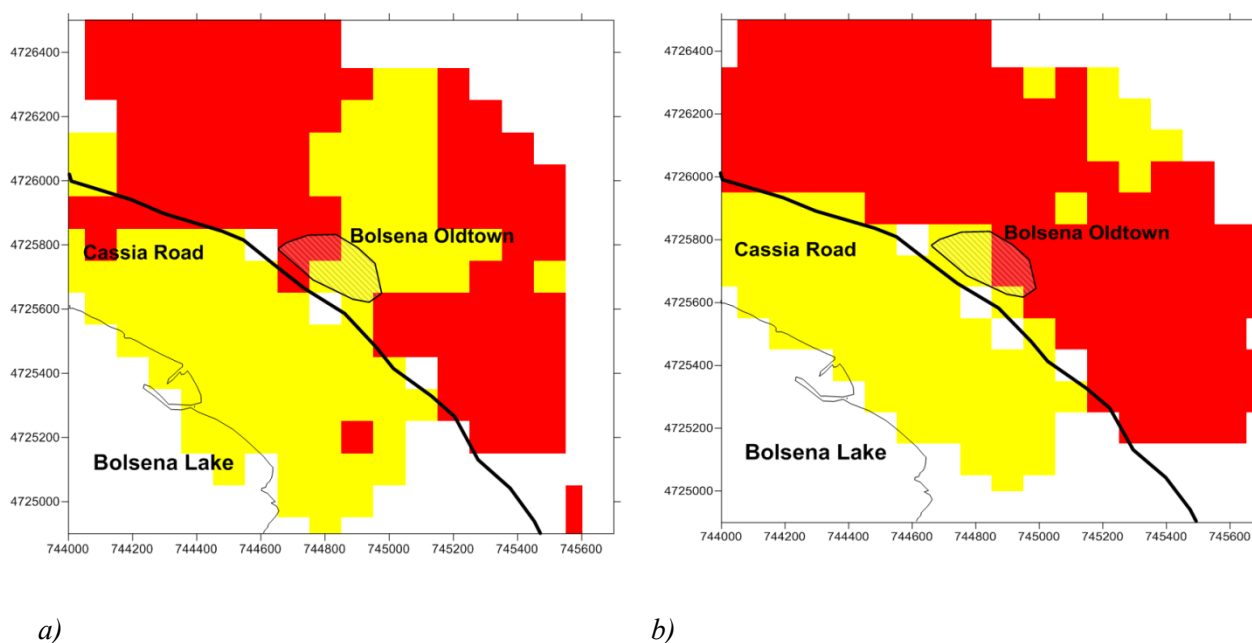
Fig. 5.8 Maps of Radon Index, in red high and in yellow medium, using a) Inverse Distance to Power interpolator, b) Moving Average.

The maps reporting the percentage of high Radon Index estimated in each cell using in the equation 4 the mean concentration estimated in each cell (fig. 5.7) and the standard deviation of alluvial or volcanic group depending on the geology assigned to each cell, is reported in figures 5.9a e 5.9b.
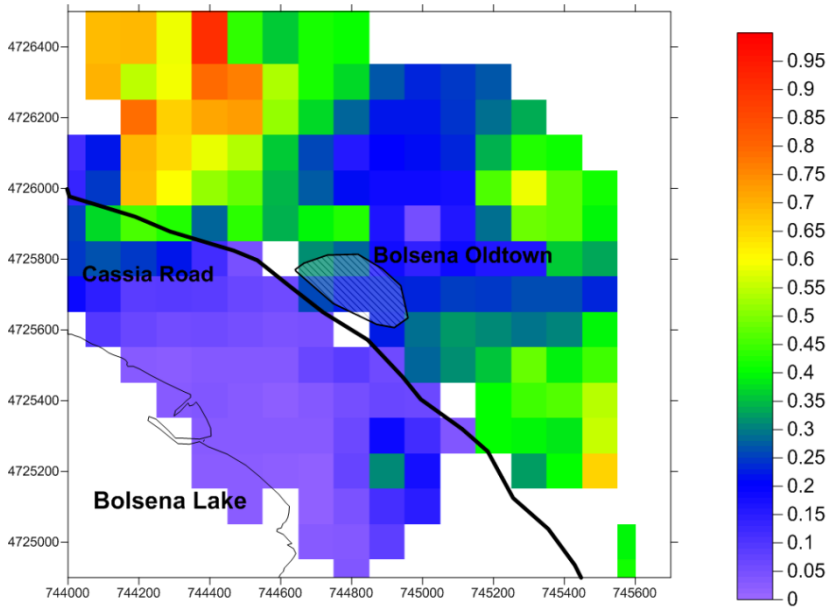
a)
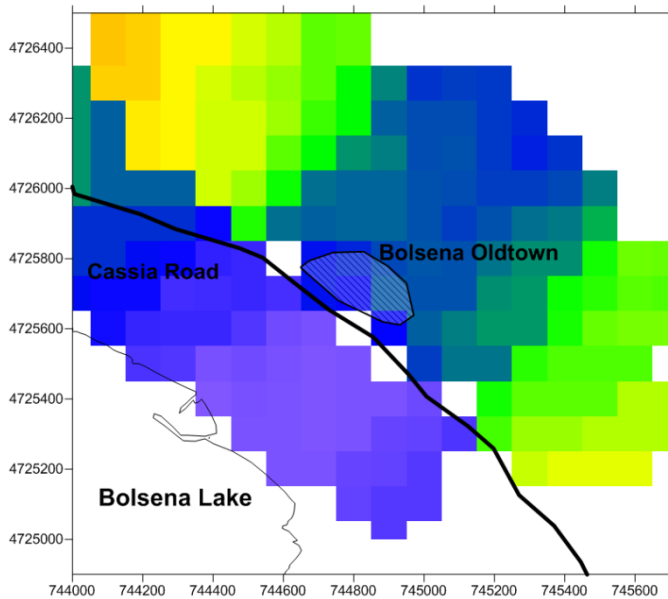
b)

Fig. 5.9 Maps of percentage of high Radon Index, using a) Inverse Distance to Power interpolator, b) Moving Average in the estimation of the mean radon concentration.

The maps highlight the presence of an area, close to the lake associated to the alluvial geology, characterized by lower risk values. This area shows percentage of high Radon index lower that 30%. The volcanic geologic area, the upper part, is characterized by percentage higher than 30% until 95% (Inverse Distance to Power) or 70% (Moving Average). White color indicates cells where less than 10 data in a radius of 500 m have been found in the same geological group.

The central part of volcanic area presents lower values than the external parts. Observing Figure 1 can be noticed that the central part of the sampling area is characterized by products from Bolsena volcanic complex and the external part by volcanic product of Orvieto volcanic complex. Grouping data from Bolsena volcanic Complex and Orvieto can be found respectively a soil gas radon concentration mean value of 64 kBq/m^3 and 80 kBq/m^3. In the previous chapter data ^{226}Ra concentration in rock samples are reported. Grouping data coming from Bolsena and Orvieto complex respectively a mean of 187 Bq/kg and 231 Bq/kg have been obtained. The higher value of ^{226}Ra concentration in rocks from Orvieto volcanic complex can justify variability of the soil gas concentrations in the volcanic part.

5.5 Conclusions

Sixty-three soil gas measurements have been carried out in Bolsena village:

a) The histogram of soil radon measurements presents two peaks associated to two different geological groups, alluvial and volcanic. The data, considering the two groups separately, fit a normal distribution (normality test) and the t-test assesses that they are statistically not comparable.

b) The surface component ^{222}Rn activity induced by ^{238}U content in the rocks seems to be dominant compared to the deep component.

c) The two geological groups are considered separately in the development of the radon soil concentration maps and the risk maps. The Inverse Distance to Power and Moving Average have been used as interpolators.

d) Both methods show that the studied area is mostly an high radon risk area, and future construction have to take into account of this risk.

References

Barnet I., Pacherová P., Neznal M., Neznal M., 2008. *Radon in geological environment – Czech experience* Czech Geological Survey Special Papers, No. 19, Prague, 2008, pp. 19-28

Beaubien, S.E., Ciotoli, G., Lombardi, S., 2003. *Carbon Dioxide and Radon Gas Hazard at the Alban Hill Area (Central Italy)*. Journal of Volc. and Geoth. Research 123, 63-80.

Bossew P, Dubois G (2006) *From Babel to the round table of Camelot: on setting up a common language and objective for European radon risk mapping.* Radon investigation in the Czech republic XI, Czech Geological Survey, Prague Canberra (1987) Radon analysis CISE 437. Canberra Industries Inc, Meriden, CT

Cinelli,G., Tondeur,F., Dehandschutter, B., 2010. *Development of an indoor risk map of the Wallon region of Belgium, integrating geological information,* Environ Earth Sci 62:809–819

Dubois G., 2005. *An overview of radon surveys in Europe.* Radioactivity environmental monitoring emissions and health unit institute for environment and sustainability JRC—European commission. EUR 21892 EN, EC, pp 168

Etiope, G, Lombardi, S., 1994. *Soil Gas ^{222}Rn in Sedimentary Basins in Central Italy: Its Implications in Radiation Protection Zoning,* Radiat Prot Dosimetry 56 (1-4): 231-233.

Isaaks EH, Srivastava RM (1989) *An introduction to applied geostatistics.* Oxford University Press, New York, p 561

Kemski J, Klingel R, Siehl A., 1996. *Classification and mapping of radon-affected areas in Germany.* Environm Int; 22, 1: S789-S798.

Kemski J, Klinger R, Siehl A, Valdivia-Manchelo M , 2009. *From radon hazard to risk prediction-based on geological maps, soil gas and indoor measurements in Germany.* Environ Geol 56:1269–1279.

Metzeltin S. and Vezzoli, L., 1983. *Contributi alla geologia del volcano di Latera (Monti Vulsini, Toscana Meridionale – Lazio Settendrionale).* Mem. Soc. Geol. Ital., 25, 247-27.

Miles JCH, Appleton JD , 2005. *Mapping variation in radon potential both between and within geological units.* J Radiol Prot 25:256–276.

Nappi,G., Chiodi, M., Rossi, S., Volponi, E., 1982. *L'Ignimbrite di Orvieto nel quadro dell'evoluzione vulcanico-tettonica dei vulsini orientali caratteristiche geologiche e tecniche.* Boll.Soc.Geol.It., 101, 327-342.

Nappi, G., Marini, A., 1986. *I cicli eruttivi dei Vulsini Orientali nell'ambito della vulcano tettonica del complesso.* Mem. Soc. Geol. Ital., 35: 679-687.

Nappi, G., Renzulli, A. and Santi, P., 1991. Evidence of incremental growth in the vulsinian calderas (Central Italy). *J. Volcanol. Geotherm. Res*. 47, 13–31.

Nappi, G., Capaccioni, B., Renzulli, A., Santi, P. and Valentini, L., 1994b. *Stratigraphy of the Orvieto-Bagnoregio Ignimbrite eruption (Eastern Vulsini District, Central Italy)*, Mem. Descript. Carta Geol. Ital. 49, 241–254

Renzulli, A., 1988. Rilevamento geo-petrografico e studio geochimico del Complesso Vulcanico di Bolsena (Vulsini orientali): relazioni tra vulcanismo e magmatismo. Tesi di Laurea in Scienze Geologiche, Università degli Studi di Urbino, pp 201 (con carta geologica dell'area alla scala 1:12.500)

SURFER, 1999. User's guide, Golden Software

Tondeur F , 2006. Mapping indoor radon in the Walloon region: kriging vs moving average, international assessment for mathematical geology, XI International Congress, Universite´ de Liege, Belgium.

Zeeb H, Shannoun F, 2009. WHO *Handbook on Indoor Radon: A Public Health perspective.* Geneva, Switzerland: World Health Organization.

Chapter 6 - Epidemiological Studies

6.1 Introduction

Radiological risks associated to natural radioactivity have been estimated in the previous chapters. This risk has been given in term of probability of develop a radiogenic cancer if the local volcanic products (radioactive sources) have been used as building material. Moreover using the measured indoor radon concentrations this risk has been given in term of probability of develop a lung cancer. From radon soil gas measurements the area has been classified as an high, medium or low radon risk area.

Bolsena area has been estimated to be mostly an high radon risk area. In the standard room built with volcanic material the risks associated to external radiation or radon inhalation are much higher than in other Italian area. The risk of lung cancer estimated using indoor radon concentrations reaches in some cases values extremely high (40%).

Next step is to see if epidemiological studies, carried out for the studied area, confirm an increase of number of cancer in the population. Unlikely in our country cancer registrations not cover all the population and some area do not present cancer registries.

6.2 The AIRTUM database

The Italian Network of Cancer Registries (AIRTUM) collects data from both general and specialized population-based cancer registries. AIRTUM verifies data quality and completeness and uses data for collaborative studies on cancer epidemiology in Italy. Cancer registration in Italy started in the 70s and has gradually extended, involving a growing proportion of the Italian resident population (Airtum, 2009).

Area	Regional coverage in 2009 %
Piemonte	25.1
Valle d'Aosta	0.0
Lombardia	35.2
Trentino Alto Adige	100.0
Veneto	48.8
Fruili Venezia Giulia	100.0
Liguria	55.0
Emilia Romagna	71.3
NORTH	48.0
Toscana	33.6
Umbria	100.0
Marche	20.0
Lazio	9.9
CENTRE	25.7
Abruzzo	0
Molise	0
Campania	28.5
Puglia	0
Basilicata	0
Calabria	0
Sicilia	22.6
Sardegna	28.5
SOUTH	15.7
ITALY	32.2

Table 6.1 AIRTUM database. % of population observed by the Italian Network of Cancer Registries (general and specialized), by region and area (Airtum, 2009)

NORTH

CENTRE

SUD
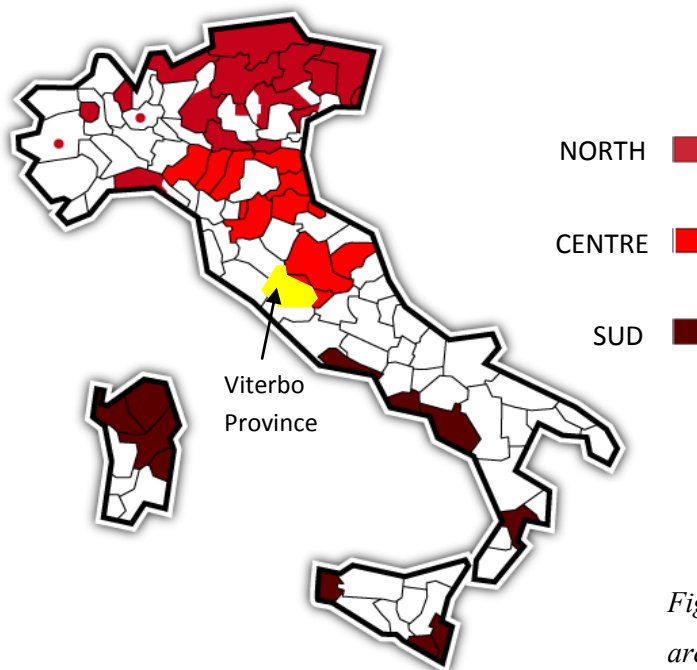
Viterbo
Province

Fig. 6.1 Map of Italy, cancer registry provinces are colored in red, brown and purple. The Viterbo provinces is colored in yellow (Airtum, 2009).

At this time, the AIRTUM database collects data from 26 general and 5 specialized (for age or cancer type) cancer registries. The density of registries is greater in the north of Italy, especially in the north-east, in comparison with the centre and the south. However, cancer registration has recently undergone significant development in the south of Italy, providing a wider dataset for this area. Table 6.1 presents the proportion of the resident population involved in cancer registry activity, for each region and for three geographic areas.

Regional coverage varies from 0% in several southern regions (Calabria, Puglia, Basilicata, Abruzzo, Molise), as well as Val d'Aosta in the north, up to 100% (e.g., Umbria, Friuli Venezia Giulia, Trento and Bolzano).

Statistical models are therefore a useful complement of cancer data collection. Models can be applied to empirical data to produce epidemiological indicators at national and regional scales and to project their estimated values to the near future. A research program, aimed at providing systematic and up-to-date estimates of incidence and prevalence for the major cancers at a regional level, has been established by the Istituto Superiore di Sanità, Rome, and the Fondazione IRCCS "Istituto Nazionale dei Tumori", Milan, in collaboration with the network of Italian Cancer Registries (AIRTum). The most complete output of the program, named "I TUMORI IN ITALIA", will be a cancer statistics data base accessible on a website (www.tumori.net).

Bolsena village is located in the Vulsini Volcanic District, in the Viterbo province, the most northerly of Lazio provinces, on the border between Toscana and Lazio (in yellow in figure 1). The Lazio region has only a cancer register in Latina province with a regional coverage of 9.9% (table 1). It means that epidemiological data for the Viterbo province are not available and for the whole Lazio region data are extrapolated from Latina province.

6.3 Lung cancer

In Italy lung cancer is the third neoplasm in men and the fourth in women, cigarette smoking is responsible of 85-90% of new cases. It was estimated that 5% of lung cancers in men is attributable to occupational exposure (Airtum, 2010). Known risk factors for lung cancer also include passive smoking and environmental exposure to radon and heavy metals.

Radon is considered the second cause of lung cancer in the general population, after smoking. In general the proportion of all lung cancers linked to radon is estimated to lie between 3% and 14%, depending on the average radon concentration in the country and on the method of

calculation (Zeeb and Shannoun, 2009). Further, radon was classified as a human carcinogen in 1988 by IARC, the WHO specialized cancer research agency. So an increase of lung cancer can be directly associated to a radon problem in the area. Assuming that the percentage of smoking population is the same in each part of Italy the lung cancer incidence has been studied for Italian region.

In general two epidemiological measures are used: *prevalence* and *incidence*. *Prevalence* is a measure of how commonly a disease or condition occurs in a population, it measures how much of some disease or condition there is in a population at a particular point in time. The prevalence is calculated by dividing the number of persons with the disease or condition at a particular time point by the number of individuals examined.

$$Prevalence\ Rate = \frac{\text{all new and pre} - \text{existing cases during a time period}}{\text{population during the same time period}}$$

The *incidence* measures the rate of occurrence of new cases of a disease or condition. Incidence is calculated as the number of new cases of a disease or condition in a specified time period (usually a year) divided by the size of the population under consideration who are initially disease free. Incidence shows the likelihood that a person in that population will be affected by the condition.

$$Incidence\ Rate = \frac{\text{new cases occurring duting a given time period}}{\text{population at risk during the same time period}}$$

In the present work only incidence rates for lung cancer have been taken into account because less affected by other parameters such as the process of population aging, the improved survival depending on regional health service.

The estimated incidence rates for 1970-2010 for lung cancer (http://www.tumori.net/it/banca_dati/query.php) considering a mixed population, weighted on male and female populations, are taken into access Incidence estimates refer to the age class 0-84 years. In figure 6.2 the trends of incidence rates are reported considering separately northern (fig. 6.2a), central (Fig. 6.2b) and southern regions of Italy (Fig. 6.2c).
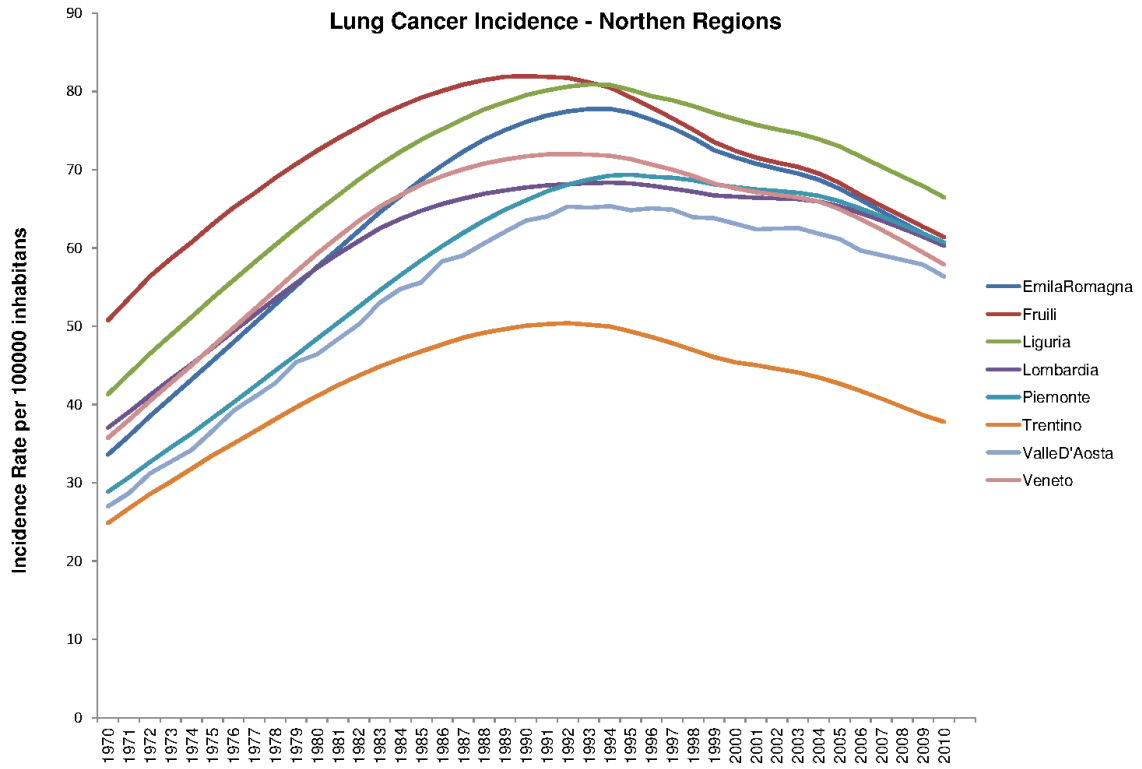
a)
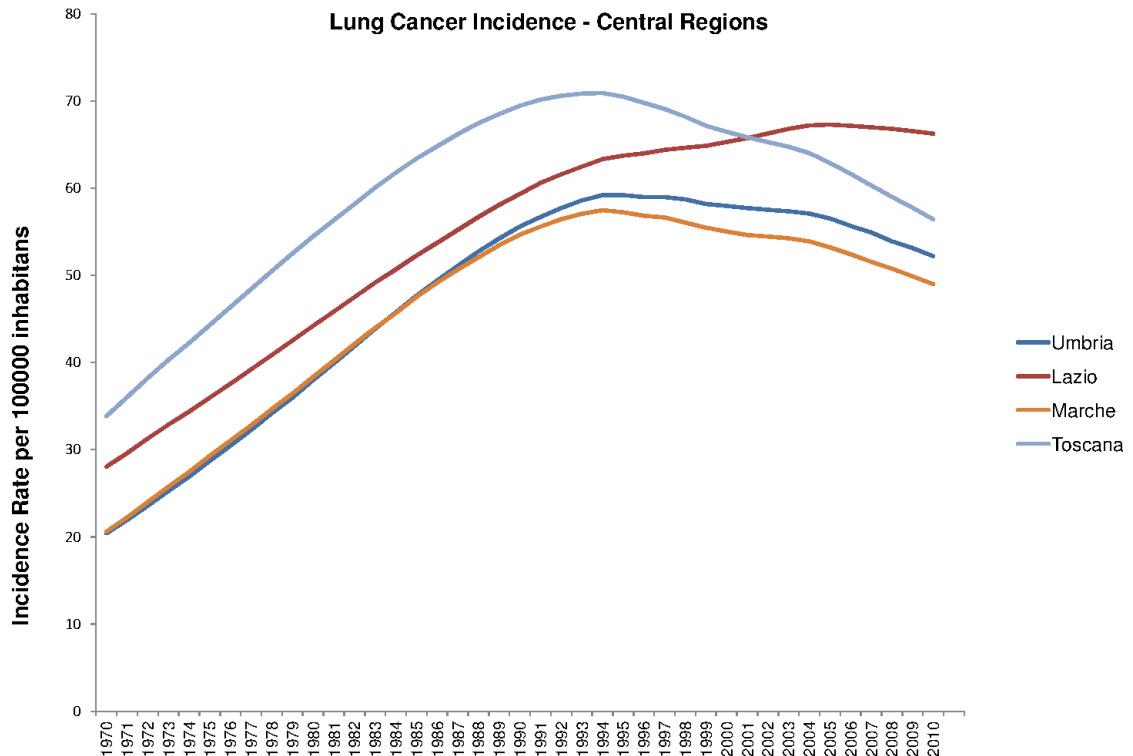
b)
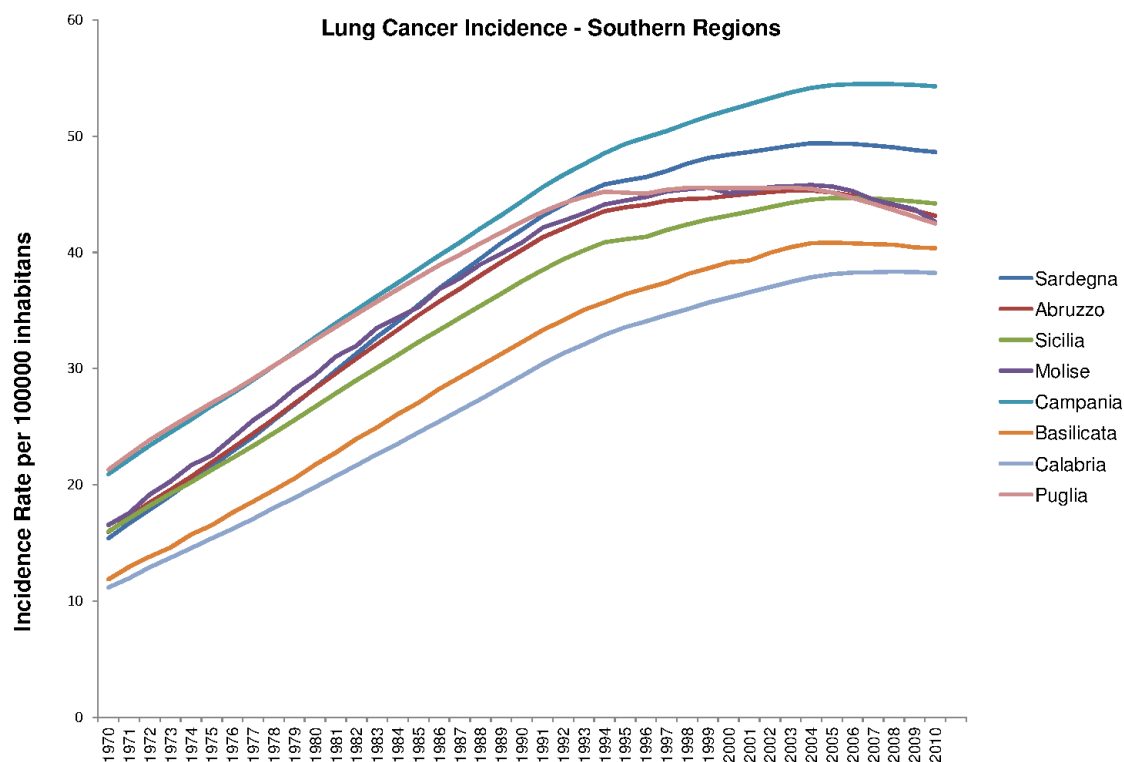
c)

Fig. 6. 2 Trends of lung cancer incidence between 1970-2010 considering in Italy northern (a), central (b) and southern regions (c).

A strong difference between the trends of northern and southern areas can be notice. All the northern regions present a peak around the 1990's while the southern regions an increasing trend until the 2000's, after it seems to be a constant. The central regions, except Lazio, present the same trends of northern ones, with the characteristic peak in the 1990's. Two explanations can be given to justify the peak of the northern regions:

a) the cancer risk has followed the Italian trends in process of industrialization in the 1900's, increasing with the progressive emptying of the countryside and the process of urbanization, and with the change in the rhythms and styles of life and work that has involved millions of Italians (Airtum, 2006);

b) the percentage of smokers has decreased in the male population since the 1970's and this has certainly played a major role in the reduction of the male lung cancer incidence since the 1990's (Grande et al, 2007; Baili at al., 2007).
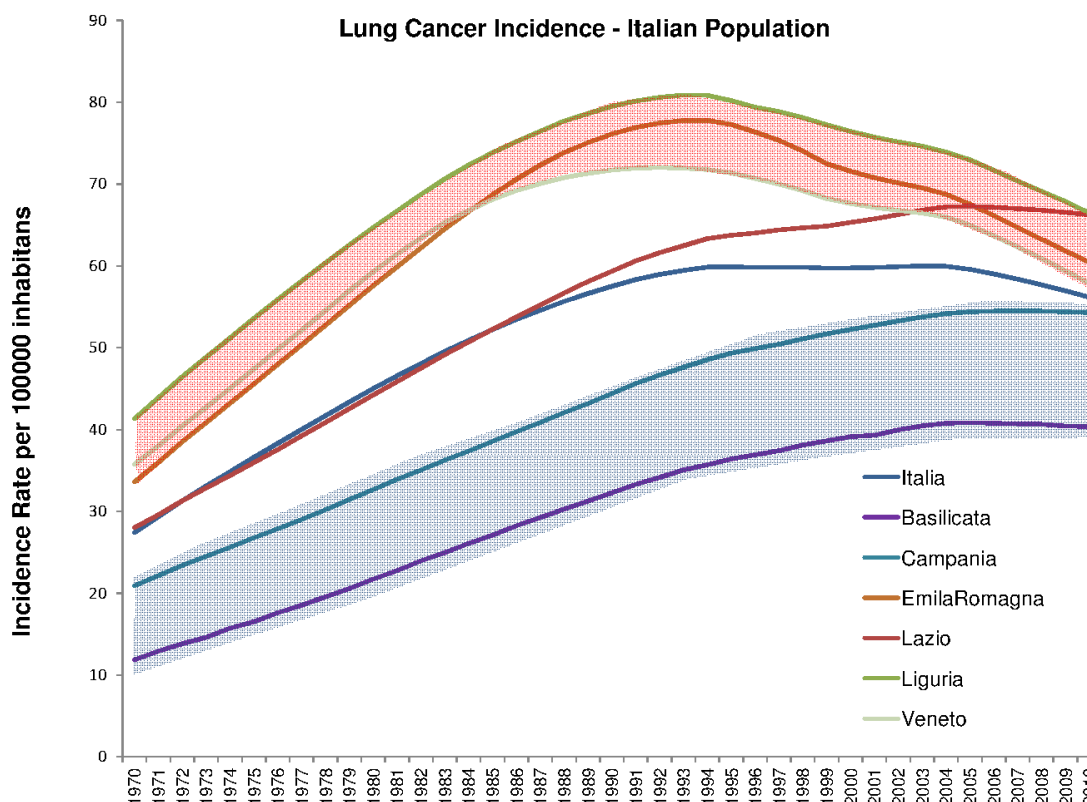
Fig. 6.3 Trends of lung cancer incidence between 1970-2010 considering a mix of northern, southern and central regions, including the Italian average.

Lazio region and some representative northern and southern regions are reported in figure 6.3 for comparison. Incidence rates present an increasing trend, the values are substantially greater than the southern regions.

Lazio region shows a trend similar to the southern regions(blu-fig. 6.3), an increasing trend but the values are substantially higher than these latter. The incidence rate of Lazio region in 2010 is the highest value of Italy.

It can be supposed that the trend of Lazio region, different from the trends of the other regions, can be due to environmental exposure to radon.

Latina province is not located in a volcanic area, but observing geological maps (http://www.isprambiente.gov.it/Media/carta_geologica_italia/tavoletta.asp?foglio=158) some correlations (fig. 6.4) with the volcanic districts can be found.
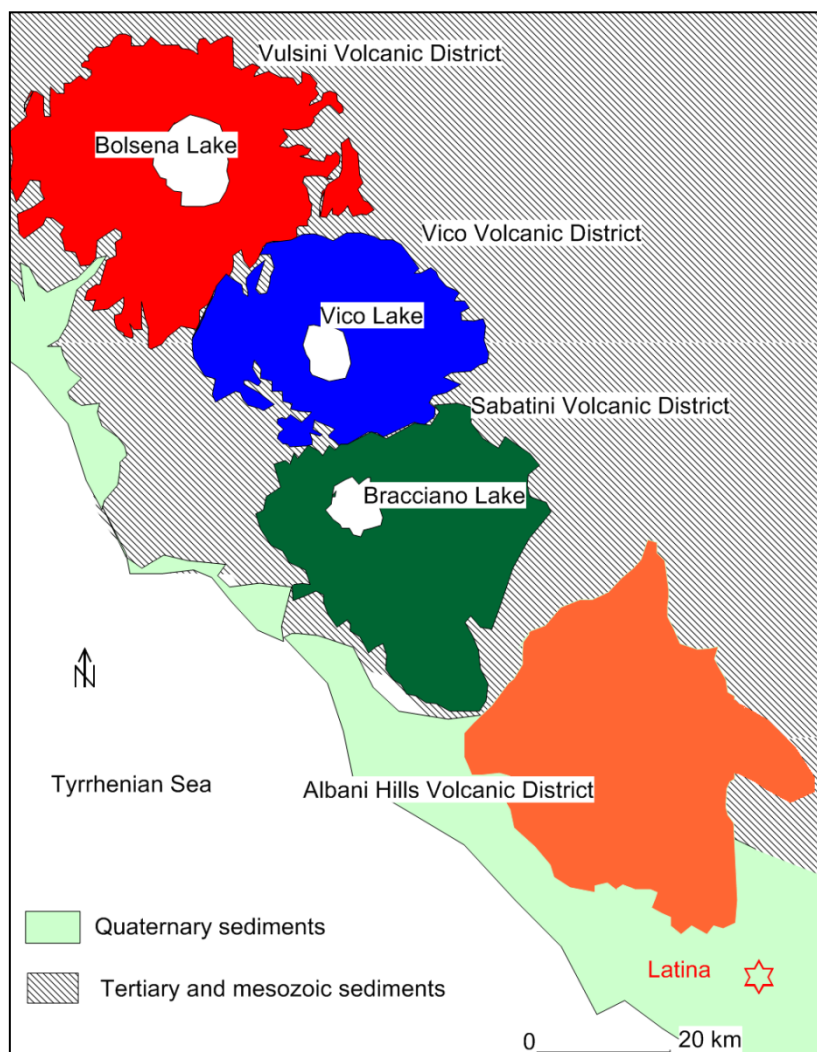
Fig. 6.4 Geological sketch map of the Latium region.

Lazio region presents four volcanic districts: Vulsini (amply studied in this work), Vico, Sabatini and Albani Hills (Fig. 6.4). The products of these volcanoes are widely analyzed in literature, and they are characterized by high concentration of ^{238}U, ^{232}Th and ^{40}K due to subduction-related metasomatic enrichment of incompatible elements in the mantle source coupled with magma differentiation within the upper crust (Conticelli and Peccerillo, 1992).

In fact the Latina province stands at the food of Albani Hills Volcanic District, the most southerly of the four Quaternary volcanic complex. The lithology of Latina province is mostly characterized by quaternary sediments, with some small area of tuff. These sediments have inside sand from decomposition of the volcanic products.

Moreover in this province, as well as in all Latium region, the volcanic tuffs from the four volcanic districts have been widely used as building material thanks to their intrinsic properties described above (De Rita and Ciriaco, 2006; Funiciello et al, 2006).

These considerations on lithology and building materials allow to use epidemiological data from Latina cancer registry also for other areas of Lazio but conscious that there are extrapolated data and not fully representative of our studied area.

Next year (2012) a new cancer registry will be activated in Viterbo province. The data coming from these area will be very important for the present study because they will be representative of the analyzed area.

References

Airtum Working Group, 2006. *Incidence, mortality and estimates*. Epidemiol Prev. 2006 Jan-Feb;30(1 Suppl 2):8-10, 12-28, 30-101 passim. English, Italian.

Airtum Working Group, 2009 *I tumori in Italia – Rapporto 2009. Sopravvivenza*. Epidemiol Prev 2007: 33 (4-5) suppl 1: 14-18.

Airtum Working Group, 2010. *I tumori in Italia – Rapporto 2010. Commenti ai risultati riguardanti i 15 tumori più frequenti*. Epidemiol Prev 2010: 34 (5-6) 150-186.

Baili, P., De Angelis, R., Casella, I., Grande, E., Inghelmann, R., Francisci, S., Verdecchia, A, Capocaccia, R., Meneghini, E. and Micheli A., 2007.Italian cancer burden by broad geographical area). Tumori, 93: 398-407.

Conticelli, S., Peccerillo, A., 1992, *Petrology and geochemistry of potassic and ultrapotassic volcanism in central Italy: petrogenesis and inferences on the evolution of the mantle sources*. Lithos, 28, 221-240.

De Rita, D., Ciriaco, G., 2006, *A case study - Ancient Rome was built with volcanic stone from the Roman land, Cap VI, Tuffs-Their Proprieties, Uses, Hydrology and Resources*. The Geological Society of America.127-131.

Funiciello, R, Heiken, G., Levich, R., Obenholzner J., Petrov V., 2006, *Construction in regions with tuff deposits*, Tuffs-Their Proprieties, Uses, Hydrology and Resources. The Geological Society of America.119-126.

Grande, E., Inghelmann, R., Francisci, S., Verdecchia, A., Micheli , A., Baili, P., Capocaccia, R., De Angelis R., 2007.Regional estimates of all cancer malignancies in Italy. Tumori, 93: 345-351.

Verdecchia A, De Angelis R, Francisci S, Grande E: Methodology for estimation of cancer incidence, survival and prevalence in Italian regions. Tumori, 93: 337-344, 2007.

Zeeb H, Shannoun F, eds. WHO Handbook on Indoor Radon: A Public Health perspective. Geneva, Switzerland: World Health Organization; 2009.

Chapter 7 – Conclusions

Concerning the improvement of the analytical methods, in this thesis an important result has been obtained for *in situ* γ-spectrometry using Sodium Iodide detector. Thanks to the Monte Carlo based calibration developed in the present work a quantitative analysis of ^{238}U, ^{232}Th and ^{40}K can be performed posing the detector above the ground or indoor building materials. It is very useful in the situations in which a sample cannot be collected for in laboratory analysis, like for ancient buildings and houses. Moreover this kind of calibration allows us to disengage from calibrations sources, i.e., calibration pads widely used, that have a cost and may deteriorate.

The Vulsini Volcanic District, well known area of high natural background has been chosen as area of study. The volcanic products, mostly consisting of lithified pyroclastic deposits (ignimbrites, auct.), have been largely used as building material since a very early age. Moreover, during the Middle age, their upper almost flat surface coupled with their overlooking position and stability have promoted the development of villages on top of the pyroclastic plateaux. Houses made of tuffs together with their location on volcanic basement have produced remarkable high external and internal indoor exposure for population living in the area.

Rocks sampled from the Latera and Bolsena complexes of the Vulsini Volcanic District show high contents of natural radionuclides: ^{238}U (6-32 ppm), ^{232}Th (31-120 ppm), and K (0.7 to 8 %). This exceptional enrichment in natural radionuclides is possibly due to a coupled effect of source composition and magma evolution at shallow levels. Lithification due to glass → zeolites conversion does not provide significant enrichment/depletion of ^{238}U and ^{232}Th, while they appear to undergo a remarkable enrichment during acid hydrothermal alteration.

The indoor radon campaign carried out in the Bolsena Village show values from 243 to 3152 Bq/m^3, more than the threshold value recommended by the European Commission (EC, 1990). The highest values measured in building made of tuffs, where the cumulative risk of developing a lung cancer reaches extremely high values, in the range 20-40%.

Simulation of a "standard" room, assumed built with the different sampled volcanic rocks of the Vulsini Volcanic District, have provided the lifetime risk of lung cancer due to radon inhalation and the cancer risk from the other pathways. External exposure and radon inhalation are the dominant contributions to the total risk, the others being negligible. The probability of radiogenic cancer

morbidity due to external doses ranges from 0.77 to 3.22 %, while that of fatal lung cancer due to radon inhalation ranges from 0.88 to 8.20 % for ever smokers and from 0.16 to 1.46 % for never smokers. In the "standard" room it has been estimated that at 0.3 h^{-1} air exchange building rate the radon becomes the dominant contributor to dose.

Soil gas measurements show a mean doubtless higher than that using all Italian data, fully comparable with those of the Ciampino and Marino Districts (Alban Hills). The surface component ^{222}Rn activity induced by ^{238}U content in the rocks seems to be dominant compared to the deep component. Data can be grouped into two different geological groups, statistically not comparable. The two geological groups are considered separately in the development of the radon soil concentration maps and the risk maps by means geostatistical techniques. The studied area is mostly an high radon risk area, and future construction have to take into account of this risk.

Epidemiological data available were not fully appropriate to confirm or not an increase of number of cancer in the population of Vulsini area. In fact in our country cancer registrations, performed by the Italian Network of Cancer Registries (AIRTUM), not cover all the population and some area do not present cancer registries. Epidemiological data for the Viterbo province are not available and for the whole Lazio region data are extrapolated from Latina province. So only assumptions can be done waiting cancer registry for the Viterbo province.

The main artificial radionuclides detected in ambient aerosol at two elevated stations in northern Italy under the influence of the Fukushima plume transit were ^{131}I(0.020-0.548 Bq/m^3), ^{137}Cs(0.012-0.250 Bq/m^3) and ^{134}Cs (0.010-0.222 Bq/m^3). A comparison of peak inhalation doses from Fukushima nuclides, natural gamma emitters and the overall average dose from all sources in the studied area indicate that the contribution of the accident to background radiation doses is factually negligible with respect to those naturally related to the Bolsena area. Infact, the comparison between doses due to natural radioactivity in the Vulsini Volcanic District and those due to artificial radioactivity consequential to nuclear accidents has shown that the natural ones in some case can have definitely higher values.

Indoor and soil radon concentrations, contents of natural radionuclides in the volcanic products and their evaluation show that the Vulsini Volcanic District is with no doubts a Radon-prone area.

Acknowledgements

Appendix I

C NaI placed on soil, cylinder with radius fixed at 100 cm, and thickness at 30 cm, mono-energetic isotropic volumetric source 2.614 Mev

C cells Cards
61 1 -3.6667 -13 -4 3 IMP:P=1 $NaI
73 7 -2 -19 -1 36 IMP:P=1 $ suolo
63 3 -1.205E-3 (-4 13 -12 2):(-3 2 -13) IMP:P=1 $ air space
64 4 -2.7 (-11 12 -4 2):(1 -2 -11) IMP:P=1 $ al
65 3 -1.205E-3 -19 -18 1 #61 #63 #64 IMP:P=1 $ air outside
66 0 19:-36:18 IMP:P=0 $ air outside
c end of the cells cards

c surface cards
1 pz 0 $ base cylinder al
2 pz 0.05 $inner cylindrical al
3 pz 0.25 $ base NaI
4 pz 7.85 $ top NaI
11 cz 4.1 $ outer al NaI
12 cz 4.05 $ inner al NaI
13 cz 3.8 $ outer NaI
18 pz 100 $ outtop
19 cz 100 $ out
36 pz -30
c end surface

SDEF ERG=2.614 CEL=73 POS=0 0 0 axs=0 0 1 RAD=d1 EXT=d2 PAR=2
SI1 0 100
SI2 -30 0
c tallies
MODE P
F8:P 61
E8 0 0.00001 0.001 1020i 3
FT8 GEB 0.0153 0.04294373 0
CUT:P 1j 0.05 3j
c end tallies

c Material cards
m1 11000 0.5 53000 0.5 $ NaI
m2 14000 0.33333 8000 0.66667 $ PM
m3 7014 0.81122 8016 0.18878 $ air
m4 13000 1 $ al
m5 14000 -0.326 20000 -0.107 11000 -0.11 8000 -0.457 $ glass
m6 6000 2 1000 4 $ polyetilen
m7 14000 -0.2161 22000 -0.004 13000 -0.0817 26000 -0.0451 25000 -0.0012 &
 12000 -0.0243 20000 -0.0508 11000 -0.0062 19000 -0.0233 15000 -0.0022 &
 1000 -0.0302 8000 -0.5151 $ soil V01
c end material cards

PTRAC file=asc write=all
c

NPS 300000000

C NaI placed on rock, cylinder with radius fixed at 125 cm, and thickness at 50 cm. mono-energetic isotropic volumetric source 2.614 Mev

C cells Cards
61 1 -3.6667 -13 -4 3 IMP:P=1 $NaI
73 7 -2 -19 -1 36 IMP:P=1 $ suolo
63 3 -1.205E-3 (-4 13 -12 2):(-3 2 -13) IMP:P=1 $ air space
64 4 -2.7 (-11 12 -4 2):(1 -2 -11) IMP:P=1 $ al
65 3 -1.205E-3 -19 -18 1 #61 #63 #64 IMP:P=1 $ air outside
66 0 19:-36:18 IMP:P=0 $ air outside
c end of the cells cards

c surface cards
1 pz 0 $ base cylinder al
2 pz 0.05 $inner cylindrical al
3 pz 0.25 $ base NaI
4 pz 7.85 $ top NaI
11 cz 4.1 $ outer al NaI
12 cz 4.05 $ inner al NaI
13 cz 3.8 $ outer NaI
18 pz 100 $ outtop
19 cz 125 $ out
36 pz -50
c end surface

SDEF ERG=2.614 CEL=73 POS=0 0 0 axs=0 0 1 RAD=d1 EXT=d2 PAR=2
SI1 0 125
SI2 -50 0
c tallies
MODE P
F8:P 61
E8 0 0.00001 0.001 1020i 3
FT8 GEB 0.0153 0.04294373 0
CUT:P 1j 0.05 3j
c end tallies
c Material cards
m1 11000 0.5 53000 0.5 $ NaI
m2 14000 0.33333 8000 0.66667 $ PM
m3 7014 0.81122 8016 0.18878 $ air
m4 13000 1 $ al
m5 14000 -0.326 20000 -0.107 11000 -0.11 8000 -0.457 $ glass
m6 6000 2 1000 4 $ polyetilen

m7 14000 -0.2161 22000 -0.004 13000 -0.0817 26000 -0.0451 25000 -0.0012 &
 12000 -0.0243 20000 -0.0508 11000 -0.0062 19000 -0.0233 15000 -0.0022 &
 1000 -0.0302 8000 -0.5151 $ soil V01
c end material cards
PTRAC file=asc write=all
c

NPS 625000000

C NaI detector placed on rock, mono-energetic isotropic volumetric source(cylinder with 50 cm thickess,125 cm radius) ^{40}K (1.46 Mev)

C cells Cards
61 1 -3.6667 -13 -4 3 IMP:P=1 $NaI
73 7 -2 -19 -1 36 IMP:P=1 $ Roccia
63 3 -1.205E-3 (-4 13 -12 2):(-3 2 -13) IMP:P=1 $ air space
64 4 -2.7 (-11 12 -4 2):(4 -5 12 -11):(-21 20 5 -6): &
      (-14 15 6 -8):(1 -2 -11):(8 -9 -14) IMP:P=1 $ al
62 2 -1.207 (-5 22 -13):(-10 5 -6):(6 -7 -16) IMP:P=1 $ PM
68 6 -1.123 -24 -23 9 IMP:P=1 $ digibase
67 5 -2.2 -13 4 -22 IMP:P=1 $ glass
65 3 -1.205E-3 -19 -18 1 #61 #63 #68 #64 #62 #67 IMP:P=1 $ air outside
66 0 19:-36:18 IMP:P=0 $ air outside
c end of the cells cards

c surface cards
1 pz 0 $ base cylinder al
2 pz 0.05 $inner cylindrical al
3 pz 0.25 $ base NaI
4 pz 7.85 $ top NaI
5 pz 11.1 $ beginning cone
6 pz 12.3 $ end cone
7 pz 22.1 $ top PM
8 pz 22.3 $ inner top cylinder al
9 pz 22.35 $ top cylinder al
10 kz 14.9 1 $ cone
11 cz 4.1 $ outer al NaI
12 cz 4.05 $ inner al NaI
13 cz 3.8 $ outer NaI
14 cz 2.9 $ outer al PM
15 cz 2.85 $ inner al PM
16 cz 2.6 $ outer PM
18 pz 100 $ outtop
19 cz 125 $ out
20 kz 15.15 1 $ cone
21 kz 15.2 1 $ cone
22 pz 8.35 $ glass
23 pz 30.35 $ top DigiBase
24 cz 3.15 $ DigiBase
36 pz -50
c end surface

```
SDEF ERG=1.46 CEL=73  POS=0 0 0 axs=0 0 1  RAD=d1 EXT=d2 PAR=2
SI1 0 125
SI2 -50 0
c tallies
MODE P
F8:P 61
E8 0 0.00001 0.001 1020i 3
FT8 GEB 0.0153 0.04294373 0
CUT:P 1j 0.05 3j
c end tallies
c Material cards
m1 11000 0.5 53000 0.5 $ NaI
m2 14000 0.33333 8000 0.66667 $ PM
m3 7014 0.81122 8016 0.18878 $ air
m4 13000 1 $ al
m5 14000 -0.326 20000 -0.107 11000 -0.11  8000 -0.457 $ glass
m6 6000 2 1000 4 $ polyetilen
m7 14000 -0.2161 22000 -0.004 13000 -0.0817 26000 -0.0451 25000 -0.0012 &
 12000 -0.0243 20000 -0.0508 11000 -0.0062 19000 -0.0233 15000 -0.0022 &
 1000 -0.0302 8000 -0.5151 $ V01
c end material cards
PTRAC file=asc write=all
c
RAND STRIDE=1450
c
NPS 5000000000
```

Appendix II - Comparison between natural and artificial doses[4]

1 Introduction

From the March 11th 2011 devastating tsunami in Japan a cloud containing radioactivity formed in air over the Fukushima nuclear power plant. In occasion of this contingency radioactivity data have been collected by our research group at Monte Cimone and Montecuccolino stations.

This data are discussed, including comparison between local natural background of airborne particulate and artificial radioactivity in connection with the arrival of the radioactive plume, and its persistence and evolution.

Effective doses to the Italian population due to inhalation of the radionuclides detected have been estimated and comparison between the natural and the artificial components has been done.

An educational trip in June 2011 has been organized for student of Energy and Nuclear Engineering of the University of Bologna to visit the area of the Chernobyl Nuclear Power Plant (Ukraine). Dose rates directly measured in the vicinity of Chernobyl nuclear power plants, where nuclear disaster has occurred, are presented for comparison with doses received from population living in the Vulsini Volcanic District.

1.1 Fukushima Accident

On March 11th 2011 at 14:46 JST (05:46 UTC) a 9.0-magnitude earthquake struck the western Pacific Ocean at a relatively shallow depth of 32 km, with its epicenter at 38.322°N 142.369°E, approximately 72 km east of the Oshika Peninsula of Tōhoku (Japan) and 150 km north-east of Fukushima Dai-ichi Nuclear Power Station (USGS, 2011).

At the time of the quake, units 1-2-3 were under operation at full power and units 4-5-6 in periodic inspection outage. In particular, all the fuel assemblies of unit 4 were placed in the spent fuel pool,

---

[4] Part of this chapter consists of a paper by L.Tositti, E. Brattich, G.Cinelli, A. Previti and D. Mostacci, "*Comparison of radioactivity data measured in PM10 aerosol samples at two elevated stations in northern Italy during the Fukushima event*. Journal of Environmental Radioactivity. Published online.

whereas in unit 5 and 6 the core was loaded (NISA, 2011). Automatic shutdown took place at the first three units following the acceleration due to the earthquake. Subsequently all the reactors have been cooled, initially, using off-site power and then, when these latter failed, resorting to emergency diesel generators. Following the earthquake, a 15 m tsunami arrived about 47 min later, topping the plant seawall and disabling the diesel generators located in the basement of the turbine buildings (JMA, 2011). When emergency batteries eventually failed, the cores of unit 1-2-3 became seriously damaged by the lack of cooling, and large amounts of radionuclides were released, initially because of venting of the primary circuit and subsequently because of severe damage to the reactor building due to probable hydrogen explosions induced by zirconium-water H_2 reaction. Unit 4 building was damaged as well, and radioactivity released from the spent fuel pool. Unit 5 and 6, on the other hand, reached cold shutdown status on March 20th 2011 without significant problems (NISA, 2011).The emission of radionuclides started on 12th March 2011. Iodine-131 and cesium isotopes, among the various radionuclides involved, were released in large amounts.

According to the Rhenish Institute for Environmental Research at the University of Cologne (Germany), a cloud containing radioactivity formed in air over the Fukushima nuclear power plant. The radionuclides were then transported across the Pacific, northward of Japan in the direction of the Arctic Ocean, entered the Atlantic Ocean over Iceland and then diffused over Europe, where they arrived despite dispersion and washout along the trip (Jakobs, 2011). In Europe the first signs of the releases were noted seven days later and the first peak of activity level was registered between March 29th and 30th. The first data on radioactive fallout in Europe were reported from March 24th, 2011, by scientists of Aristotle University of Thessaloniki (40°38'N, 22°58'E), Greece (Manolopoulou et al., 2011).

According to NISA, the Japanese Nuclear and Industrial Safety Agency, the source term consisted of around 150 PBq of ^{131}I and 6 to 12 PBq of ^{137}Cs. Peak values registered in Europe from March 28th until 5th April ranged from less than 1 mBq m^{-3} up to 6 mBq m^{-3} for the particulate fraction of ^{131}I (Masson et al., 2011).

1.2 Measurement Sites

Air sampling was carried out at two locations (see Figure 1): Montecuccolino, starting 1st April 2011, and Mt. Cimone, starting 8th April 2011.

Fig.1 Locations of Montecuccolino and Mount Cimone stations in the northern Italian Apennines (Planiglobe, kk&w - digital cartography).

Montecuccolino

Montecuccolino is a nuclear sciences laboratory of the University of Bologna, founded in the 1960's and still active in the field of nuclear reactor, plasma physics and radiation protection. The Montecuccolino laboratory (44° 27' N, 11° 19' E) is located on the foothills of Bologna, 3.5 km away from downtown, at an altitude of 273 m above sea level. It hosts also the Institute for Radiation Protection of ENEA (Italian National agency for new technologies, Energy and sustainable economic development). Due to the presence of the research nuclear reactors in the past there has always been an intense activity in radiation measurements, and this was utilized following the Fukushima Dai-ichi accident.

Mt. Cimone

The Mt. Cimone Station is a research platform for the observation of meteorological and climatologic parameters of international relevance with an active role within the WMO-GAW

network, recently upgraded to "global station" ranking. Mt. Cimone (44°12' N, 10°42' E) is the highest peak of the Northern Apennines (2165 m a.s.l.), the mountain range dividing the north of Italy from central Italy and the Mediterranean basin. In addition to having a 360° free horizon and to being far from cities and industrialized areas, Mt. Cimone has an elevation such that the measurement station "O. Vittori" lies above the planetary boundary layer during most of the year (Winkler et al., 1998), so that it can be considered representative for the South-European free troposphere (Bonasoni et al., 2000; Fischer et al., 2000), besides being regarded as the most representative WMO-GAW station in Italy. For these reasons, the measurement site affords a suitable location to investigate the influence of regional and long-range transport of polluted air masses on the background free troposphere.

It is worth noting that in the past this station served also as one of the Italian monitoring sites for weapon test fallout by total beta measurement, an activity discontinued in the 1990's (Dietrich et al., 1997). Radioactivity measurements in the aerosol fraction and in the gas (radon) and in the particulate phase have been carried out by the Environmental chemistry and radiochemistry laboratory of the Department of Chemistry "G. Ciamician" of the Bologna University since the mid 1990's. This was in the framework of a collaboration with the ISAC-CNR laboratory of Bologna aimed at the study of stratosphere-to-troposphere exchange through measurement of ^{7}Be (Bonasoni et al., 1999; Bonasoni et al., 2000a; Bonasoni et al., 2000b; Sandrini, 2002; Cristofanelli et al., 2003; Tositti et al., 2004; Cristofanelli et al., 2006; Baldacci, 2006; Cristofanelli et al., 2007; Cristofanelli et al., 2009; Tositti et al., 2011). A time series of ^{7}Be, ^{210}Pb and PM$_{10}$ aerosol mass load data is available for this laboratory starting from 1998.

2 Material and methods

2.1 Experimental activity

The ^{7}Be, ^{210}Pb and aerosol mass loading in the form of PM$_{10}$ have been measured at Mt. Cimone since the early 1990's, however, a steady measurement activity began in 1998 following acquisition of a PM$_{10}$ high volume sampler. The preference for PM$_{10}$ sampling rests on the well-known size distribution of the radionuclides considered, which tend to populate the fine fraction (< 1.0 μm) (Winkler et al., 1998) as a consequence of their physical origin, to wit nuclear spallation reaction in free gas molecule/atoms in the atmosphere for ^{7}Be and decay of gaseous ^{222}Rn to ^{210}Pb. Once formed, both radionuclides become rapidly associated to the finest aerosol particles, becoming

prone to long-range transport. The same fate is shared by those components of radioactive plumes whose radioisotopes are released through high temperature processes and accidents, so that they are first vaporized and thereafter attach onto fine particles, as observed for weapon test fallout and the Chernobyl accident. Still, the 10 μm cut-off allows the substantially quantitative collection of the coarser fraction of aerosols of mineral origin following soil resuspension processes. The supermicron fraction typically of crustal origin (and locally including sea salt contribution) may contain K, U and Th radioisotopes associated to the mineral phases detectable in γ-spectra as a function of meteorological conditions.

At Mt. Cimone, aerosol sampling was carried out with a time resolution of about 48 hours by means of a PM_{10} high-volume sampler (Thermo Environmental Instruments Inc. – Flow rate = 1.13 m^3 min^{-1}) using a rectangular glass fiber filter (20.3 cm x 25.4 cm, exposed area: 407 cm^2). The volume sampled in a period amounted to approximately 3250 m^3. Once collected, samples were transferred to the Laboratory of Environmental Chemistry and Radiochemistry of Bologna University where they were conditioned at a constant temperature (20° C) and relative humidity (30%) prior to weighing for the determination of net mass loads of ambient aerosol. Since high altitude stations such as Mt. Cimone (2173 m a.s.l.) are representative of large regions, but may only partially catch the situation in the lower troposphere, a second sampling point was set at Montecuccolino at the end of March 2011, using analogous sampling conditions and extending the comparison from the activity concentrations of artificial radionuclides to the other γ-emitters detectable in aerosol samples such as [7]Be and ^{210}Pb tracing respectively downward and upward transports.

The γ-emitters in aerosol samples were analyzed on a planar Hyper Pure Germanium crystal detector (HPGe) with a 1500 mm^2 active surface, FWHM 0.73 keV at 122 keV, and energy range 0-900 keV. Spectra were accumulated for 1 day, to optimize peak analysis. Spectra were processed with the software package GammaVision-32, version 6.07, ORTEC.

Efficiency calibration is determined with a blank glass fiber filter traced with accurately weighted aliquots of a standard solution of mixed radionuclides (QCY48, Amersham) supplemented with ^{210}Pb, homogeneously dispersed in drops over the filter surface. Once dried under a hood in ambient conditions, the calibration filter was folded into a polystyrene container in the same geometry as the unknown samples. Quantitative analysis on samples was carried out by subtracting the spectrum of a blank filter in the same geometry, while uncertainty on peaks (k = 1, 68% level of confidence) was calculated propagating the combined error over the efficiency fit previously determined with

the counting error. Minimum detectable activity was calculated making use of the Traditional ORTEC method with a peak cut-off limit of 40%.

Activity data was corrected to the midpoint of the time interval of collection and for the decay during spectrum acquisition. As expected the latter correction was significant only for ^{131}I owing to the short half-life.

Qualitative analysis of the aerosol spectra was carried out using a selected isotope library extracted by the basic ORTEC mask library. As a rule, typical isotopes searched in spectra are ^{7}Be, ^{210}Pb, ^{40}K, γ emitters from the uranium and thorium families, ^{137}Cs and ^{22}Na. This list was supplemented with a further selection of artificial nuclides based on the experience gathered at the time of the Chernobyl accident and above all on the analysis of a couple of fresh Fukushima samples in the month of March 2011. The samples analyzed in our laboratory were obtained by collecting dust from the turbines of a airliner which flew between Tokyo and Milan during the period of maximum airborne radioactivity in Japan. Both samples were very active compared to typical ambient samples and led to identification of the following artificial radionuclides attributed to the release from Fukushima: ^{132}Te, ^{131}I, ^{132}I, ^{133}I, ^{134}Cs, ^{136}Cs and ^{137}Cs. As a result the isotope library was supplemented, for the present study, with all the "exotic" species detected due to the decay of the less abundant, short-lived Fukushima radionuclides. In the present work, results of gamma spectrometry are reported, using the emission at 661.62 keV for ^{137}Cs, 604.66 and 795.76 keV for ^{134}Cs, 364.48 keV for ^{131}I and 185.99 keV for ^{226}Ra. The ^{226}Ra activity was corrected taking into account the contribution of the ^{235}U peak at 185.71 keV, considering the natural isotopic composition of uranium (Gilmore, 2008).

Fallout was also sampled in the city of Bologna collecting bulk (wet+dry) deposition on the roof of the Department of Chemistry during the periods: 18/03-05/04/2011, 01-11/04/2011, 11-27/04/2011, 27/04-18/05/2011. Fallout samples were collected in a barrel with an open surface of 471 cm^2. The samples were recovered by acidification and analyzed in 1 dm^3 Marinelli beakers by low-level low-background gamma spectroscopy.

To integrate the experimental data apparently deriving from an exotic source, back-trajectories analysis was applied. The use of back-trajectories in atmospheric research is presently widespread. In fact they allow both to characterize typical circulation patterns in a given location and to provide a diagnostic tool (either in retrospective or in forecast mode) useful to associate atmospheric composition variation to circulation. In the present work, 3D-kinematic back-trajectories were calculated using the NOAA - ARL (National Oceanic and Atmospheric Administration − Air

Resources Laboratory) Hybrid Single Particle Lagrangian Integrated Trajectory model (HYSPLIT –
4) ((Draxler and Rolph, 2003; http://www.arl.noaa.gov/ready/hysplit4.htm), employing archived
GDAS1 (Global Data Assimilation System) global analysis meteorological data provided by NCEP
(National Weather Service's National Center for Environmental Prediction).

2.2 Dose Estimation

Effective doses and their contribution to the total annual dose to individuals in Italy were estimated,
to evaluate the potential radiological impact to the Italian population due to the arrival of the
radionuclides from the Fukushima Dai-ichi damaged reactors. Estimates refer only to the measuring
site of Montecuccolino, in view of its proximity to a densely populated area, whereas Mt. Cimone is
a research station located in a remote, unpopulated environment.

The effective doses due to inhalation of artificial radionuclides (^{137}Cs, ^{134}Cs and ^{131}I) and natural
radionuclides (^{226}Ra, ^{7}Be and ^{210}Pb) were estimated following specifications in the Italian Law
(Legislative Decree 230/1995, implementing the Council Directive 96/29/EURATOM, based on the
recommendations of the ICRP60). To produce an upper bound estimation of the dose, an inhalation
rate of 1.2 m^3/h, i.e., that of a working adult, and inhalation dose coefficients for children under 1
year of age, the highest activity-to-dose conversion factors, were considered. Iodine is present both
within particulate and in gaseous form, but in the present work only the particulate form was
measured: a particulate-to-total ratio of 0.3 was assumed in dose calculation. This value was chosen
on the basis of Japanese and European experimental data collected during the Fukushima accident
(Masson et al., 2011) and on the basis of Chernobyl data (Battiston et al., 1988). The activity
concentrations of the radionuclides measured in Montecuccolino during the days of 4th and 5th April
2011, the days when the highest concentration of artificial radionuclides was measured, were used.

Measures of radioactivity have been performed directly by our research group during the
educational trip in the area around Chernobyl nuclear power plant (Fig.s 2-3). It remembers that the
nuclear accident at the Chernobyl Nuclear power plant occurred on 26 April 1986.

The air doses rates (µSv/h) have been carried out using Gamma-Scout® and РКСБ-104 (Belvar)
Geiger counters.

In Japan after the nuclear accident the area around the Fukushima Dai-ichi Nuclear Power Plant has
been closely monitored. The data of air dose rates have been collected by JAEA (Japan Atomic

Energy Agency) and MEXT (Ministry of Educational, Culture, Sports, Science and Technology: Japan) and are available in http://www.mext.go.jp/english/.

*Fig.2 Photograph of Chernobyl Nuclear Power Plant, on the left the rest of reactor number 4 (L.Tositti).*

Fig.3 Photograph of the evacuated and not repopulated Pripyat village (L.Tositti).

3 Results and discussion

The occurrence of the Fukushima accident suggested inclusion in the monitoring activity of a number of artificial radionuclides usually neglected, with the exception of ^{137}Cs which occasionally has been detected in the high volume samples collected in this framework. In particular, because of the favourable position of Mt. Cimone, samples from May-June 1998 showed the transit of the ^{137}Cs plume released from Algeciras steel plant due to melting of radio-contaminated metal (Papastefanou et al., 2005; Quélo, 2007; Pham et al., 2011). The ^{137}Cs concentration reported on that occasion was of the order of a few mBq m^{-3} against the usual absence of this nuclide from γ-spectra due to the absence of soil resuspension on the mountain top. As for the other artificial radionuclides, the choice was made in keeping with what was discussed in the experimental section.

The results of γ-spectrometry for each sample collected are reported in Figure 4 for Mt. Cimone and Figure 5 for Montecuccolino. Artificial radionuclide activities are presented in Figure 4a and Figure 4b, whereas natural radionuclides activities are reported in Figure 5a and Figure 5b.
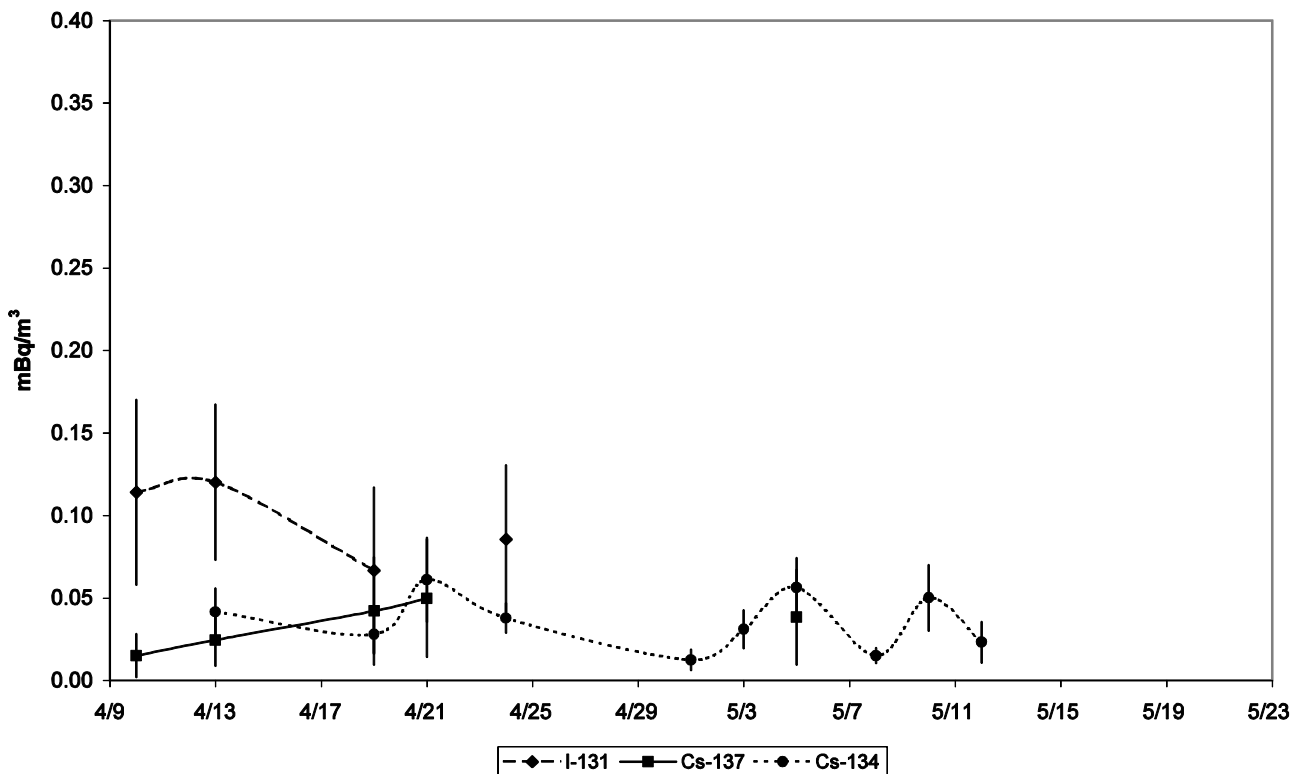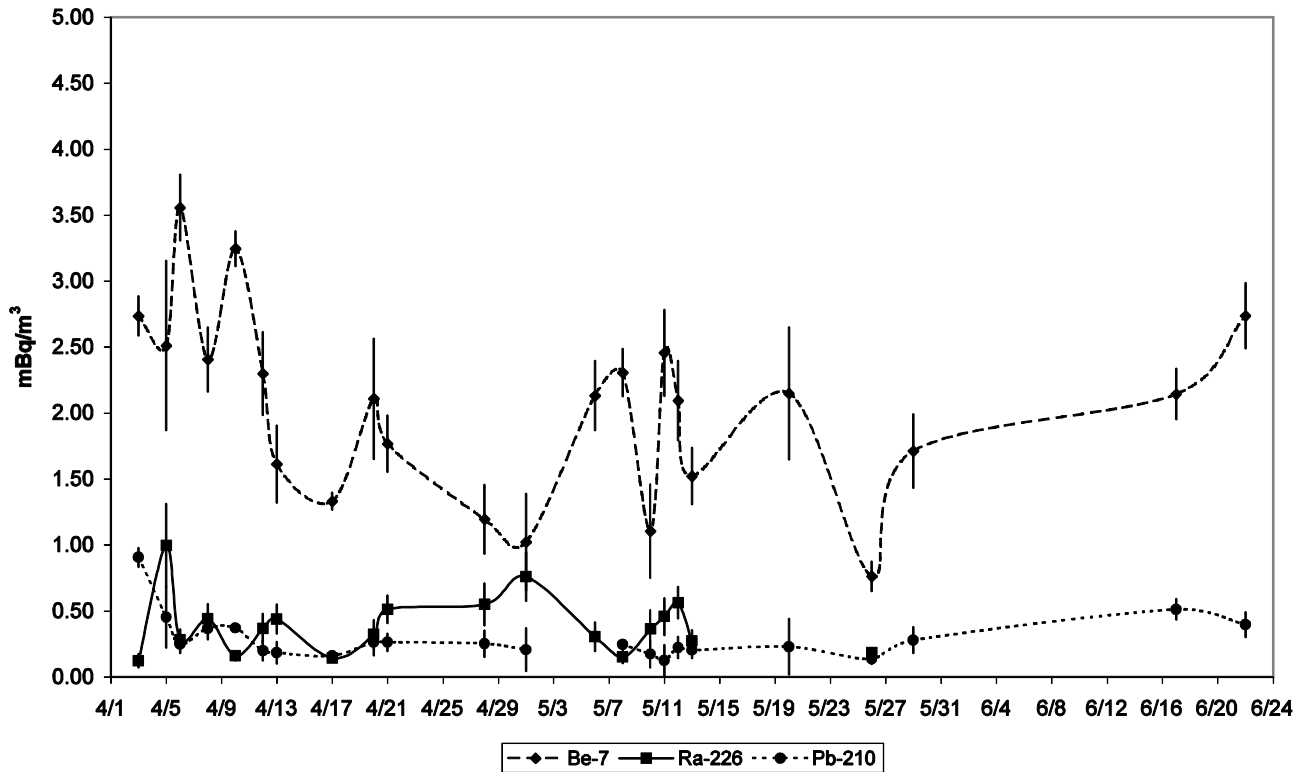

a)
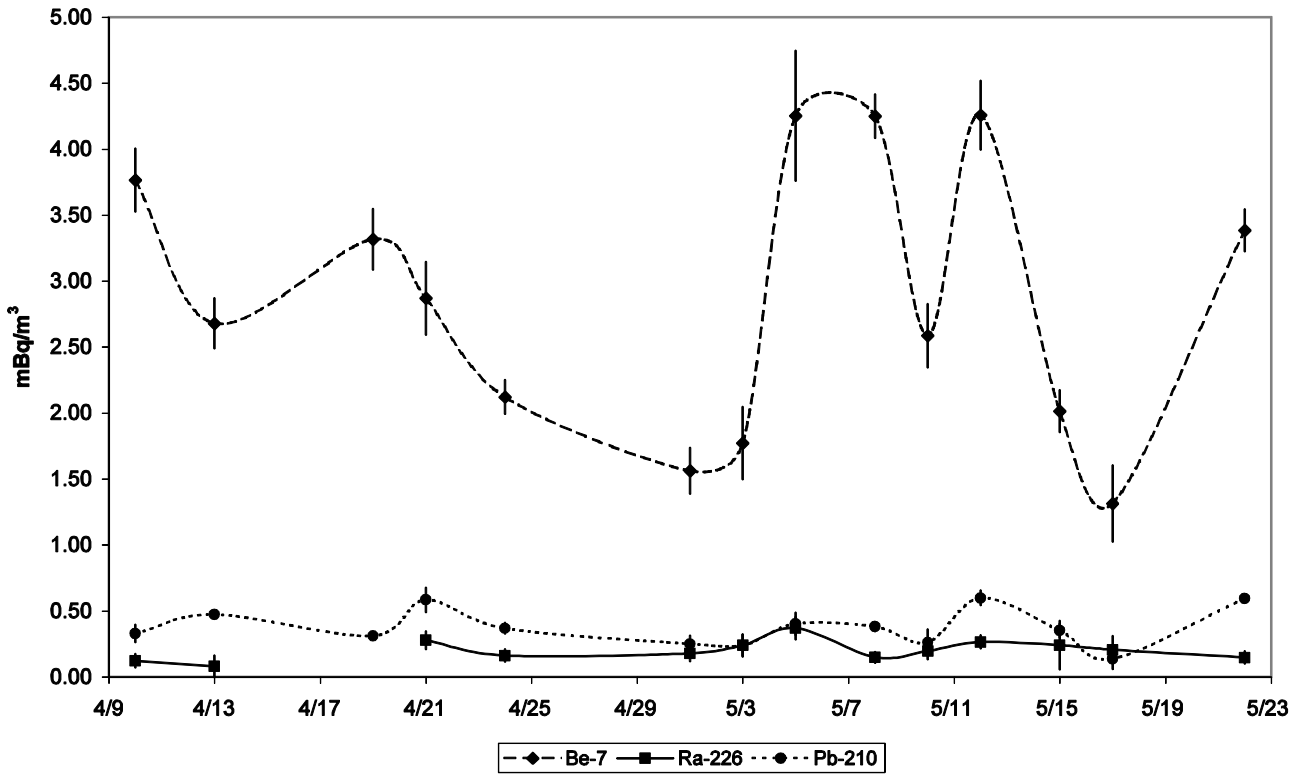
b)

Fig. 4 Activities measured in mBq/m³ (corrected for standard conditions) with N-type planar detector at Mt. Cimone site: (a) artificial emitters ^{131}I ^{137}Cs ^{134}Cs, (b) natural emitters ^{7}Be ^{226}Ra ^{210}Pb.
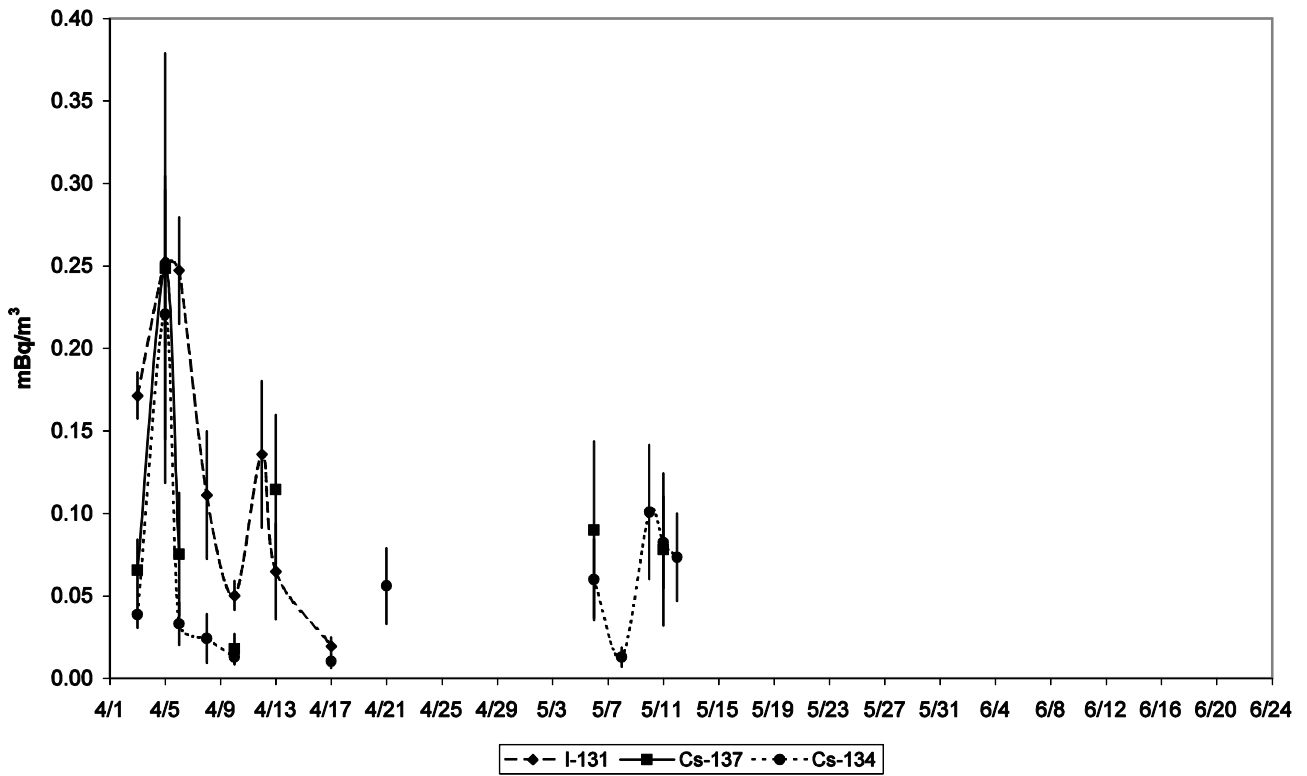
a)

b)

Fig.5 Activities measured in mBq/m³ (corrected for standard conditions) with N-type planar detector at Montecuccolino site: (a) artificial emitters ^{131}I ^{137}Cs ^{134}Cs, (b) natural emitters ^{7}Be ^{226}Ra ^{210}Pb.

The values for ^{131}I ranged from 0.020 to 0.250 mBq/m³, those for ^{137}Cs from 0.015 to 0.250 mBq/m³ and finally those for ^{134}Cs from 0.010 to 0.220 mBq/m³. The average recorded values of Fukushima radionuclides are in good agreement with data collected over the Italian peninsula, generally from ground level stations as reported from the Institute for Environmental Protection and Research (ISPRA, http://www.isprambiente.gov.it/site/it-IT/Documenti_emergenza_nucleare_Giappone/; Abstracts of the Workshop "Twenty-five years after the Chernobyl accident: studies, remarks and recent findings", 2011). Our data are consistent with those observed over the European continent, as discussed in Masson et al. (2011), which show a rather large degree of homogeneity of the plume following redistribution processes in the troposphere.

Comparing the maximum activity concentration observed in our time series and that one recorded at Fukushima and Sugitsuma (available at MEXT http://radioactivity.mext.go.jp/en/monitoring_around_FukushimaNPP_dust_sampling/2011/05/1306 621_053110.pdf), the mean transit time between Japan and Northern Italy was roughly estimated as

eleven days. As a result, the approximate dilution factor of the plume radioactivity based on ^{137}Cs (the longest lived of the detected γ-emitters) was estimated of about 5 orders of magnitude.

Good agreement was found between the activities (either natural or artificial) measured at both stations, as per Table 1, upon comparing average values at the two sites with a Student's t-test. The t-test value indicated that for all the radionuclides reported, with the sole exception of ^{7}Be and ^{226}Ra, the means of the observed values at the two sites were not statistically different at the 0.05 confidence level. The values for ^{7}Be are slightly higher at Mt. Cimone because of the greater altitude of the location and the negative gradient of this radionuclide due to its cosmogenic origin. On the contrary, the values for ^{226}Ra were slightly lower because of the crustal origin of this radionuclide. Concerning ^{210}Pb, values would be expected higher close to the ground, but data at the two sites were comparable. Such comparable values for ^{210}Pb are expected during the warm season when, as a result of active turbulent motions which stir the innermost tropospheric layer above the Mt. Cimone top, this site lies within the Planetary Boundary Layer (PBL); during the cold season, instead, the PBL and free troposphere are decoupled largely preventing upward transport of ^{210}Pb .

Comparison of activity data on Fukushima radionuclides with those on the natural components clearly shows that the background aerosol radioactivity (namely ^{7}Be and ^{210}Pb) was on the average one order of magnitude higher than the artificial component. In all the samples in which the Fukushima radionuclides were detected, associated experimental uncertainty was very high due to low concentrations, as a result of both dispersal-dilution and wet removal, frequent in the region (especially at Mt. Cimone) during spring time. As for ^{7}Be and ^{210}Pb, the values were also typical for the season, that is at an average concentration between the winter minimum and the summer maximum.

The average ^{134}Cs/^{137}Cs ratio at the two sites was found to be 0.9, in good agreement with the 0.95 average European value recorded during the period March 20th – April 4th (Masson et al.,2011), and very different from the 0.5-0.6 value reported after the Chernobyl accident (Arvela et al., 1990; De Cort et al., 1998).

In Figure 6, 3D kinematic fifteen days back-trajectories calculated using the HYSPLIT-4 model for the site of Mt. Cimone on the 4th April 2011, i.e. the day with the maximum observed ^{137}Cs value, are shown. Only Mt.Cimone backtrajectories are reported due to the coincidence of the output for Montecuccolino. The analysis of back-trajectories of the period end of March – beginning of April confirmed the westerly Japanese origin of the considered air masses, which is very well captured and described by the one shown in Figure 4.

NOAA HYSPLIT MODEL
Backward trajectories ending at 0000 UTC 04 Apr 11
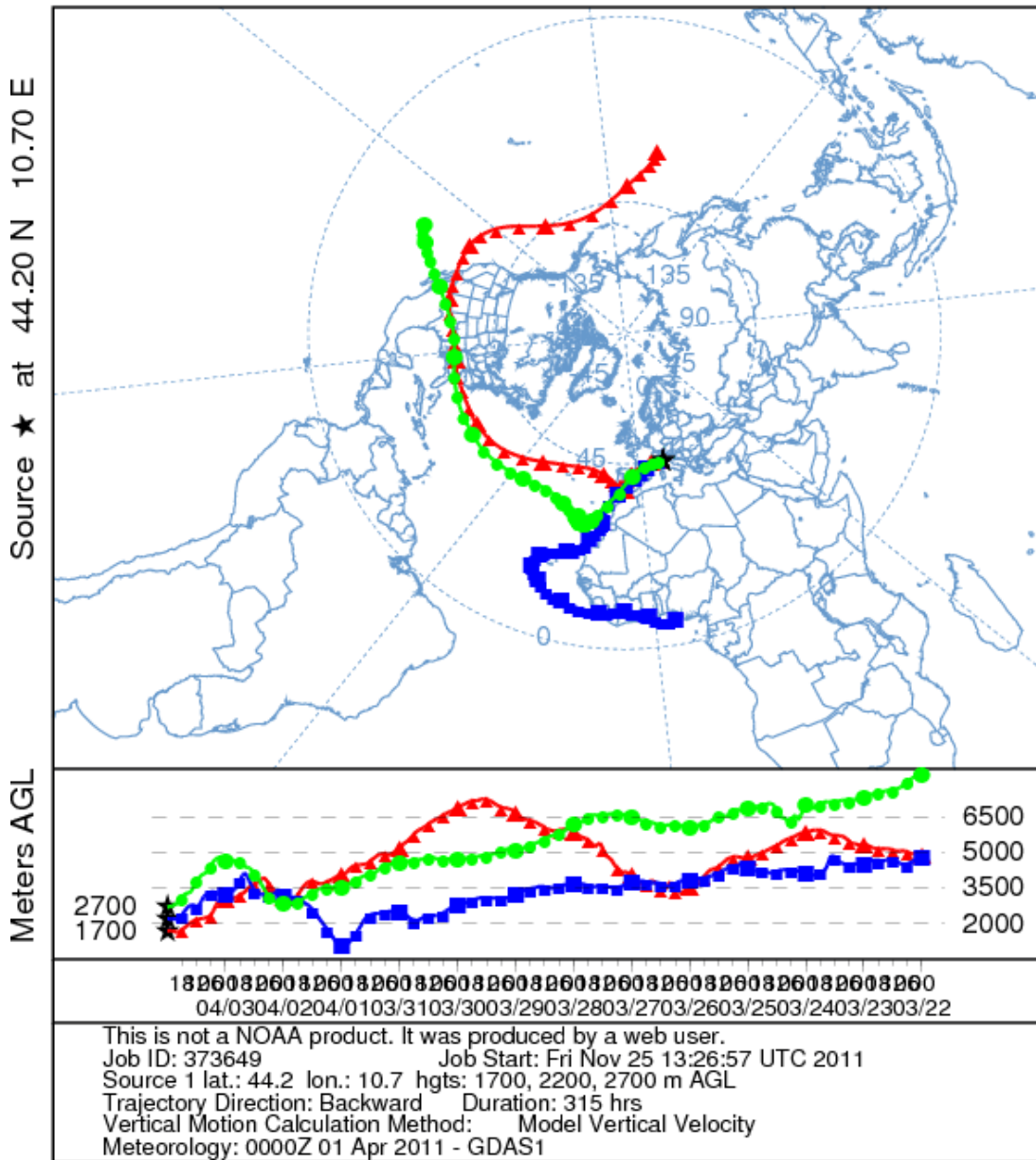GDAS Meteorological Data

Fig.6 15 days back-trajectories for 4th April 2011 (00:00 UTC), day of maximum detected 137Cs value, for Mt. Cimone (44°12' N, 10°42' E), calculated by the HYSPLIT-4 model (http://www.arl.noaa.gov/ready/hysplit4.htm) for three arrival heights (1700, 2200 and 2700 m a.s.l.).

From the time series of the artificial radionuclides the influence of emissions from Fukushima appears to have ceased in Italy in the first half of May 2011 (Torri, 2011). For the sake of completeness the data of fallout sampled in the same period is reported: total ^{137}Cs deposition analyzed between March 18th and May 18th 2011 resulted to be 27.1 ± 5.9 Bq/m^2.

The increase in radiological risk due to the Fukushima plume in Italy can be evaluated against the doses due to the natural radionuclides that are always present. Dose calculations were conducted under the worst case hypotheses discussed in section 2.2. The doses calculated for all the radionuclides considered are reported in Table 2. The dose contribution of the nuclides deriving from the Fukushima accident, calculated for a hypothetical one year constant exposure, was assessed at 1.1 μSv/year, to be compared to the 50 μSv/year due to the natural components, including [7]Be, ^{210}Pb, [226]Ra. This latter in turn amounts to only a minor fraction of the annual dose to members of the public from all sources (natural, medical, etc.), which in Italy averages approximately 4500 μSv/year (Dionisi et al., 2005).

3.1 Comparison of dose rates in Chernobyl, Fukushima and Bolsena

Air dose rates taken directly around Chernobyl nuclear power plant and in Bologna city and available data for the area around Fukushima nuclear power plant are used for comparison with air dose rates directly measured in Bolsena village (Table 3). Considering an uniform irradiation the equivalent doses numerically are equal to the effective ones.
Moreover using the conversion factor $3 \cdot 10^{-9}$ Sv/ (Bq$\cdot$m$^{-3}\cdot$h) (Legislative Decree 230/1995) and the indoor radon concentrations, measured in different buildings of Bolsena village (see table 1, Chapter 4), the effective dose rates has been calculated (table 3).

The highest values is that calculated in the cellar of Bolsena (described in the Chapter 4), about 7 times more than at 100 m from the reactor number 4 of Chernobyl.
In figure 7, in which the outer values are not considered (near reactor in Chernobyl, Futuba county Namie town Akougi Teshichiro - Japan and cellar in Bolsena),again Bolsena village presents values higher than Chernobyl and Fukushima area.

Location	Date	Code	Distance from reactor (km)	Effective Dose Rate (μSv/h)
Ukraine				
Pripyat	08/06/2011	1C	3	[1]1.7
Near Reactor	08/06/2011	2C	0.1	[1]12
Chernobyl Village	08/06/2011	3C	10	[1]0.14
Kiev	07/06/2011	4C	130	[1]0.08
Japan				
Iwaki city Miwa-town Saiso	17/10/2011	1F	39 S-W	[2]0.2
Iwaki city Hisanohama town Hisanohama aza Kitaaramaki	17/10/2011	2F	31 S	[2]0.3
Tamura city Miyakoji town Furumichi aza Teranomae	17/10/2011	3F	25 W	[2]1.0
Futuba county Namie town Akougi Teshichiro	17/10/2011	4F	31 N-W	[2]15.2
Minami Soma city Kashima ward Terauchi Motoyashiki	17/10/2011	5F	32 N	[2]0.5
Italy				
Bologna town	17/10/2011	BO		[1]0.15
Bolsena village	17/03/2011	Bol1		[1]1.1
Bolsena (house made of tuff)	03/2011	Bol2		[3]3.83
Bolsena (house made of tuff+plaster)	03/2011	Bol3		[3]2.28
Bolsena (house made of concrete)	03/2011	Bol4		[3]0.99
Bolsena (cellar caved in tuff)	09/2010	Bol5		[3]90

[1]measured by Geiger-Muller counter

[2]data available in
http://radioactivity.mext.go.jp/en/monitoring_around_FukushimaNPP_monitoring_out_of_20km/2011/03/index.html
[3]Considering indoor radon concentrations

Table 1 Effective dose rates (μSv/h) measured around Chernobyl (Ucraine) and Fukushima (Japan) Nuclear Power Plants, in Bolsena and Bologna (Italy).
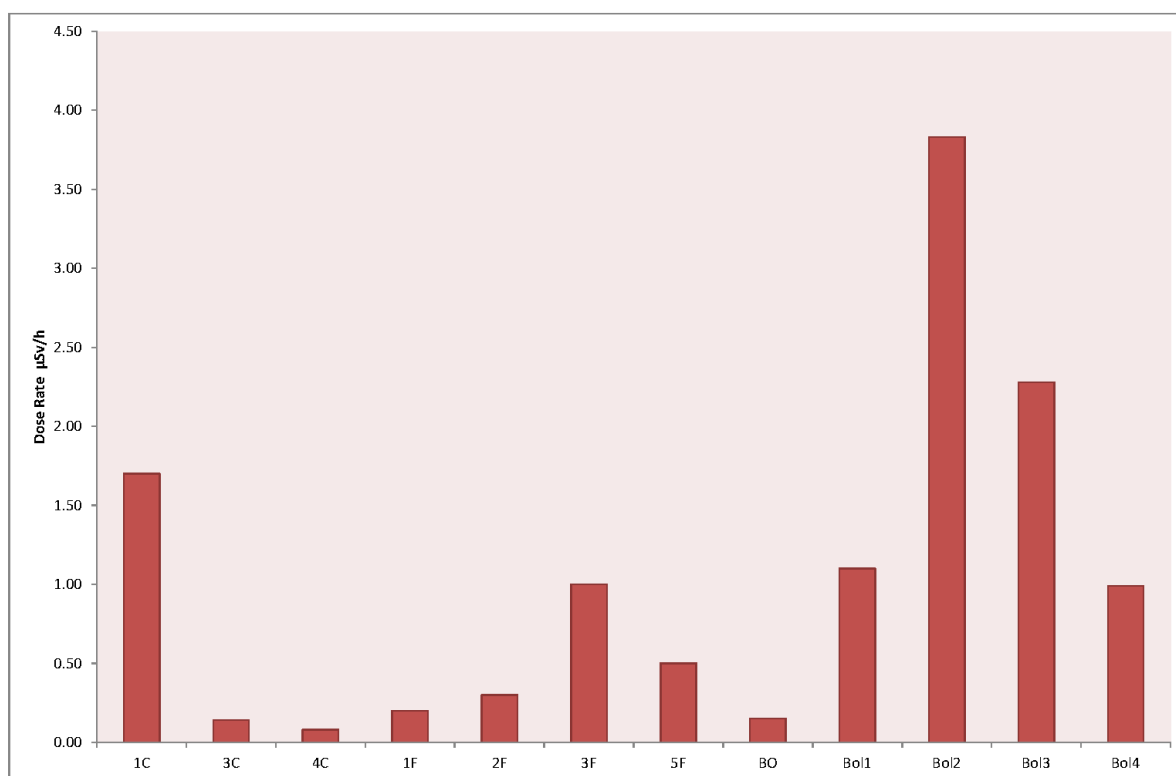
*Fig.7 Comparison between dose rates (*μSv/h) reported in table 3 neglecting the outer value (see text).

4 Conclusions

In this work the data of airborne radioactivity in ambient aerosol at two elevated stations in northern Italy under the influence of the Fukushima plume transit are reported. The main artificial radionuclides detected were [131]I (0.020-0.548 mBq/m^3), [137]Cs (0.012- 0.250 mBq/m^3) and [134]Cs (0.010-0.222 Bq/m^3).The order of magnitude of the gamma emitters from Fukushima accident detected at both stations are consistent with those collected at other locations both in the Italian peninsula. A comparison of peak inhalation doses from Fukushima nuclides, natural gamma emitters and the overall average dose from all sources in the studied area indicate that the contribution of the accident to background radiation doses is factually negligible.

Comparing dose rates measured nowadays in two sites, where nuclear accidents happened, Chernobyl and Fukushima, it can be highlight how some particular area like Bolsena presents highest values of dose rate only due to natural sources.

References

1st International Expert Meeting on Sources and Measurements of Natural Radionuclides Applied to Climate and Air Quality Studies, 2004, (Gif-sur-Yvette, France, 3-5 June 2003) (WMO TD No. 1201), available at ftp://ftp.wmo.int/Documents/PublicWeb/arep/gaw/gaw155.pdf

Battiston, G.A., Degetto, S., Gerbasi, R., Sbrignadello, G., Tositti, L., 1988. Fallout Distribution in Padua and Northeast Italy after the Chernobyl Nuclear Reactor Accident, *J.Environ.Radioactivity*, 8, 183-191.

Bonasoni, P., Evangelisti, F., Bonafè, U., Feldmann, H., Memmesheimer, M., Stohl, A., Tositti, L., Kromp-Kolb, L.H., and Colombo, T., 1999. Stratosphere-troposphere exchanges: case studies recorded at Mt. Cimone during VOTALP project.

Bonasoni, P., Evangelisti, F., Bonafe, U., Ravegnani, F., Calzolari, F., Stohl, A., Tositti, L., Tubertini, O., and Colombo, T., 2000. Stratospheric ozone intrusion episodes recorded at Mt. Cimone during the VOTALP project: case studies. *Atmospheric Environment,* 34, *1355-1365.*

Bonasoni, P., Stohl, A., Cristofanelli, P., Calzolari, F., Colombo, T., and Evangelisti, F., 2000. Background ozone variations at Mt. Cimone Station. *Atmospheric Environment*, 34, 5183-5189.

Cristofanelli, P., Bonasoni, P., Collins, W., Feichter, J., Forster, C., James, P., Kentarchos, A., Kubik, P.W., Land, C., Meloen, J., Roelofs, G.J., Siegmund, P., Sprenger, M., Schnabel., C., Stohl, A., Tobler, L., Tositti, L., Trickl, T., and Zanis, P., 2003. Stratosphere-to-troposphere transport: A model and method evaluation. Journal of Geophysical Research, Vol. 108, No. D12, 8525, doi:10.1029/2002JD002600

Cristofanelli, P., Bonasoni, P., Tositti, L., Bonafè, U., Calzolari, F., Evangelisti, F., Sandrini, S., and Stohl, A., 2006. A 6-year analysis of stratospheric intrusions and their influence on ozone at Mt. Cimone (2165 m above sea level). Journal of Geophysical Research, Vol. 111, D03306, doi:10.1029/2005JD006553

Cristofanelli, P., Bonasoni, P., Carboni, G., Calzolari, F., Casarola, L., Zauli Sajani, S., and Santaguida, R., 2007. Anomalous high ozone concentrations recorded at a high mountain station in Italy in summer 2003. *Atmospheric Environment*, 41, 1383-1394.

Cristofanelli, P., Calzolari, F., Bonafè, U., Duchi, R., Marinoni, A., Roccato, F., Tositti, L., Bonasoni, P., 2009. Stratospheric Intrusion Index (SI[2]) from baseline measurement data. *Theor Appl Climatology*, 97, 317-325.

Davies, T.D., Schuepbach, E., 1994. Episode of high ozone concentrations at the earth's surface resulting from transport down from the upper troposphere/lower stratosphere: a review and case studies. *Atmospheric Environment*, 28, 53-68.

Davies, T.D., Schuepbach, E., 1994. Episode of high ozone concentrations at the earth's surface resulting from transport down from the upper troposphere/lower stratosphere: a review and case studies. *Atmospheric Environment*, 28, 53-68.

Dietrich, E., Favale, B., Passamonti, V., 1997, Trentasei Anni di Misure di Radioattività Beta nell'Aria sull'Italia al Livello del Suolo.Valori Medi Mensili dal 1957 al 1992. CNR-IFA Internal Report 97-15.

Dionisi, Fontani, Innocenzi, Menna, Parisi, Salierno, Torri, Zeppa, Wells. 2005, APAT. *Enviromental Data Yearbook*.

Fischer, H., Kormann, R., Klüpfel, T., Gurk, C., Königstedt, R., Parchatka, U., et al., 2000. Ozone production and trace gas correlations during the June 2000 MINATROC intensive measurement campaign at Mt. Cimone. *Atmospheric Chemistry and Physics*, 3, 725-38.

Gilmore, G., 2008, Practical Gamma-Ray Spectrometry, John Wiley & Sons.

Jakobs, H., 2011. Potential Dispersion of the Radioactive Cloud After a Nuclear Accident in Fukushima. Rhenish Institute for Environmental Research at the University of Cologne. 17 March, 2011. EURAD:UNI-KOELN.DE.

Lozano, R.L., Hernández-Ceballos, M.A., Adame, J.A., Casas-Ruíz, M., Sorribas, M., 2011. Radioactive impact of Fukushima accident on the Iberian Peninsula: Evolution and plume previous pathway. Environment International 37, 1259-64.

Manolopoulou, M., Vagena, E., Stoulos, S., Ioannidou, A., Papastefanou, C., 2011. Radioiodine and radiocesium in Thessaloniki, Northern Greece due to Fukushima nuclear accident. *Journal of Environmental Radioactivity*, 102, 796-797.

Masson et al., 2011. Airborne radionuclides released by the Fukushima Daiichi NPP all over Europe, submitted.

Papastefanou, C., and Ioannidou, A., 1995. Aerodynamic size association of [7]Be in ambient aerosols. *Journal of Environmental Radioactivity*, 34, 3545-3561.

Torri, G., 2011. La rete di monitoraggio RESORAD e la sua risposta all'incidente di Fukushima. Twenty-five years after the Chernobyl accident: studies, remarks and recent findings, 21-22-23 June 2011, Udine, Italy (http://www.arpa.fvg.it/fileadmin/Temi/Radiazioni/Radiazioni_ionizzanti/Chernobyl_25/presentazioni_convegno/TORRI.pdf).

Winkler, R., Dietl, F., Frank, G., and Thiersch, J., 1998. Temporal variation of ^{7}Be and ^{210}Pb size distributions in ambient aerosols. *Atmospheric Environment*, 32, 983-991.

World Meteorological Organization – Global Atmospheric Watch, 1994. Report on the measurements of atmospheric turbidity in BAPMo N. Report N 94, 1-73.

http://www.nisa.meti.go.jp/english/files/en20110412-4.pdf,

http://www.nisa.meti.go.jp/english/press/2011/07/en20110715-1-2.pdf (Nuclear and Industrial Safety Agency, Japan).

http://www.mext.go.jp/english/

http://www.jma.go.jp/en/tsunami/observation_04_20110313180559.html (Japan Meteorological Agency)

http://www.isac.cnr.it/cimone/ (Monte Cimone)

http://www.riu.uni-koeln.de/ (Rhenish Institute for Environmental Research at the University of Cologne)

http://www.irsn.fr/FR/popup/Pages/irsn-meteo-france_19mars.aspx, http://www.irsn.fr/FR/popup/Pages/irsn-meteo-france_30mars.aspx (IRSN plume dispersion modeling)

http://www.isprambiente.gov.it/site/it-IT/Documenti_emergenza_nucleare_Giappone/

Curriculum Vitae

Giorgia Cinelli was born on 12th January 1983 in San Benedetto del Tronto (AP), Italy. He grew up in Ascoli Piceno and here attended A. Orsini High School between the ages of 14 and 19. She moved in Bologna and began studying Energy and Nuclear Engineer at Alma Mater Studiorum University, Bologna. She graduated in October 2005 in bachelor thesis and stated the master period. After six months spent in Bruxelles during Erasmus project she performed her master thesis and graduated in March 2009 with laudem.

In January 2009 she began the PhD of which this thesis is the result and in this period she became qualified expert in protection of radiation of the first level.